

Energy Management and Control for a Wind Energy System

by

Someshwar Singh

**Bachelor in Electrical Engineering, Uttar Pradesh Technical University,
India, 2006**

**A THESIS SUBMITTED IN PARTIAL FULFILLMENT OF THE
REQUIREMENTS FOR THE DEGREE OF**

Master of Science in Engineering

In the Graduate Academic Unit of Electrical Engineering

Supervisor(s): J. H. Taylor, Ph.D.
Electrical and Computer Engineering
Examining Board: L. Chang, Ph.D.
Electrical and Computer Engineering
External Examiner: G. Srinivasan, Ph.D.
Faculty of Business Administration

This thesis is accepted

Dean of Graduate Studies

THE UNIVERSITY OF NEW BRUNSWICK

March, 2011

©Someshwar Singh, 2011

To Papa and Amma & Dr. James H. Taylor

Abstract

All commercial electrical energy producers and consumers are connected to an electrical grid covering a pre-defined geographical area through transmission lines. The electrical grid facilitates buying and selling of electrical energy through a day-ahead bidding process, under a set of prior known rules and procedures between producers and consumers; it also maintains generation:load balance within $\pm 1.5\%$ limits for stable operation of the grid.

A wind energy system is an arrangement of mechanical and electrical components which converts kinetic energy of the air moving over the earth's surface into electrical energy. Due to the intermittent nature of wind, wind energy sources are considered to be unreliable sources of electrical energy and therefore rather than participating in day-ahead markets most wind energy utilities enter into contracts with the local conventional suppliers. However, these contracts offer a low price compared to the electricity markets.

The main focus of this work was to provide a solution to important aspects of a wind energy facility required to participate in an electricity market, i.e., power production forecasting, uncertainty estimation and bidding strategies. This work took the history of wind-speed forecast and actual data provided by Environment Canada and calculated the forecast error distributions. A representative wind-speed realization was then modeled as the sum of a deterministic term and a stochastic term. The deterministic term was the forecast provided by Environment Canada, while the stochastic component, the error in the forecast, was modeled as a first-

order gaussian markov process; it was demonstrated that wind-speed forecast error distributions are approximately normal, and their statistics (mean and standard deviation) were determined.

Wind-speed realizations were then input to a wind generator model developed in MATLAB[®]/Simulink[®] to get wind power realizations. The uncertainties in the wind speed-realizations were transferred to the wind power realizations as well. Monte Carlo Simulations were performed to assess the expected future power production for any delivery period and the likely range of wind power production using the wind-speed forecast error statistics. The statistics of wind power prediction obtained by performing Monte Carlo Simulation gave an idea of the risk involved in wind power production; then the question arose as to how much to bid into an electricity market to obtain a maximum profit. This dilemma was resolved in this work, by the development of an optimal bidding strategy.

It is well established that a combination of an uncertain production unit with a certain production unit reduces the overall uncertainty and risk. Therefore, the prospects of adding a natural gas microturbine or buying power from the grid were assessed to reduce uncertainty in the power production.

This work gave an insight into designing energy management and control software for a renewable energy system. With the conclusions drawn from the above outlined work, it was suggested that further research be done to validate the normality of wind-speed forecast error with more data; also it is strongly recommended that for performing Monte Carlo trials the wind power generator model in MATLAB[®]/Simulink[®] is not appropriate and should be replaced with a mathematical model to decrease the computational time.

Acknowledgements

The author sincerely thanks Dr. James H. Taylor for his guidance and advice during the course of this work. Special thanks to Dr. G. Srinivasan for guiding me to understand the economics aspect of this work. The author would like to express his appreciation to Dr. K. Englehart, Dr. M. Stevenson, Dr. B. Petersen and Sean Perry for their advice on various matters. The author would also like to express his gratitude to staff of the Department of Electrical and Computer engineering for their selfless support and assistance.

The author is grateful to the Atlantic Innovation Fund and to Dr. Taylor and to Dr. Liuchen Chang for the financial support afforded during the course of this work.

Genuine thanks to Shweta Gupta as well to those who shared time, experience, hopes and friendship.

Table of Contents

Dedication	ii
Abstract	iii
Acknowledgments	v
Table of Contents	vi
List of Tables	x
List of Figures	xi
Abbreviations	xvi
1 Introduction	1
1.1 Literature Review	3
1.2 Objectives	6
1.3 Contribution	7
1.4 Thesis Outline	8
2 Wind-speed forecast error modeling	9
2.1 Background	9
2.2 Approach	11
2.2.1 Chi-Square Test	16

2.2.2	Gaussian Distribution Fitting	17
2.3	Markov Processes	19
2.3.1	Autocorrelation Function	19
2.3.2	Order of a Markov Process	20
2.4	Solving a First Order Markov Process	22
3	Modeling a wind power generator	24
3.1	Performance of a Grid-Connected Wind Power Generator	29
4	Uncertainty estimation in power forecasts	32
4.1	Monte Carlo Simulations	32
4.1.1	Prediction Error Realizations	34
4.1.2	Power Predictions	35
4.1.3	Confidence Intervals	37
4.1.4	Selection of Time Step (h)	38
4.2	Test Results	39
4.2.1	Effects of n on the confidence limits	42
5	Modeling a gas microturbine	46
5.1	Performance of a C60 Microturbine	48
5.1.1	Fuel Input	48
5.1.2	Heat Rate	49
5.1.3	Electrical Efficiency	49
5.1.4	Heat Recovery	49
5.2	Cost of Power using a C60 Microturbine	50
5.2.1	Capital Cost Factor	50
5.2.2	Fuel Cost	51
5.2.3	Maintenance Cost	51
5.2.4	Total Cost	52

5.3	Comparing a Microturbine vs. Grid-based Power	52
6	Bidding under uncertainty	53
6.1	Overview of an Electricity Market	53
6.1.1	Bids	54
6.1.2	Accepted Market Price and Quantities	54
6.1.2.1	Consumer Surplus	55
6.1.2.2	Producer Surplus	56
6.1.2.3	Social Welfare	57
6.1.3	Reserve Power	60
6.2	Bidding Quantities Formulation	61
6.3	Test Results	66
7	Thesis observations	68
7.1	Summary and Conclusion	68
7.2	Future Work	70
	Bibliography	71
	Appendix	77
A	χ^2 test results	77
A.1	24 hour Prediction block test result	77
A.2	12 hour Prediction block test results	78
A.3	6 hour Prediction block test results	79
A.4	3 hour Prediction block test results	80
A.5	1 hour Prediction block test results	81
B	Comparing cumulative probabilities (wind-speed forecast error)	88
C	Grid-connected wind power generator	93

List of Tables

2.1	Summary of test results	17
4.1	Values of ψ for various values of β	37
5.1	Full load specifications	48
5.2	Cost of energy using microturbine as power system	52
5.3	Cost of energy using microturbine as combined heat and power system	52
6.1	Electricity market solution for two participants	59
6.2	Summary of chi-square test results	62

List of Figures

2.1	Time line for bidding, acceptance, delivery and forecasting	12
2.2	Scheme for data collection	13
2.3	Mean and variance of error in forecasted wind speed	15
2.4	Comparing cumulative probabilities for time block 01:00:00 to 1:59:59	18
2.5	Comparing cumulative probabilities for time block 09:00:00 9:59:59 .	18
2.6	Fitting an ACF for FOM and SOM processes	21
3.1	Wind turbine system	24
3.2	Characteristics of an induction machine [33]	27
3.3	Power factor	28
3.4	Input/output sharing between script file and model file	30
3.5	Wind speed realization	31
3.6	Power forecast	31
4.1	Wind power realization generation	36
4.2	Forecasted wind speed	39
4.3	Two wind-speed forecast error realizations ($e^{(i)}$)	40
4.4	Two wind-speed forecast realizations ($v_r^{(i)}$)	40
4.5	Two wind power realizations ($P_p^{(i)}$)	41
4.6	Wind power statistics, 75 MCS trials	41
4.7	Wind power sample mean with 90% confidence bands	43
4.8	Estimated kurtosis	44

4.9	Wind power sample standard deviation with 90% confidence bands	44
5.1	Components of a gas microturbine system	46
6.1	Consumer surplus	55
6.2	Deriving consumer surplus	55
6.3	Producer surplus	56
6.4	Deriving producer surplus	56
6.5	Social welfare	57
6.6	Comparing cumulative probabilities for time block 01:00:00 to 1:59:59	63
6.7	Comparing cumulative probabilities for time block 13:00:00 to 13:59:59	63
6.8	Bidding quantities	67
A.1	Prediction block 00:00 to 23:59:5	77
A.2	Prediction block 00:00 to 11:59:59	78
A.3	Prediction block 12:00 to 23:59:59	78
A.4	Prediction block 00:00 to 5:59:59	79
A.5	Prediction block 6:00 to 11:59:59	79
A.6	Prediction block 12:00 to 17:59:59	79
A.7	Prediction block 18:00 to 23:59:59	79
A.8	Prediction block 00:00 to 2:59:59	80
A.9	Prediction block 3:00 to 5:59:59	80
A.10	Prediction block 06:00 to 8:59:59	80
A.11	Prediction block 9:00 to 11:59:59	80
A.12	Prediction block 12:00 to 14:59:59	80
A.13	Prediction block 15:00 to 17:59:59	80
A.14	Prediction block 18:00 to 20:59:59	81
A.15	Prediction block 21:00 to 23:59:59	81
A.16	Prediction block 00:00 to 0:59:59	81

A.17 Prediction block 1:00 to 1:59:59	81
A.18 Prediction block 2:00 to 2:59:59	82
A.19 Prediction block 3:00 to 3:59:59	82
A.20 Prediction block 04:00 to 4:59:59	82
A.21 Prediction block 5:00 to 5:59:59	82
A.22 Prediction block 6:00 to 6:59:59	83
A.23 Prediction block 7:00 to 7:59:59	83
A.24 Prediction block 08:00 to 8:59:59	83
A.25 Prediction block 9:00 to 9:59:59	83
A.26 Prediction block 10:00 to 10:59:59	84
A.27 Prediction block 11:00 to 11:59:59	84
A.28 Prediction block 12:00 to 12:59:59	84
A.29 Prediction block 13:00 to 13:59:59	84
A.30 Prediction block 14:00 to 14:59:59	85
A.31 Prediction block 15:00 to 15:59:59	85
A.32 Prediction block 16:00 to 16:59:59	85
A.33 Prediction block 17:00 to 17:59:59	85
A.34 Prediction block 18:00 to 18:59:59	86
A.35 Prediction block 19:00 to 19:59:59	86
A.36 Prediction block 20:00 to 20:59:59	86
A.37 Prediction block 21:00 to 21:59:59	86
A.38 Prediction block 22:00 to 22:59:59	87
A.39 Prediction block 23:00 to 23:59:59	87
B.1 Prediction block 00:00 to 0:59:59	88
B.2 Prediction block 1:00 to 1:59:59	88
B.3 Prediction block 2:00 to 2:59:59	89
B.4 Prediction block 3:00 to 3:59:59	89

B.5	Prediction block 04:00 to 4:59:59	89
B.6	Prediction block 5:00 to 5:59:59	89
B.7	Prediction block 6:00 to 6:59:59	89
B.8	Prediction block 7:00 to 7:59:59	89
B.9	Prediction block 08:00 to 8:59:59	90
B.10	Prediction block 9:00 to 9:59:59	90
B.11	Prediction block 10:00 to 10:59:59	90
B.12	Prediction block 11:00 to 11:59:59	90
B.13	Prediction block 12:00 to 12:59:59	90
B.14	Prediction block 13:00 to 13:59:59	90
B.15	Prediction block 14:00 to 14:59:59	91
B.16	Prediction block 15:00 to 15:59:59	91
B.17	Prediction block 16:00 to 16:59:59	91
B.18	Prediction block 17:00 to 17:59:59	91
B.19	Prediction block 18:00 to 18:59:59	91
B.20	Prediction block 19:00 to 19:59:59	91
B.21	Prediction block 20:00 to 20:59:59	92
B.22	Prediction block 21:00 to 21:59:59	92
B.23	Prediction block 22:00 to 22:59:59	92
B.24	Prediction block 23:00 to 23:59:59	92
C.1	Grid-connected wind power generator model [34]	94
C.2	Nine MW wind farm model [34]	95
D.1	Prediction block 00:00 to 0:59:59	96
D.2	Prediction block 1:00 to 1:59:59	96
D.3	Prediction block 2:00 to 2:59:59	97
D.4	Prediction block 3:00 to 3:59:59	97

D.5	Prediction block 04:00 to 4:59:59	97
D.6	Prediction block 5:00 to 5:59:59	97
D.7	Prediction block 6:00 to 6:59:59	97
D.8	Prediction block 7:00 to 7:59:59	97
D.9	Prediction block 08:00 to 8:59:59	98
D.10	Prediction block 9:00 to 9:59:59	98
D.11	Prediction block 10:00 to 10:59:59	98
D.12	Prediction block 11:00 to 11:59:59	98
D.13	Prediction block 12:00 to 12:59:59	98
D.14	Prediction block 13:00 to 13:59:59	98
D.15	Prediction block 14:00 to 14:59:59	99
D.16	Prediction block 15:00 to 15:59:59	99
D.17	Prediction block 16:00 to 16:59:59	99
D.18	Prediction block 17:00 to 17:59:59	99
D.19	Prediction block 18:00 to 18:59:59	99
D.20	Prediction block 19:00 to 19:59:59	99
D.21	Prediction block 20:00 to 20:59:59	100
D.22	Prediction block 21:00 to 21:59:59	100
D.23	Prediction block 22:00 to 22:59:59	100
D.24	Prediction block 23:00 to 23:59:59	100

List of Symbols and Acronyms

Symbols

B_a	Friction on rotor side
B_{gc}	Friction of the mechanical coupling
β	Correlation time constant for FOM
β_1, β_2	Correlation time constants for SOM
χ^2	Chi-square
C	Unit cost of production
C_p	Rotor efficiency
$\$$	Canadian dollar
$\Delta(t)$	Time interval
η	Gear ratio
e	Prediction error
E	Expectation operator
f	Frequency of the grid
$F(x)$	Cumulative distribution of a random variable X
$f(x_i)$	Probability density function of X_i
Γ_a	Aerodynamic torque
Γ_g	Electrical torque
h	Time step
H_0	Null hypothesis variable
I	Current
J_r	Moment of inertia of wind turbine
J_g	Moment of inertia of electrical generator
kW_e	Electrical power
kW_{th}	Thermal power
K_r	Stiffness of the wind turbine rotor
K_{gc}	Stiffness of the mechanical coupling
λ	Final market price
μ	Mean
$\hat{\mu}$	Estimated mean

Symbols Contd...

n	Number of trials
N	Number of data points
O	Observed frequency
P_h	Prediction horizon
ϕ	Angle between useful power and apparent power
P	Number of poles
P_d	Demand quantity
P_f	Wind power production forecast using the EC forecast
P_g	Generation quantity
P_p	Power prediction
P_s	Selling price
Q_r	Spectral density
Q	Quantity to be bid
r_{ee}	Autocorrelation function
ρ	Air density
R	Rotor blade radius; transmission line resistance
R_{up}	Regulation-up price
R_{dw}	Regulation-down price
σ	Standard deviation
$\hat{\sigma}$	Estimated standard deviation
s	Slip of the motor
S	Variance
\hat{S}	Estimated variance
t	Time in hours
t_f	Final time
T	Time period
θ_t	Angular position of the rotor
θ_g	Angular position of the generator
θ_{gc}	Angular position of the mechanical coupling
τ	Time lag
u	random input
v_f	Forecasted wind speed
v_a	Actual wind speeds
v_r	Stochastic realization of wind speed
v	Wind speed
V	Voltage
w	Number of hours covered in a distribution
ω_g	Generator rotor speed
ω_{gc}	Mechanical coupling angular speed

Symbols Contd...

ω_r	Rotor angular speed
ω_s	Rotor synchronous speed
x_i	Random deviates of the random variable X_i
\bar{x}	Upper confidence band
\underline{x}	Lower confidence band

Acronyms

AST	Atlantic Standard Time
ACF	Autocorrelation Function
BTU	British Thermal Unit
CHP	Combined Heat and Power
CCF	Capital Cost Factor
DD	Delivery Day
EPAORD	Environmental Protection Agency's Office of Research and Development
ETV	Environmental Technology Verification
EC	Environment Canada
FOM	First-order Markov
FC	Fuel Cost
GHG	Green House Gas
GMP	Gauss-Markov Process
GWh	Gigawatt hour
GW	Gigawatt
GRIB	GRIdded Binary
HHV	Higher Heating Value
ISO	Independent System Operator
KW	Kilowatt
KWh	Kilowatt hour
LHV	Lower Heating Value
MP	Markov Process
MCS	Monte Carlo Simulation
MW	Megawatt
MWh	Megawatt hour
MC	Maintenance Cost
NAERC	North American Electric Reliability Council
NBSO	New Brunswick System Operator
PDF	Probability Density Function
PSIG	Pounds Per Square Inch Gauge
SOM	Second-order Markov
TC	Total Cost
WD	Weibull Distribution
USA	United States of America
WE	Wind Energy

Chapter 1

Introduction

The integration of wind power generator with electricity markets presents planning and operational difficulties, mainly due to the intermittent nature of wind. This nature makes it hard to make a firm power commitment which is a major requirement of electricity markets in allocation of power generation to meet the load, and, as a consequence wind energy sources are considered to be unreliable sources of electric power.

Typically electricity market structures, as operated by an Independent System Operator (ISO) include day-ahead, hour-ahead and real-time markets. The ISO, to ensure stability of electrical grid, accepts hourly bids from suppliers and buyers, called market participants, in a day-ahead (for the following day) market . The ISO then accepts only those supply bids which fulfill maximum consumer demand at minimum price. At the time of delivery, if the deviation of any participant is more than $\pm 1.5\%$ from their committed quantity, there is a salvage price, also called regulation-down price, for over-production, and a penalty, also called regulation-up price, for under-production. These regulation prices basically reflect the cost of re-scheduling other generators to make up for any deviation [40, 42, 37], and are intended to encourage market participants to be as accurate as possible in their day-ahead bids.

The inherent uncertainty in wind makes it hard for a Wind Energy (WE) utility to

predict their generation within a range of $\pm 1.5\%$. The WE utilities face a challenge to operate in day-ahead electricity markets and are subject to high financial risk in trading. Therefore, rather than participating in day-ahead markets most WE utilities enter into contracts with local conventional suppliers. However, these contracts offer a low price compared to the electricity markets [50, 16].

Some ISOs have introduced new electricity market rules to improve participation of the wind power utilities; these rules allow wind generation to be sold in hour-ahead markets and receive the hour-ahead market prices without any penalty [43]. But ISOs do not consider wind production as a capacity resource, because they have to provide a backup generation source to compensate for the possibility of unanticipated low- or no-wind conditions causing unexpected shortfalls at wind generation facilities [3, 29]. This issue does not arise with a conventional generator because their production can be known in advance with almost certainty.

In most North American Markets, since installed wind capacity is low, their production can essentially be absorbed into the market without any degrading of the system. But as installed capacity increases, there is a common agreement among researchers [3] that wind capacity should be acknowledged by encouraging wind energy participation in day-ahead markets. The ISO of NordPool, a prominent Nordic electricity market, has successfully implemented this, and the results shown by Morthorst [37] show that approximately 20% of total power consumption in Denmark is supplied by wind power and electricity market prices fell approximately between 7 to 13% in the year 2005; since wind energy has low cost of production its participation in the electricity market decreases over all electricity market prices.

The participation of wind energy in a day-ahead market is currently discouraged due to its high uncertainty. If WE utilities can adequately address the issue of uncertainty and variability in wind power generation then they will be allowed to participate in the market for fair pricing, and that will motivate them to invest in better forecasting methods for maximum profit, and the cost associated with running

a backup generation. (If the dispatch of a backup generator is linked to wind power production, it may not be possible to run that unit at optimal cost).

The participation in the day-ahead market requires a day ahead-commitment. Any deviation from the committed power will lead to a regulation-up price or regulation-down price which decreases profits. Since a WE utility's production is intermittent, their profits can suffer due to regulation prices. Therefore, a WE utility needs accurate power forecasts and strategies for bidding.

This research provides a solution for wind power forecasting incorporating local meteorological conditions and a strategy for bidding in a day-ahead market for maximum profit in face of regulation prices. This thesis also provides insight into the feasibility of dispatching a natural gas microturbine in order to reduce the variability of a wind power generator or wind farm.

1.1 Literature Review

There are growing concerns and efforts all over the world to reduce Green House Gas (GHG) emissions. The electrical utilities are one of the major GHG emitters because a significant amount of their production comes by burning fossil fuels (coal, petroleum, natural gas, etc.). The fossil fueled generators are the second major emitters of GHGs after the transportation sector in Canada [12]. The GHGs are oxides of carbon (CO_x), methane (CH_4), oxides of nitrogen (N_xO), sulphur hexachloride (SF_6), perfluorocarbons, and hydrofluorocarbons.

As the world looks for environmentally friendly electricity generation alternatives, the wind energy sector has seen a phenomenal growth in terms of installed capacity. The world's total wind power generation capacity grew by 31% in 2009 [15]. The development of wind power projects in Canada has also seen a rapid increase in the past 6 years after the federal and the provincial governments took various initiatives, although not as aggressive as other industrialized countries, for creating wind energy

demand. The total installed capacity of wind power generation has increased from 322 MW in 2003 to 2.4 GW by the end of the year 2008, an increase of 645% [5].

Despite this growth, the power generation from wind in Canada accounts for only 1% of its total electricity generation, which is much less than the percentage of power generation from wind by any other industrialized country [15]; given the fact that Canada has good wind energy sites as compared to Germany where almost 20 % of electricity demand is met by wind energy [15, 17, 6], there is clearly a high potential for increased WE production in Canada.

One of the reasons for slow growth of the wind energy sector in Canada is that it has enjoyed relatively cheaper electricity prices compared to other industrialized countries due to its abundant hydroelectric, natural gas and coal resources [6]. But as the demand for electricity grows and generation capacities of the existing facilities shrink, there is growing concern about meeting the demand and keeping the electricity prices low because the best rivers are already exploited to their maximum and thermal coal prices doubled in 2008 compared to the 2007 [5]. In addition, most industrialized countries are taking steps to force utilities to pay for the burden imposed on the environment through GHG emissions. This will directly effect the choice of fuel used in new power generating units and hence the price of electricity produced [5].

The recent development in the wind energy sector is heavily supported by energy policies of many countries. The main principle of energy policy is to offer a guaranteed premium on top of the electricity market energy prices for fixed periods of time. The premium offered for any particular project is designed to make it possible for efficiently operated wind energy installations to be cost-effective. The premium reduces the risk of investment in wind energy projects and thus creates an environment for rapid growth [4, 16, 14].

A study by the Canadian Wind Energy Association has concluded that in the

long term the cost of energy by wind generator will be competitive, without any government support, compared to coal, natural gas, hydro power plants. The study assumes that prices of fossil fuel are going to increase rapidly, and that the capital cost of wind turbines will decrease as supply catches up to demand and wind power technologies continue to improve [5].

The favorable government policies will ensure a good growth in wind energy sector. However, regarding integrating wind generated electricity into an electricity market, there remain some issues. Electricity markets accept day-ahead bids from participants for the following day. Once the bids are submitted, the system operators provide the accepted quantities and prices to the market participants [40, 42, 37]. Since there is a long time between the day-ahead commitment and the delivery, any difference between accepted and actual quantities can be settled in hour-ahead or real-time markets [25].

Since installed capacity of wind power generation is low, wind power production can essentially be absorbed into an hour-ahead market without any degrading of the system. But as installed capacity increases, one of the easiest way to ensure smooth operation of electricity markets and wind energy growth is by increasing the participation of wind production in day-ahead electricity markets [3, 29, 50].

The WE utility faces the challenge of producing accurate power generation forecasts before entering into the electricity market. Wind power forecasting requires wind speed modeling and prediction. There have been many approaches to modeling wind speed. Time series models are used extensively [11, 53, 10], which assumes that wind speeds have a Weibull or Rayleigh distribution, but researchers [22, 28] have shown that neither of these distributions are quite appropriate. Other researchers [49] have modeled wind speed using a stochastic Markov Chain (MC) approach.

Holttinen [26] has argued that wind production should be taken into hours-ahead market rather than day-ahead market by showing that power forecast error can be significantly reduced and revenue of the wind power utility can be increased by as

much as 8 % if the time between bidding and delivery is reduced to 2 hours compared to when it is 3 hours, 4 hours and so on. The comparison of various forecast time horizons is made using the Wind Power Prediction Tool [26], which takes a local weather forecast as input.

It has been demonstrated that wind speed forecasts are more accurate if the forecasting techniques incorporate local weather conditions and knowledge of prediction errors [26, 47, 30, 1].

The power forecast is obtained by passing predicted wind speeds to a wind power generator model which converts the kinetic energy in the wind speed into electrical energy. The MathWorks provides a complete model of a wind power generator in MATLAB[®]/Simulink[®] [34].

There is inherent uncertainty in predicted wind speeds that gets transferred to the power predictions as well. Since there are regulation prices for under-production and over-production which can significantly reduce revenue of the wind power utility, a bidding strategy is required to decide how much power to bid, given the uncertainties in power production, to achieve maximum profit in face of regulation-up and regulation-down prices [54].

1.2 Objectives

The objectives of this thesis are as follows:

1. Develop a method for generating wind speed forecasts based on the weather data provided by Environment Canada
2. Develop a method for generating wind power predictions and statistics for various prediction horizons
3. Develop an optimal bidding strategy which maximizes the expected profits in day-ahead electricity markets (market-based decision criteria)

4. Study the feasibility of adding a natural gas microturbine, in order to reduce the net variability of wind power generation

1.3 Contribution

This thesis provides a solution for important aspects of energy management and control of a wind energy facility, i.e., power forecasting, uncertainty estimation and a bidding strategy. Environment Canada (EC) provides wind speed forecasts every day for the next 48 hours. This work took the history of wind speed forecasts and actual data available from EC and then estimated the forecast error statistics. Wind-speed realizations were then modeled and simulated as the sum of a deterministic component and a stochastic component. The deterministic component is the wind speed forecast provided by Environment Canada, while the stochastic component, the error in the various forecasts, was modeled as a Markov process. A Markov process formulates the behavior of the physical process in terms of state. The state is the smallest collection of numbers, functions or some quantitative information that must be specified at time $t = t_0$ in order to predict the behavior of the system at $t \geq t_0$.

The reason for modeling the wind-speed forecast error, not wind speed, is because many researchers have shown that the assumption that wind speed follows Weibull distribution is not quite appropriate [28, 56]; also there is no well developed model for random variables possessing a Weibull distribution [10, 53]. Furthermore, Lange [31] and Landberg [30] have shown that wind prediction error follows a normal distribution, and there are many well developed models for random variables possessing normal distribution. Since it was found that our local forecast error data possess an approximately normal distribution, therefore modeling the prediction error this way is justified.

Solving the forecast error Markov process gave realizations of forecast error. The wind-speed realization was then obtained by adding a forecast error realization to the

forecasted wind speed. The wind speed realization was then input to a wind power generator model to get a wind-power forecast. The uncertainty in the power forecast was estimated using Monte Carlo Simulations (MCS). MCS converts uncertainty in the input variables of a model into the statistics of outputs.

The statistics of the wind-power forecast were then used in a new stochastic optimization function designed for this research, to provide the optimal quantities to be bid which maximize the profit in face of regulation prices. In calculating the bidding quantities we do not assume that the distribution of power forecast is known, which is a new approach.

1.4 Thesis Outline

Chapter 2 explains techniques to generate estimated wind speed error distributions, and model them using an appropriate Markov process; it also describes generating realizations of forecast error. Realizations of error were then added to the forecasted wind speeds to get wind-speed realizations. Wind-speed realizations were passed through a wind power generator model to obtain power production realizations which then be used to generate their statistics. Chapter 3 describes the working of a wind power generator and the modeling procedures in MATLAB[®]/Simulink[®]. Chapter 4 provides the details of realizing wind speed and power forecasts; it also provides insight into the uncertainty estimation in the power forecasts using MCS. Once the statistics of forecasted wind power are known then the possibility of adding a natural gas microturbine to reduce the uncertainty in wind power production is considered. Chapter 5 explains modeling the cost of energy per unit using a natural gas microturbine. Chapter 6 first gives an overview of an electricity market workings and then explains the bidding strategy. Finally, Chapter 7 is the summary and conclusion.

Chapter 2

Wind-speed forecast error modeling

2.1 Background

The intermittent nature of wind power generation pose operational difficulties to electricity markets. An electricity market, operated by an ISO, must always maintain a balance between supply and demand of electricity at each instant of time; if there is any variation in load, then there must be reserves at the ISO's disposal to make up any insufficiency. Generally, to maintain stable operation of the grid, the ISO accepts hourly bids starting at 09:00 and ending at 11:00 Atlantic Standard Time (AST) for the following day (00:00 to 23:59:59), from the market participants [42]. The submitted bids can be made valid up to the next five days. The system operator then runs an optimization algorithm to calculate a price at which maximum demand has been fulfilled at minimum cost.

Participants have to fulfill their obligation at the time of delivery. After the delivery day, deviations from the hourly accepted quantities are calculated for each market participant and regulation prices will be charged to the defaulters [26]. A detailed discussion on electricity market operation is given in Chapter 6.

The WE utility faces the challenge of producing accurate power generation forecasts before entering into the electricity market because the power forecast errors have significant impact on its revenue. Thus, a WE utility requires wind-speed forecasts and wind-speed forecast error statistics to assess and manage the risk involved in the bidding process in order to achieve maximum revenue.

The wind-speed forecast and wind-speed forecast error statistics can be used not only to assess the expected future power production for any delivery period but also the likely range of wind power production using the wind-speed forecast error statistics. This is achieved using Monte Carlo Simulation (MCS, described in more detail in chapter 4).

MCS essentially uses wind-speed prediction error statistics to generate likely “realizations” of the wind-speed forecast error for the future delivery period. These error realizations can be added to forecasted wind speeds (for the future delivery period) to obtain stochastic realizations of the wind speed. The realizations of wind speed can then be input to a wind power generator model to get realizations of power production.

If a large number of power production realizations are generated then a statistical analysis can provide risk-assessment decision parameters such as the average power production, the minimum and the maximum wind power over the future delivery period that can be anticipated with, for example, 95% probability. Also, the statistics based on the large number of power production realizations can be used to design a strategy which enables a WE utility to calculate the optimal power quantities to be bid over the delivery period for maximum revenue.

In this chapter we discuss wind-speed prediction error calculation and modeling, and the generation of realizations of wind speed for use in a wind power generator model to use in producing realizations of anticipated wind power production for use in MCS analysis.

2.2 Approach

This thesis took a different approach for modeling the wind speed which is based on the forecasts provided by the Environment Canada (EC). It took the history of wind-speed forecasts and of actual data available from Environment Canada and then generated the corresponding forecast errors. The advantage of using data from EC is that the local weather conditions are already taken care by the EC's models; Landberg [30] and Holttinen [26] have shown that forecasting is improved significantly by taking local meteorological conditions into account.

A wind-speed realization was modeled as the sum of a deterministic component and a stochastic component. The deterministic component is the wind-speed forecast provided by the Environment Canada, Fredericton, for a specific sample point in Fredericton, in GRIBed Binary (GRIB) format. Environment Canada's Fredericton station provides weather forecasts every day at 08:00 for the next 48 hours in 3 hour blocks including wind speeds in GRIB format at multiple resolutions for over 817 Canadian stations or sample points [18]. GRIB is a mathematically concise data format commonly used in meteorology to store historical and forecasted weather data. The stochastic component, the error in the various forecasts, was modeled as a Markov process; it was found that hourly distributions of forecast errors are normal (gaussian), and Markov process modeling is well known technique to generate a normal random process by passing gaussian white noise through a simple filter [23].

The prediction errors were calculated by comparing the forecasted wind speed in the GRIB files with the actual wind speeds for the same prediction time; 291 GRIB files and the actual wind speed for the year 2003 provided by Environment Canada Fredericton were used. The GRIB files are missing for July and August, 2 days in May, 5 days in August, 3 days in September and 2 days in December. The actual data is available for all the forecasted time points. A routine was developed in MATLAB[®]

to read data from GRIB files into the MATLAB[®] workspace directly [9]. The actual data is in hourly blocks while forecast data is in three-hour blocks; therefore the missing two hour data points of each block in the GRIB file were filled using the persistence technique. The persistence technique assumes that speed will be the same at $t + k$ hours as at t hours, $k = 1, 2$ [26].

Figure 2.1 shows the time line for bidding quantity clearance at the New Brunswick

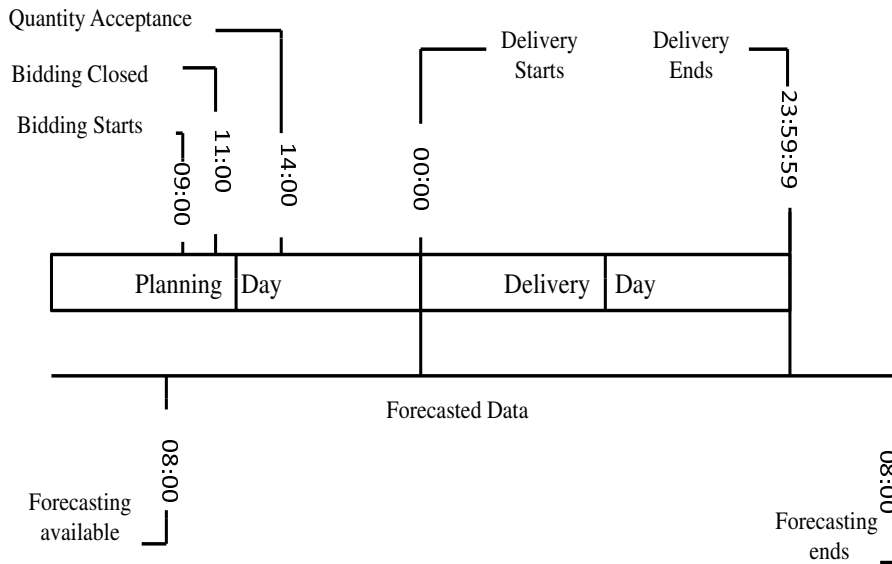


Figure 2.1: Time line for bidding, acceptance, delivery and forecasting

electricity market operated by the New Brunswick System Operator (NBSO), Fredericton, and also the time line for the availability of forecast data from EC. The wind-speed forecast provided by EC is available every day at 08:00 AST for the next 48 hours in 3 hour blocks. Since NBSO accepts bids from 09:00 to 11:00 AST for the following day (Delivery Day, 00:00 to 23:59:59), thus, in order to submit the bids, the wind power forecasts for the time 00:00 to 23:59:59 must be known before 11:00, the day before (Planning Day). The wind power forecasts for the Delivery Day (DD) require the wind- speed forecasts (wind-speed realizations), which were obtained by adding stochastic realizations of wind-speed error to the forecasted wind

speeds provided by EC.

It has been shown by Holttinen [26] that error in the wind power prediction increases as forecast grows older; therefore power prediction error can be reduced significantly if time between bid close and delivery is short. From figure 2.1 it is clear that the wind-speed forecast provided by Environment Canada is 16 to 40 hours old over the DD.

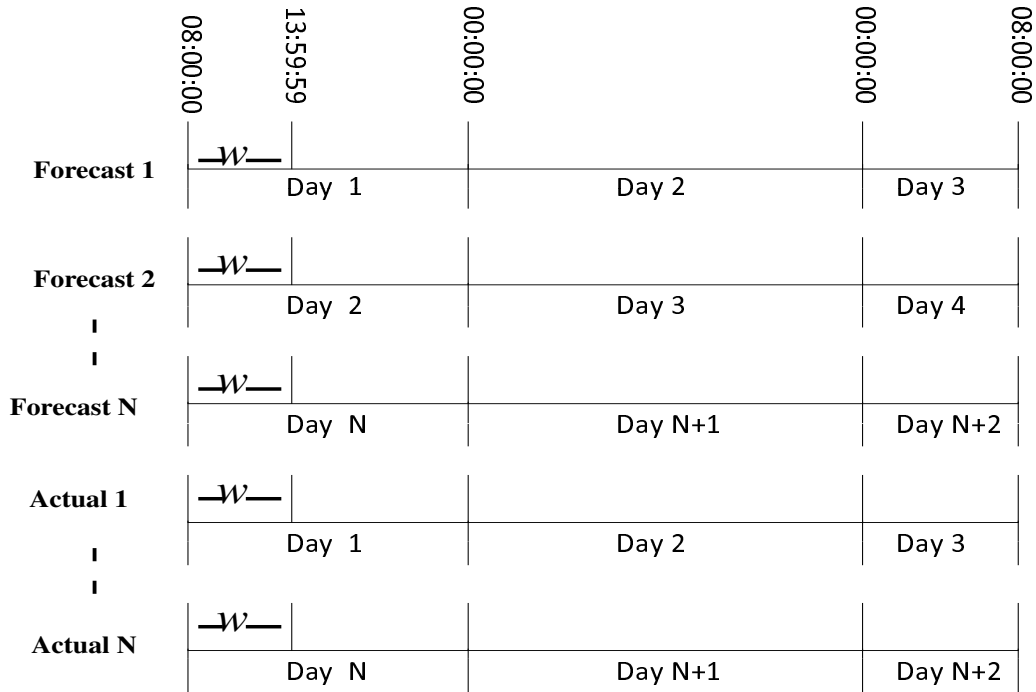


Figure 2.2: Scheme for data collection

One can then intuitively think that the mean and the variance of wind-speed forecast error should increase as prediction time increases. To validate this the wind-speed forecast errors were calculated by comparing forecasted wind speeds (v_f) with actual wind speeds (v_a) for a prediction horizon of 48 hours, according to the scheme shown in figure 2.2, where w is the number of hours covered in a single prediction error distribution, e.g., six hours as shown. The Forecasts 1,...,N were compared with the actual data 1,...,N, where $N=291$.

For example, given $w=6$ hours and a prediction horizon of 48 hours then there are 8 wind-speed forecast error distributions of 6 hours; the first distribution covers the wind-speed forecast error data from 08:00 to 13:59:59 AST, the second distribution covers 14:00 to 19:59:59 AST, and so on. It should be noted that there is a time overlap between the forecasted and the actual data (figure 2.2) but data corresponding to them belongs to different categories. The time 08:00 at day 2 in Forecast 1 is 24 hours old while the 08:00 at day 2 in Forecast 2 is 00:00 hours old.

Let $v_f(i, j)$ represent the value of the wind speed in Forecast i at the j^{th} hour while $v_a(i, j)$ represent the corresponding actual wind speed. Also let $\hat{\mu}^{(r)}$ represent the sample mean and $\hat{S}^{(r)}$ represent the sample variance of the wind-speed forecast error of the r^{th} distribution, where $r = 1, 2, \dots, (\frac{P_h}{w})$; P_h is the prediction horizon. For example, given $w=6$ hours and a prediction horizon of 48, then there are 8 wind-speed forecast error distributions of 6 hours (discussed above), and thus there are 8 sample means and sample variances each denoted as $\hat{\mu}^{(r)}$ and $\hat{S}^{(r)}$, where $r = 1, 2, \dots, 8$. The $\hat{\mu}^{(r)}$ and the $\hat{S}^{(r)}$ are calculated using equation (2.1) and (2.2) respectively:

$$\hat{\mu}^{(r)} = \frac{1}{Nw} \sum_{j=8+(r-1)w}^{8+(rw-1)} \sum_{i=1}^N (v_f(i, j) - v_a(i, j)) \quad (2.1)$$

$$\hat{S}^{(r)} = \frac{1}{Nw - 1} \sum_{j=8+(r-1)w}^{8+(rw-1)} \sum_{i=1}^N (v_f(i, j) - v_a(i, j) - \mu^{(r)})^2 \quad (2.2)$$

The mean and variance for prediction time block $w = 1$ (using the persistence technique to fill in the forecasted data) is shown in figure 2.3, and it can be easily noticed that the mean and variance of the prediction error for this data do not increase significantly as prediction time increases; in fact they follow 24 hour cycles. Therefore, although the data used in this thesis will be 16 hours old at the time of its usage it will have little affect on the prediction results as compared to when it

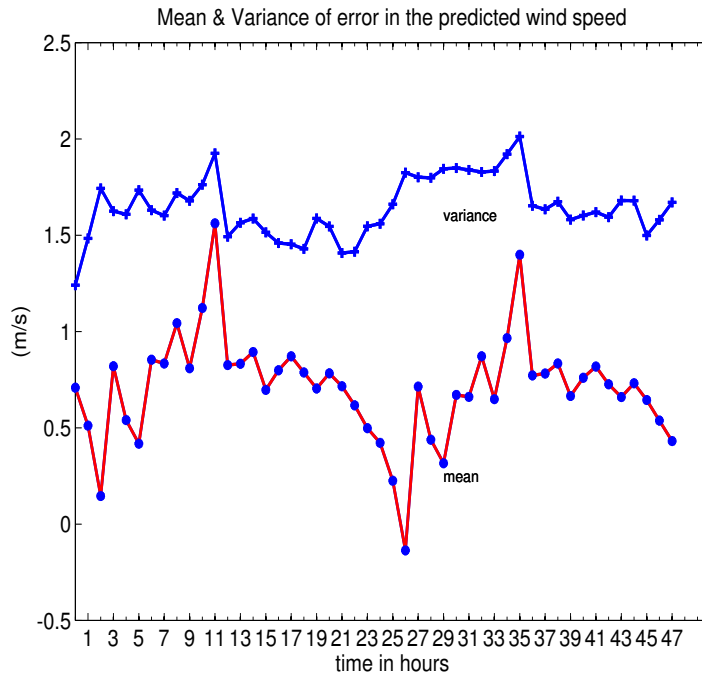


Figure 2.3: Mean and variance of error in forecasted wind speed

was 00:00 hours old. The main reason for this counterintuitive result could be the limitation of the model discussed in [26] for forecasting wind speeds. The advantage of using the standard schedule is that solutions developed in this thesis can be directly incorporated into the existing rules of grid operation.

The next step was to analyze the probability distribution of wind-speed forecast error for various prediction time blocks so that an appropriate method can be chosen to model the probability distributions. The probability distributions for 24h, 12h, 6h, 3h, and 1h prediction time blocks in a 24 hour prediction horizon (00:00 to 23:59:59) are shown in Appendix A. The distributions were then tested for normality using a statistical Chi-Square (χ^2) test because it is claimed that the wind-speed forecast error follows a normal distribution for 12h and 24h prediction horizons [31, 30] .

2.2.1 Chi-Square Test

The χ^2 test tests a null hypothesis H_0 that a sample data set follows a specified distribution, i.e., that there is no significance difference between their distribution. It divides the samples into k bins and then calculates a test statistic χ^2 given as,

$$\chi^2 = \sum_{i=1}^k \frac{(O_i - E_i)^2}{E_i} \quad (2.3)$$

where O_i = observed frequency and E_i = expected frequency. The expected frequency is given as,

$$E_i = n \int_{\underline{x}_i}^{\bar{x}_i} f(x) dx = n(F(\bar{x}_i) - F(\underline{x}_i)) \quad (2.4)$$

where $f(x)$ is the specified probability density function, $F(x)$ is the corresponding cumulative distribution, and $\bar{x}_i, \underline{x}_i$ bound the i^{th} bin. The test statistic follows, approximately, a χ^2 distribution with a degree of freedom $k - 3$, and the hypothesis is defined as follows:

$$\text{if } \chi^2 < \chi_\alpha^2, H_0 = 0, \text{ the Hypothesis will be accepted.} \quad (2.5)$$

otherwise,

$$H_0 = 1, \text{ the Hypothesis will be rejected.} \quad (2.6)$$

where χ_α^2 corresponds to the known distribution with $k - 3$ degree of freedom and an α level of significance.

The chi-square test results, using MATLAB[®] command ‘chi2gof’ for various time blocks are summarized in table 2.1 and given in detail in Appendix A. The table basically tells the probability (in %) that a given distribution is normal (the probabilities less than 10^{-4} were rounded off to zero). The test results show that wind-speed forecast error will not be normally distributed for 12h and 24h prediction

0																							24 h block		
0											0											12 h block			
0					0					0					0					6 h block					
0			0			0			0			0			0			0			3 h block				
6	95	19	7	0	10	6	51	35	5	0	0	55	0	28	46	50	41	33	0	60	38	1	1	1 h block	
																									time in
0	1	2	3	4	5	6	7	8	9	10	11	12	13	14	15	16	17	18	19	20	21	22	23	hours	
All probabilities are in percentage (%)																									

Table 2.1: Summary of test results

time blocks; so the claim in [31, 30] is not valid for the given data; the reason could be that wind-speed error distributions vary from region to region [30]. But 11 one hourly prediction distributions are normally distributed with probability ranging from 33 to 95%, 2 ranging from 10 to 33% and 11 below 10%. At this point, in a case where probabilities are low, it is usually desirable to repeat the test with a larger sample size, irrespective of whether the initial statistical chi-square test gives low probability that the distribution is normal. But given the limitation on data (291 points for each hour), a different approach to investigate the normality of wind-speed forecast error distribution was considered.

2.2.2 Gaussian Distribution Fitting

To investigate the normality of wind-speed forecast error distributions further, each one-hourly distribution was fitted by the normal distribution using the MATLAB[®] command ‘normfit’. After that, using the statistics obtained from the ‘normfit’, 1000 synthetic normal forecasting error samples were generated for each hourly distribution. Then the cumulative distribution was plotted for the generated sample

along with the actual distribution for the same bin width for each hour as given in Appendix B. The cumulative distribution function is given as:

$$F(x) = P(X \leq x) \tag{2.7}$$

where $F(x)$ is the corresponding cumulative probability and x_i is random deviates of the random variable X_i .

The plots in Appendix B show that the normal cumulative sample distributions closely follow the actual cumulative distributions for each one-hour data window. There is not a significant variation between the two distributions (as an example, two cumulative comparison plots, one for time 01:00:00 to 1:59:59 and other one for 09:00:00 9:59:59 are shown in figure 2.4 and figure 2.5). Therefore, it was

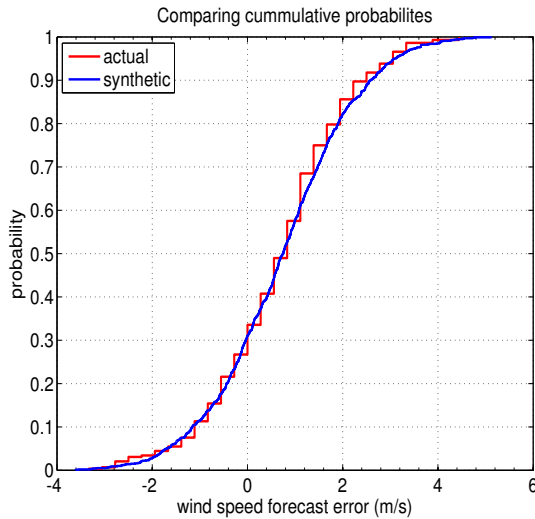


Figure 2.4: Comparing cumulative probabilities for time block 01:00:00 to 1:59:59

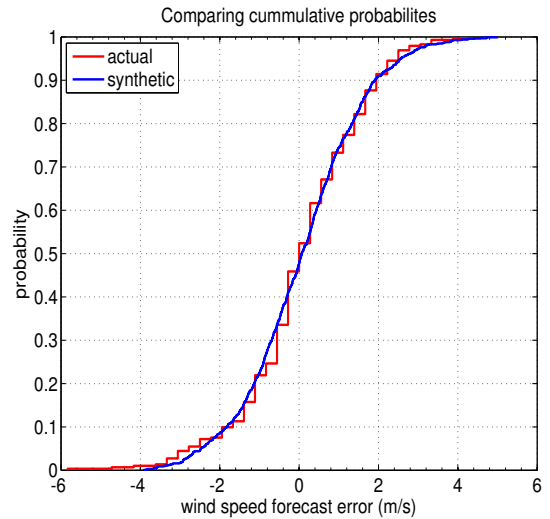


Figure 2.5: Comparing cumulative probabilities for time block 09:00:00 to 9:59:59

assumed that all the hourly distributions are normally distributed; given the nature of wind-speed forecasting, the very slight variation between the actual and cumulative distribution at a few points will not have any significant impact on the quality of forecasting.

2.3 Markov Processes

Once it is established that hourly wind-speed forecast error distributions can be assumed to be approximately normal, then the random process can be generated as a Gauss-Markov Process (GMP). A continuous process is a Markov Process (MP) if the probability distribution for the current state (range of values) depends only the most recent past state, and if the restriction is added that distribution of the current state is normal then it is called GMP [23]. For example, a continuous process $e(t)$ is a First Order Markov (FOM) process if for every k and

$$t_1 < t_2 < \dots < t_k \quad (2.8)$$

it is true that,

$$F[e(t_k)|e(t_{k-1}), \dots, e(t_1)] = F[e(t_k)|e(t_{k-1})] \quad (2.9)$$

where in this study, e denotes wind-speed forecast error.

2.3.1 Autocorrelation Function

Given a string of wind-speed forecast error data, e_i , $i = 1, 2, \dots, N$, taken at a constant time intervals. The lag τ Autocorrelation Function (ACF) is defined as,

$$r_{ee}(\tau) = \frac{\sum_{i=1}^{N-\tau} (e_i - \mu)(e_{i+\tau} - \mu)}{\sum_{i=1}^N (e_i - \mu)^2} \quad (2.10)$$

where μ is the true mean of the data; if $\hat{\mu}$ or the sample mean is used then this estimate is biased. In this study the MATLAB[®] function ‘autocorr’ was used which has a small bias for large N . Typically, a one dimensional ACF for a random variable exhibits exponential behavior [23].

2.3.2 Order of a Markov Process

A random process $e(t)$ with an empirical lag τ ACF calculated using equation (2.10) may be reasonably well approximated by the following equation [23]:

$$r_{ee}(\tau) = \exp(-\beta|\tau|) \quad (2.11)$$

where β is the correlation time constant of the data. This ACF can be associated with a first-order differential equation [23],

$$\frac{de}{dt} + \beta e = u(t) \quad (2.12)$$

Alternatively, a random process $e(t)$ with an empirical lag τ ACF calculated using equation (2.10) may be fit by the following equation [23]:

$$r_{ee}(\tau) = \left[\frac{2\beta_1\beta_2(\beta_1 + \beta_2)}{(\beta_2 - \beta_1)^2} \right] \left[\frac{e^{-\beta_1|\tau|}}{2\beta_1} + \frac{e^{-\beta_2|\tau|}}{2\beta_2} - \left(\frac{e^{-\beta_1|\tau|} + e^{-\beta_2|\tau|}}{\beta_1 + \beta_2} \right) \right] \quad (2.13)$$

This ACF can be associated with second-order differential equation [23],

$$\frac{d^2e}{dt^2} + (\beta_2 + \beta_1)\frac{de}{dt} + \beta_1\beta_2e = u(t) \quad (2.14)$$

Equation (2.12) is termed as a First-Order Markov (FOM) process, while equation (2.14) is called a Second-Order Markov (SOM) process; β_1 and β_2 are the correlation time constants for the SOM. For a GMP the input $u(t)$ is sum of a gaussian white noise process and possibly a deterministic term.

The ACF calculated according to the equation (2.10) for the wind-speed forecast error data is shown in the figure 2.6. The formula is evaluated only up to 20 lags (τ) or 20 hours; beyond that it is almost zero. From figure 2.6, wind-speed forecast error autocorrelation value are seen to fall off exponentially. The calculated ACF was then fitted with the theoretical autocorrelation functions, equation (2.11) for a

FOM model, and equation (2.13) for a SOM model using a nonlinear least-square fit technique (MATLAB[®] function ‘fit’) as shown in figure 2.6. From that figure it is clear that the FOM model is almost identical to the SOM model fit. The correlation time constant found for the FOM was $\beta=0.2982$ hour (95% confidence bounds [0.2645, 0.3313]), and the correlation time constants found for the SOM were $\beta_1=30.96$ hour (95% confidence bounds [-459.7, 521.6]) and $\beta_2=0.2933$ hour (95% confidence bounds [0.2389, 0.3477]) respectively. The confidence bounds of β_1 of the SOM are very high, i.e., the value is essentially meaningless as demonstrated in figure 2.6, and thus it can be ignored. Therefore the FOM fit was selected over the SOM fit.

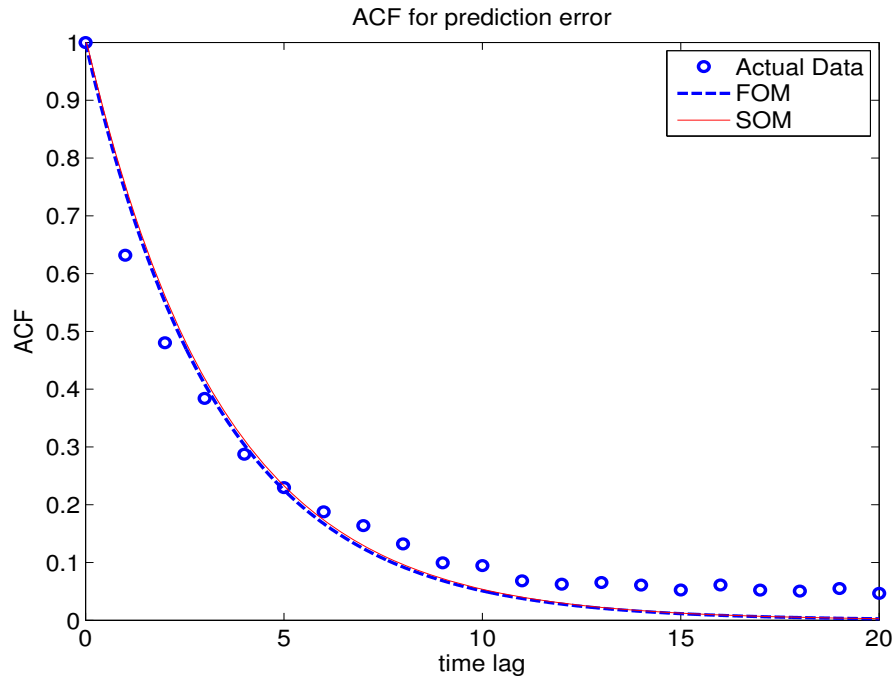


Figure 2.6: Fitting an ACF for FOM and SOM processes

Once the correlation time constant was found the spectral density Q of the white noise that produces σ_e was calculated [23] as:

$$Q = 2\beta\sigma_e^2 \quad (2.15)$$

After that, solving the differential equation (2.12) will give wind-speed forecast error dynamics. It should be noted that the statistical properties (mean, variance) of the error data changes on an hourly basis, and therefore this characteristic was incorporated in solving the prediction error dynamics by changing the statistics of the random input $u(t)$ on an hourly basis.

2.4 Solving a First Order Markov Process

The FOM process was solved using the Euler technique. The FOM model equation (2.12) can be rewritten as:

$$\frac{de}{dt} = u(t) - \beta e \quad (2.16)$$

The first-order approximation of the Taylor series solution given as,

$$e(t_0 + h) \simeq e(t_0) + h \left. \frac{de}{dt} \right|_{t=t_0} \quad (2.17)$$

implies that starting at point $t = t_0$, the value after small time step h , $e(t_0 + h)$ can then be approximated by the value $e(t_0)$ plus the time step multiplied by the slope of the function, i.e., the derivative of function $e(t)$ at $t = t_0$. With this background the Euler technique method for solving an FOM is as follows:

1. Choose an initial condition $e(t_0)$, a time step h , and a terminal time t_f ; set $t = t_0$.
2. Select a random value of input $u(t)$, add this to the deterministic component of $u(t)$.
3. Substitute $e(t)$ into equation (2.16) to determine de/dt .
4. Substitute that value into equation (2.17) for an approximate value of $e(t + h)$.
5. Let $t = t + h$, $e(t) = e(t + h)$.

6. Repeat steps 2 to 5 until t equals the termination time t_f .

The FOM process describes the dynamics of the prediction error over time (24 hour); solving the FOM using Euler's technique for random initial conditions and random inputs, chosen according to the statistics of the prediction error data, produced realizations of prediction error, and adding those to the forecasted wind speeds gave wind-speed realizations (detailed discussion in chapter 4). The wind-speed realizations were then passed through a wind power generator model to assess the power production. The modeling of the wind power generator was done in MATLAB[®]/Simulink[®], as described in chapter 3.

Chapter 3

Modeling a wind power generator

The wind power generator is an arrangement of mechanical and electrical components which converts kinetic energy of the air moving over the earth's surface into electrical energy. The main components of the wind power generator are the turbine rotor, shaft, gearbox, and an electric generator as shown in figure 3.1 [48]:

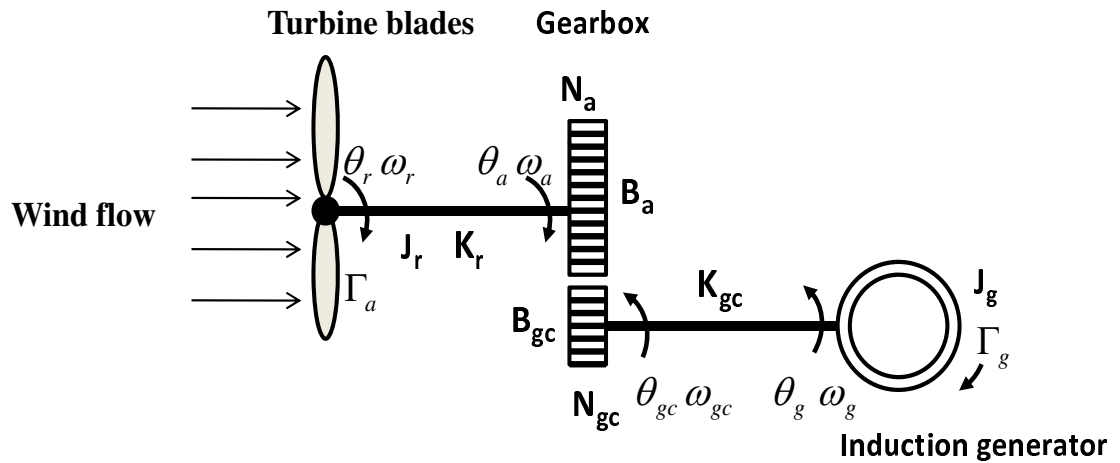


Figure 3.1: Wind turbine system

where Γ_a , θ_r , ω_r , J_r , K_r , N_a and B_a are aerodynamic torque, angular position, angular velocity, moment of inertia, stiffness, gear teeth and friction on the rotor sides, θ_{gc} , ω_{gc} , K_{gc} , N_{gc} and B_{gc} are angular position, angular velocity, stiffness, gear

teeth and friction of the mechanical coupling on the generator side, and Γ_g , θ_g , ω_g , and J_g are torque, angular position, angular velocity and moment of inertia of the electrical generator.

The kinetic energy of the wind stream flowing with speed v and density ρ when it hits the rotor blades attached to the turbine rotor or hub produces aerodynamic torque on it which causes the blade assembly to spin. The aerodynamic torque developed on the wind turbine blades is given as [19, 48],

$$\Gamma_a = \frac{1}{2\omega_r} C_p \rho v^3 \pi R^2 \quad (Nm) \quad (3.1)$$

where R is rotor blade radius (m), C_p is the rotor's efficiency to capture kinetic energy present in the air, ρ is air density, v is the wind speed (m/s), and ω_r is the rotor angular speed (rad/s). The ω_r is given as,

$$\omega_r = \frac{\lambda v}{R} \quad (3.2)$$

where λ is the tip speed ratio.

The rotation of the blade assembly turns a shaft connected to the turbine rotor. The rotor shaft then transfers its rotational energy to the rotor of a induction generator via a gear train. The gear train is placed between the rotor shaft and the induction generator; its job is to transfer the slow rotational speed of the rotor shaft to the faster rotational speed of the generator. The induction generator then converts the rotational energy of the rotor into electric energy.

The induction machine in the wind power generator arrangement is connected as motor, and its stator is energized by a three phase electrical source [33]. The three phase electrical source produces a magnetic flux rotating at a uniform speed (synchronous speed). The rotating flux cuts the rotor conductors and due to the relative velocity between the stator field and rotor an electrical torque is induced in

the rotor whose magnitude is proportional to the relative velocity between the rotor and stator field (Faraday's law) [33]. The torque, according to lenz's law, would oppose its cause, the relative velocity between the rotor and stator field. Hence, to reduce the relative velocity, the rotor starts rotating in the same direction of the stator flux.

The difference between the synchronous speed (ω_s) and the rotor speed (ω_r) is termed as the slip of the motor:

$$s = \frac{\omega_s - \omega_r}{\omega_s} \quad (3.3)$$

where, the synchronous speed of the motor is given as,

$$\omega_s = \frac{120 * f}{P} \quad (3.4)$$

where f is the frequency of the excitation and P is the number of poles. Generally, the slip is in the range of 1-3%.

Figure 3.2 shows the torque versus slip and torque versus rotor speed percent of synchronous speed curve for an induction machine [33]. It can be easily noticed that an induction machine works as a motor when the slip is positive or rotor speed is below the synchronous speed, and for negative slip (rotor speed higher than the synchronous speed) the induction machine works as a generator.

In the case of a wind turbine connected to the grid, initially the induction machine acts as a motor, and as the wind turbine causes the rotor to catch up to synchronous speed and exceed it, the operation of the induction motor changes into that of a generator (figure 3.2).

If the moment of inertia of the gear-box is small compared to those of the wind turbine rotor and generator rotor then the state-space form of figure 3.1 can be

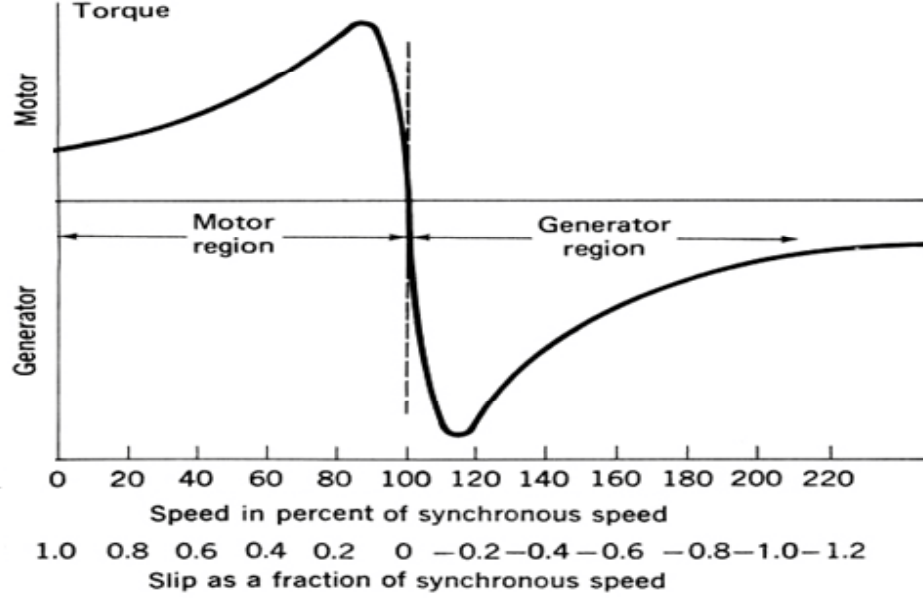


Figure 3.2: Characteristics of an induction machine [33]

written as (assuming ω_r , ω_{gc} , ω_g , $\phi_a = \theta_r - \theta_a$ and $\phi_b = \theta_g - \theta_{gc}$ are state variables):

$$\frac{d\omega_r}{dt} = \frac{1}{J_r}(\Gamma_a - K_r\phi_a) \quad (3.5)$$

$$\frac{d\omega_g}{dt} = \frac{1}{J_g}(-\Gamma_g - K_{gc}\phi_b) \quad (3.6)$$

$$\omega_a = \frac{1}{B_{gc}/\eta^2 + B_a}(K_r\phi_a + K_{gc}\phi_b/\eta) \quad (3.7)$$

$$\frac{d\phi_a}{dt} = \omega_r - \omega_a \quad (3.8)$$

$$\frac{d\phi_b}{dt} = \omega_g - \omega_a/\eta \quad (3.9)$$

where η is the gear ratio, $N_{gc}/N_r = \omega_a/\omega_{gc}$.

The wind turbine rotor can be fixed-speed or variable-speed. Fixed-speed turbines become stalled at high speed, while a variable-speed rotor turbine can operate with more flexibility over a range of speeds [48]. The wind power generators can operate as stand-alone systems or grid-connected systems. In stand-alone systems, also called off-grid systems, wind power generators are not connected to any grid or electrical

distribution and solely feed the local electric system with a possible combination of some other renewable energy components, such as solar electric. In grid-connected systems, the wind power generators feed local loads which are also connected to a electrical distribution system or grid. Thus, in case of no wind power generation, the electrical load can draw power from the electrical grid.

Induction generators are most commonly used in wind power systems because these machines cost less, require minimal maintenance, and offer varying operating conditions like over speed capabilities which make them suitable for wind turbine systems [33].

The induction generator's stator winding must be excited in order to produce electricity. Excitation provides a magnetizing current to generate the magnetic field required for the induction machine operation. The excitation is provided by reactive power which is supplied externally in a stand-alone system or from the grid in the case of grid-connected systems. In grid-connected systems it is very important to ensure that wind power generators draw minimum reactive power from the grid; otherwise it will lead to a low power factor resulting in high distribution losses.

The power factor is defined as the cosine of the angle ϕ between useful or real power and apparent power, as shown in figure 3.3. Mathematically the power factor is given

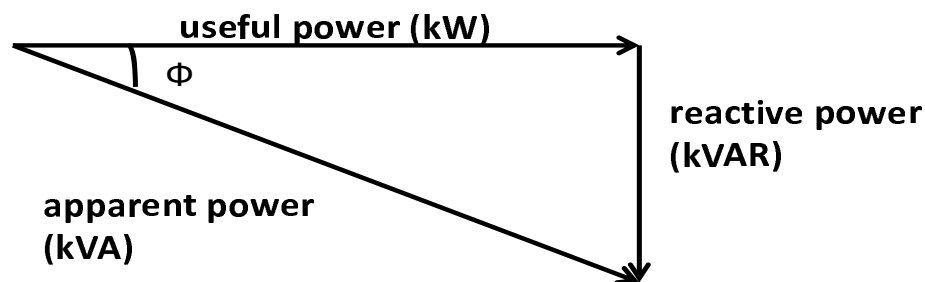


Figure 3.3: Power factor

by,

$$pf = \cos\phi = \frac{kW}{kVA} \quad (3.10)$$

From figure 3.3, if the wind turbine generator draws excess reactive power for excitation from the electrical grid then the angle ϕ will increase and hence the power factor will decrease. Decrease in power factor means that more current is required to supply a load ($P = VI\cos\phi$, V = voltage is constant) than the same load with a power factor close to unity. Excess current flowing in the distribution lines results in higher copper losses (I^2R , R is the transmission line resistance). Therefore, wind power generators require reactive power compensators to maintain a power factor close to unity [57].

3.1 Performance of a Grid-Connected Wind Power Generator

A rated 9 MW fixed-speed, grid-connected wind farm consisting of three units located in one area was used in this thesis, as shown in figure C.1; it is a customized form of the wind farm model 'power_wind_ig' given in the MATLAB[®]/Simulink[®] [34]. The model was 'customized' to incorporate the interface shown in Figure 3.4 - the routine for generating wind speed realizations was developed in MATLAB[®] script files (.m), while the wind power generator is developed in a Simulink[®] model file (.mdl). Therefore, the interface as shown in figure 3.4 was developed which takes a wind speed realization and simulation time from the script file and transfers it to the wind power generator's input port, then runs the wind power generator model to calculate power production and transfers that power back to the MATLAB[®] workspace.

The wind power generation model generates electricity for wind speed ≥ 5.6 m/s and becomes stalled for wind speed greater ≥ 10.5 m/s (the range of operation may

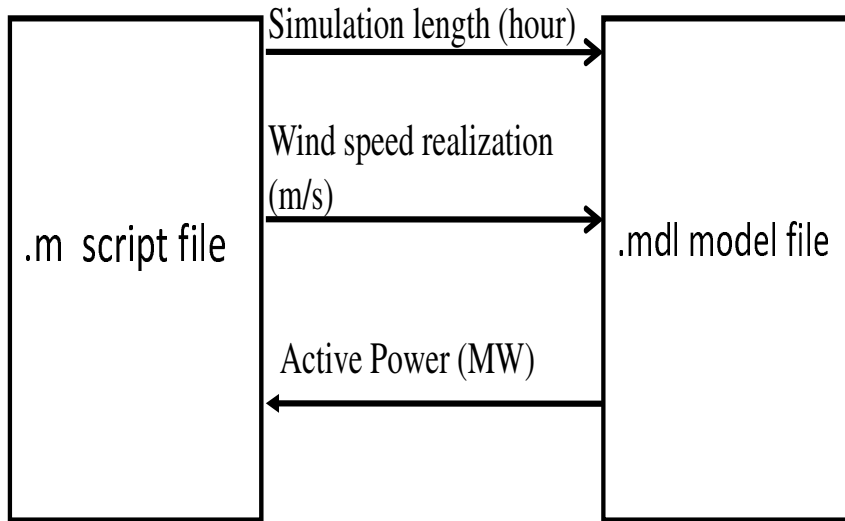


Figure 3.4: Input/output sharing between script file and model file

seem narrow, but it was found through testing that MATLAB[®]'s wind farm model stops working the moment wind speed goes below or above the specified limits). The power forecast is obtained by passing wind speed realizations to the wind power generator's input port for the wind speed (v_r shown in figure C.2). The performance of the grid-connected wind power generator was tested by passing the wind speed realization as shown in figure 3.5 to it. The active power generated by the wind power generator was measured at Bus B25 in figure C.1.

Figure 3.6 shows the active power generated by the wind power generator for this sample of wind speed realization. It can be easily be seen that when the wind speed is below or close to the cut-off wind speed the power production is zero.

The power predictions obtained by passing realizations of wind speed to the wind power generator are not perfect because of the variability present in the wind speed error. Therefore, an uncertainty analysis of the power predictions is required to assess the risk involved in it. In this thesis, the Monte Carlo Simulation technique was used for the uncertainty estimation in the power forecasts [52, 44].

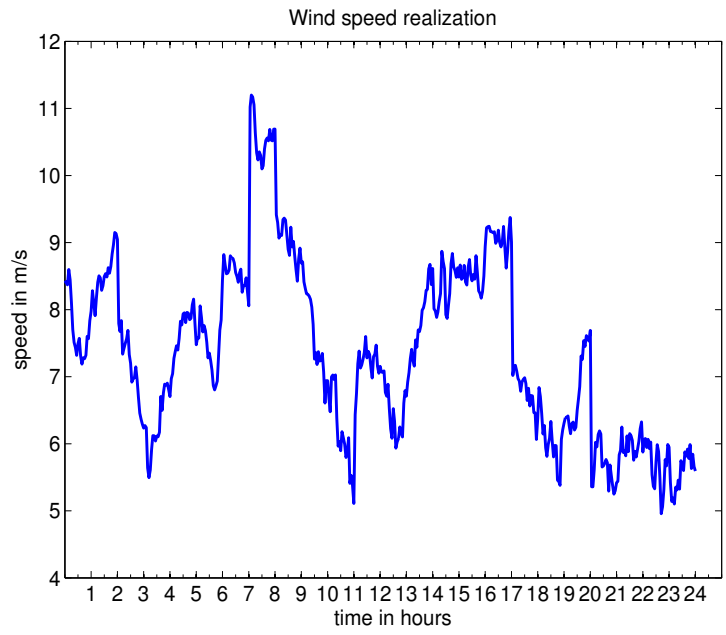


Figure 3.5: Wind speed realization

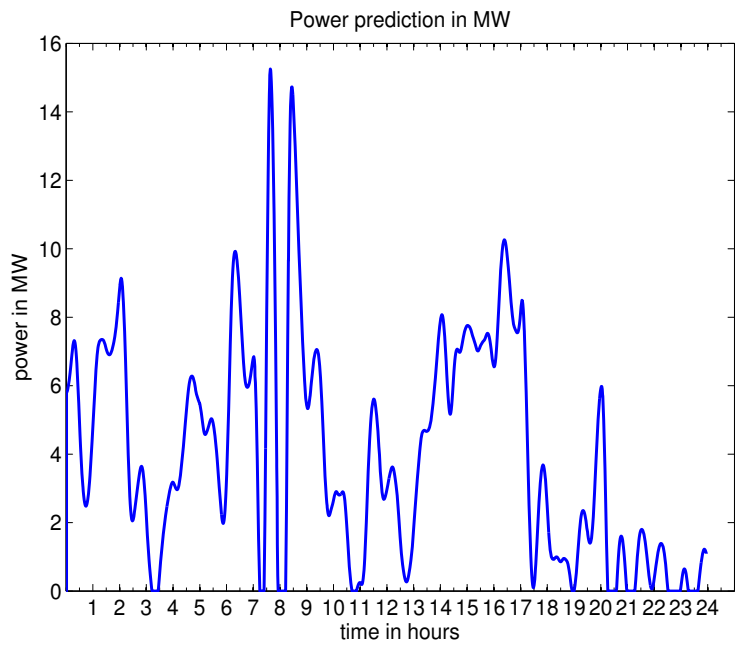


Figure 3.6: Power forecast

Chapter 4

Uncertainty estimation in power forecasts

The power predictions were obtained by passing wind speed realizations to the wind power generator. Since there are uncertainties in the realized wind speeds, the uncertainties get transferred to the power predictions as well. Therefore, Monte Carlo Simulations (MCS) were performed to quantify the risk in the power predictions. The quantification of uncertainty will permit assessing the risk of relying on the power prediction forecasts.

4.1 Monte Carlo Simulations

MCS converts uncertainty in the input variables of a system into an approximate probability distribution of the outputs. It provides an approach to the statistical analysis of the performance of a system with random inputs by direct simulation. It entails determining system response to a finite number of initial conditions and random input functions generated according to their specified statistics. Thus information required for MCS are the system model, initial condition statistics and random input statistics [52]. Generally, the initial conditions are specified by the mean and the variance of the response. The statistical properties of the random

input determines the response after the initial condition.

As mentioned in chapter 2, the state space formulation of the FOM model is given as,

$$\dot{e} = u(t) - \beta e \quad (4.1)$$

where e is the wind prediction error and $u(t)$ is the sum of a white noise process and a deterministic term. The input $u(t)$ is determined by requiring that the statistics (the mean and the standard deviation) of e match empirical values discussed in section 2.2. This process is simplified by separating e into its random component and deterministic part:

$$e = e_r + \hat{\mu}_r(t) \quad (4.2)$$

where, for $(r - 1) \leq t < r$, $r = 1, 2, \dots, 24$, the deterministic component $\hat{\mu}$ is given by equation (2.1). The random component of e then satisfies,

$$\dot{e}_r = w_n(t) - \beta e_r \quad (4.3)$$

where w_n is a gaussian white noise process. The initial condition statistics are given as,

$$E[e_r(0)] = 0 \quad (4.4)$$

$$E[(e_r(0))e_r^T(0)] = S_0 \quad (4.5)$$

where S_0 is the variance of the prediction error distribution at time $t=00:00$. The random component of e_r often characterized by its standard deviation:

$$\sigma_0 = \sqrt{S_0} \quad (4.6)$$

As mentioned in chapter 2, the statistics of the random input change on an hourly basis; therefore the statistics of the $w_n(t)$ are given as,

$$E[w_n(t)] = 0 \quad (4.7)$$

$$E[w_n(t)w_n^T(\tau)] = Q_r(t)\delta(t - \tau) \quad (4.8)$$

where, for $(r - 1) \leq t < r$, $r = 1, 2, \dots, 24$, the spectral density of the white noise $Q_r(t)$ is given by the equation (4.9) [52, 23].

$$Q_r(t) = 2\beta\hat{S}(r) \quad (4.9)$$

Equation (4.8) indicates that the input random component has zero autocorrelation for $t \neq \tau$, i.e., the quantity $w_n(t)$ is white noise as mentioned above [52].

4.1.1 Prediction Error Realizations

Given the system model, initial condition statistics and random input statistic, the MCS technique generates an ensemble or large number n of the system responses to wind speed realizations. The ensemble of system responses is generated by performing the following procedure n times: choose a random initial condition, i.e., a value $e_r(0)$, according to the statistics provided by equations (4.4) and (4.5). Then select a random input vector $w_n(mh)$; the value of white noise with spectral density $Q_r(t)$ was simulated by using the MATLAB[®] random number generator ‘randn’ to obtain a sequence of random values $w_n(mh)$, $m = 1, 2, \dots, t_f/h$ satisfying [52]

$$E[w_n(mh)] = 0 \quad (4.10)$$

and

$$E[(w_n(mh))w_n^T(mh)] = \frac{Q(mh)}{h} \quad (4.11)$$

where h is the simulation time-step, then the random input $w_n(t)$ is defined as,

$$w_n(t) = w_n(mh), \quad mh \leq t < (m + 1)h \quad (4.12)$$

where h is small time increment [52]. The input vector is then passed to the Euler integration technique, as mentioned in section 2.4, to propagate the solution from $t = 0$ to $t = h$, and so on until the final time $t_f = 23 : 59 : 59$ hours is reached [52] (only the deterministic term in step 2 is zero).

Performing n independent trials yields an ensemble of n prediction trajectories or realizations of e_r , each denoted $e_r^{(i)}(t; x^i(0), w^i(t))$ to show the dependence of trajectory on the random initial condition and random input value [52]:

$$\begin{pmatrix} e_r^{(1)}(t; x^1(0), w^1(t)) \\ e_r^{(2)}(t; x^2(0), w^2(t)) \\ \dots \\ e_r^{(n)}(t; x^n(0), w^n(t)) \end{pmatrix}$$

Adding the above realizations of e_r to the deterministic components of the prediction error (equation 4.2) gives n realizations of the prediction error, each denoted $e^{(i)}(t; e_r^i(t), \hat{\mu}(t))$ to show the dependence of trajectory on e_r and the deterministic component $\hat{\mu}$.

$$\begin{pmatrix} e^{(1)}(t; e_r^1(t), \hat{\mu}(t)) \\ e^{(2)}(t; e_r^2(t), \hat{\mu}(t)) \\ \dots \\ e^{(n)}(t; e_r^n(t), \hat{\mu}(t)) \end{pmatrix}$$

4.1.2 Power Predictions

Adding the above error realizations to the forecasted wind speeds v_f , gave the wind speed realizations $v_r(t)$, and power predictions were then obtained by passing

wind speed realizations to the wind power generator. The block diagram shown in figure 4.1, shows the process of getting wind power predictions. The limiter was placed after the addition of prediction error realization and forecasted wind speed to avoid negative values of the wind speed realization $v_r(t)$, i.e., for each trial $v_r^i(t)$

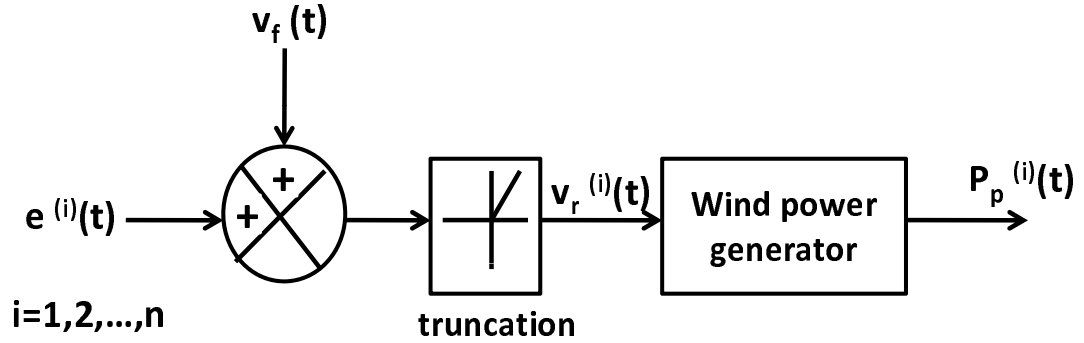


Figure 4.1: Wind power realization generation

is given as,

$$v_r^i(t) = \max [(v_f + e^i(t)), 0] \quad (4.13)$$

Each realized power prediction is determined by inputting each realized wind speed $v_r^i(t)$ to the wind power generation model.

Generating n realizations of forecast error gives n statistically meaningful realizations of wind speed, which yields an ensemble of n realized power predictions:

$$\begin{pmatrix} P_p^{(1)}(t; v_f(t), e^1(t)) \\ P_p^{(2)}(t; v_f(t), e^2(t)) \\ \dots \\ P_p^{(n)}(t; v_f(t), e^n(t)) \end{pmatrix}$$

The sample mean $\hat{m}_p(t)$ and variance $\hat{S}_p(t)$ of the power predictions was calculated by the following equations [52],

$$\hat{m}_p(t) = \frac{1}{n} \sum_{i=1}^n (P_p^i(t)) \quad (4.14)$$

$$\hat{S}_p(t) = \frac{1}{n-1} \sum_{i=1}^n (P_p^i(t) - \hat{m}_p(t))(P_p^i(t) - \hat{m}_p(t))^T \quad (4.15)$$

4.1.3 Confidence Intervals

It was desirable to determine the confidence intervals to ensure that true mean is guaranteed to lie within these intervals with a specified probability or confidence. If n is sufficiently large then the confidence interval $[\underline{m}, \overline{m}]$ in which the true mean $\mu(t)$ will lie is centered on the sample mean $\hat{m}(t)$ and the range is governed by the sample variance $\hat{S}(t)$ (or standard deviation $\hat{\sigma}$) and the level of confidence β , is given as,

$$\underline{m} = \hat{m} - \frac{\psi \hat{\sigma}(t)}{\sqrt{n}} < \mu < \frac{\psi \hat{\sigma}(t)}{\sqrt{n}} + \hat{m} = \overline{m} \quad (4.16)$$

The true value of the mean $\mu(t)$ lies between the values of lower and the upper bound of the inequality, as indicated in equation 4.16. The lower bound (\underline{m}) and upper bound (\overline{m}) quantities are referred to as the lower and upper confidence band limits. The values of ψ for various values of confidence β are given in table 4.1, with whatever level of confidence is chosen, e.g., $\beta = 0.90$ or 90% confidence, for $\psi=1.645$.

ψ	β
1	0.6827
1.645	0.90
1.960	0.95
2.576	0.99

Table 4.1: Values of ψ for various values of β

The lower and upper confidence limits $[\underline{\sigma}, \bar{\sigma}]$ of a sample $\hat{\sigma}$ is expressed as [52]:

$$\begin{aligned}\underline{\sigma} &= \underline{\rho}\hat{\sigma} \\ \bar{\sigma} &= \bar{\rho}\hat{\sigma}\end{aligned}\tag{4.17}$$

where $\underline{\rho}$ and $\bar{\rho}$ are determined by the level of confidence, β , the kurtosis of the random variable λ and the number of trails performed n , given as [52],

$$\begin{aligned}\underline{\rho} &= \frac{1}{\left[1 + \psi\sqrt{\frac{\lambda-1}{n}}\right]^{\frac{1}{2}}} \\ \bar{\rho} &= \frac{1}{\left[1 - \psi\sqrt{\frac{\lambda-1}{n}}\right]^{\frac{1}{2}}}\end{aligned}\tag{4.18}$$

The values of ψ for various values of confidence β are given in the table 4.1. The reasonable choice of λ must be determined before the confidence intervals are calculated. One option is to determine it by the following relation [52]:

$$\lambda \simeq \frac{\hat{\mu}_4}{\hat{S}^2} \equiv \hat{\lambda}\tag{4.19}$$

where $\hat{\mu}_4$ is the sample fourth central moment and \hat{S} is the sample variance.

4.1.4 Selection of Time Step (h)

The selection of the time step h is challenging and it is done heuristically. Since the Euler technique (section 2.3), relies on the derivative of the error function to approximate its trajectories, the smaller the step size, the smaller the error. A small time step of $h=.01$ hour was chosen which is very small compared to the time constant of the FOM $\beta=0.2982$ hour; for $h \ll \beta$, $w_n(mh)$ is a good approximation to a white noise process.

4.2 Test Results

MCS were performed to get a large ensemble (n) of power predictions for the given forecasted wind speeds: a wind speed error realization was generated and then the realization was added to the forecasted wind speeds. The addition of error realization with the wind speed forecast gave the wind speed realization. The realized wind speed was then passed into the wind power generator model to get a wind power prediction. Doing it in the same way for n times gave an ensemble of n power forecasts. The equation 4.14 and 4.15 were then used to calculate the statistics of wind power production.

75 MCS were performed, which ensures that the difference between true mean μ and the estimated mean $\hat{m}(t)$ will be less than roughly 11% with 90% certainty [52]. It was not possible to perform more trials since MATLAB[®] ran out of memory due to large amount of data being stored for post processing. Figure 4.2 shows the 24 hour forecasted wind speeds (v_f).

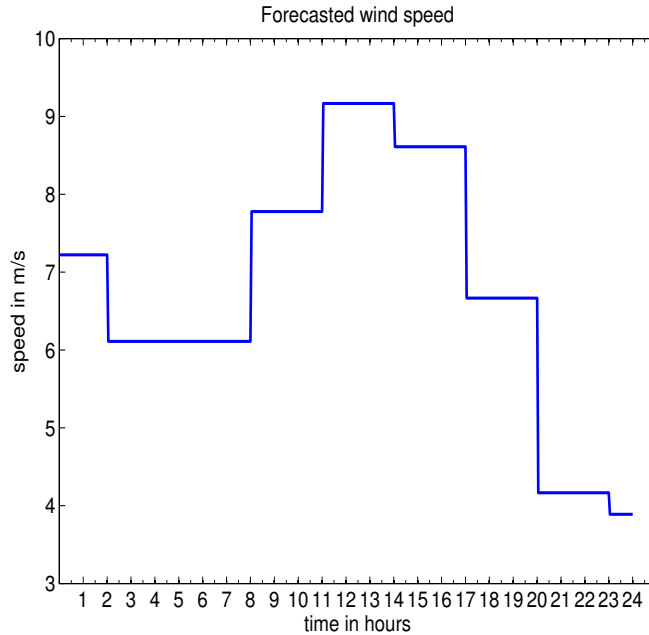


Figure 4.2: Forecasted wind speed

Figure 4.3 shows two realizations of forecast error $e(t)$. Figure 4.4 shows the

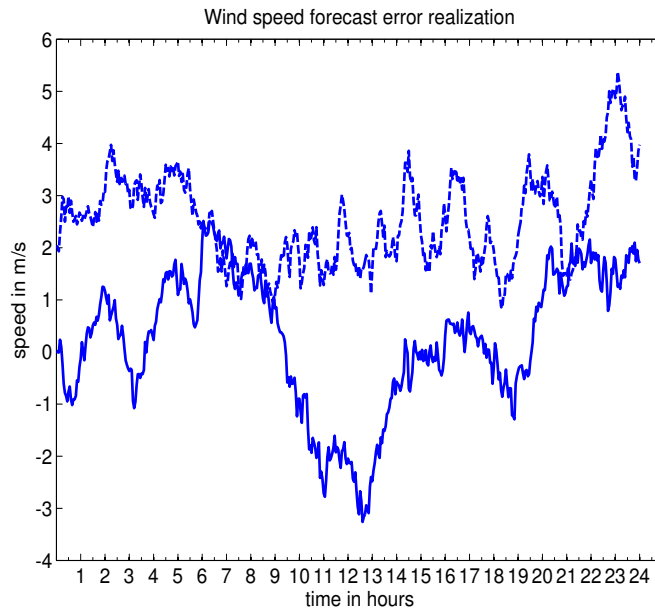


Figure 4.3: Two wind-speed forecast error realizations ($e^{(i)}$)

corresponding two realizations of wind speed v_r , i.e., the sum of signals shown in figure 4.2 and 4.3.

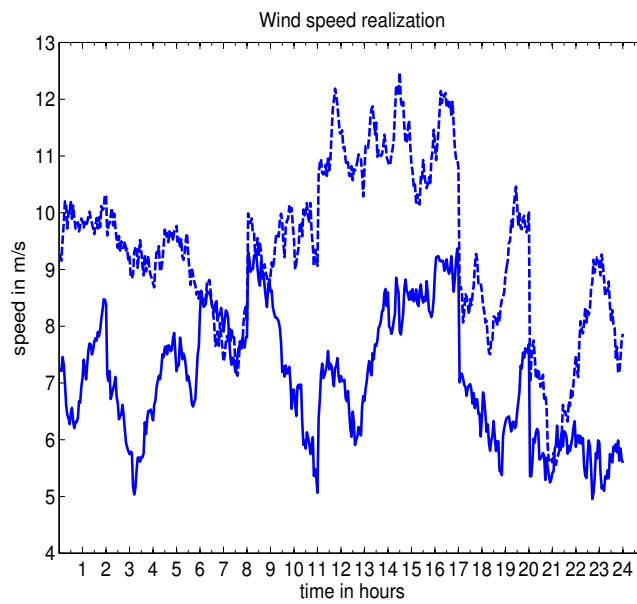


Figure 4.4: Two wind-speed forecast realizations ($v_r^{(i)}$)

Figure 4.5 shows the corresponding two realizations of power forecast P_p obtained by passing these wind speed realizations to the wind power generator model.

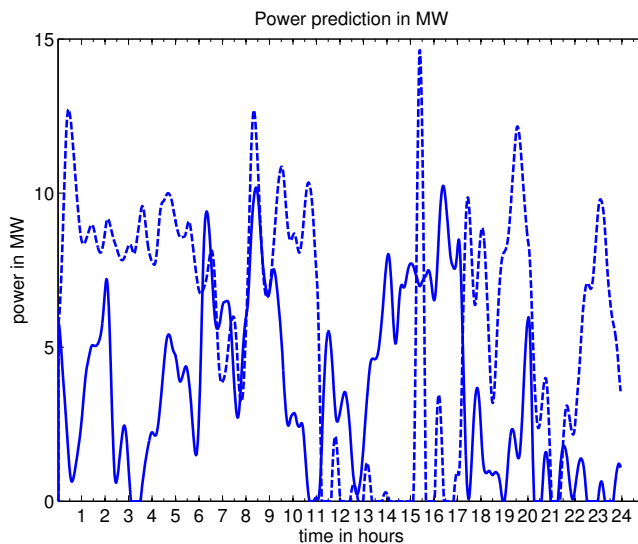


Figure 4.5: Two wind power realizations ($P_p^{(i)}$)

Figure 4.6 shows the mean and standard deviation of the wind power forecasts, obtained by performing 75 MCS trials.

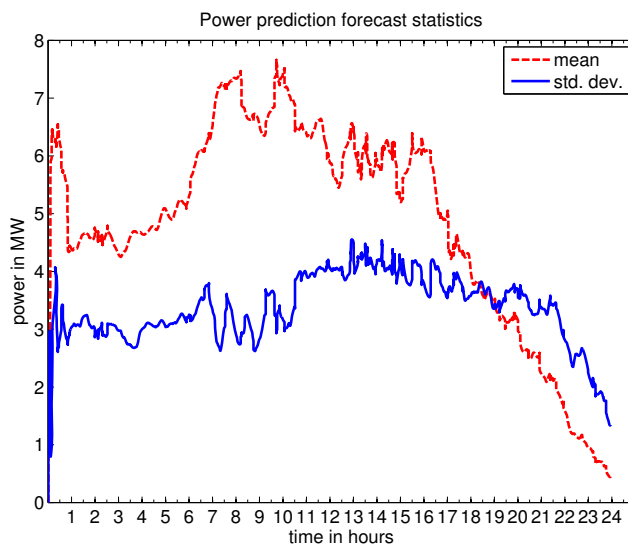


Figure 4.6: Wind power statistics, 75 MCS trials

4.2.1 Effects of n on the confidence limits

As mentioned above, confidence limits ensures that true mean lies between the lower confidence limit

$$\underline{m} = \hat{m} - \frac{\psi \hat{\sigma}(t)}{\sqrt{n}} \quad (4.20)$$

and the upper confidence limit

$$\overline{m} = \frac{\psi \hat{\sigma}(t)}{\sqrt{n}} + \hat{m} \quad (4.21)$$

with a specified level of confidence β ; The values of n corresponding to the different values of ψ are given in [52]. It must be carefully distinguished between uncertainty due to the number of trials and uncertainty due to wind-speed forecast error. We do not have any control on the uncertainty of wind-speed forecast error, but equation (4.20) and equation (4.21) demonstrates the effect of n to achieve a desired degree of a confidence limits, i.e., we can make uncertainty due to the number of trials arbitrarily small by increasing the number of MCS trials performed.

Deciding how many trials to perform requires comparing the wind power production forecast using the EC forecast, P_f , versus that produced with the wind speed forecast error model and MCS, P_p ; it is desirable to obtain a clear separation between these two results, i.e., P_f should lie outside the MCS confidence bands of P_p for it to be helpful. The mean of P_p may help a WE utility operator to decide how much power to bid in an electricity market:

1. If $E[P_p] = \hat{m}_p$ lies above P_f then the WE utility operator can be more aggressive in terms of how much power to bid.
2. If \hat{m}_p lies below P_f then the operator should be careful.
3. If \hat{m}_p is approximately equal to P_f then the operator should be neutral.

To illustrate these concepts, the statistics as shown in figure 4.6 were then substituted into equation 4.16 to provide the \hat{m}_p confidence intervals, with level of confidence

90% as shown in figure 4.7 along with the P_f plot.

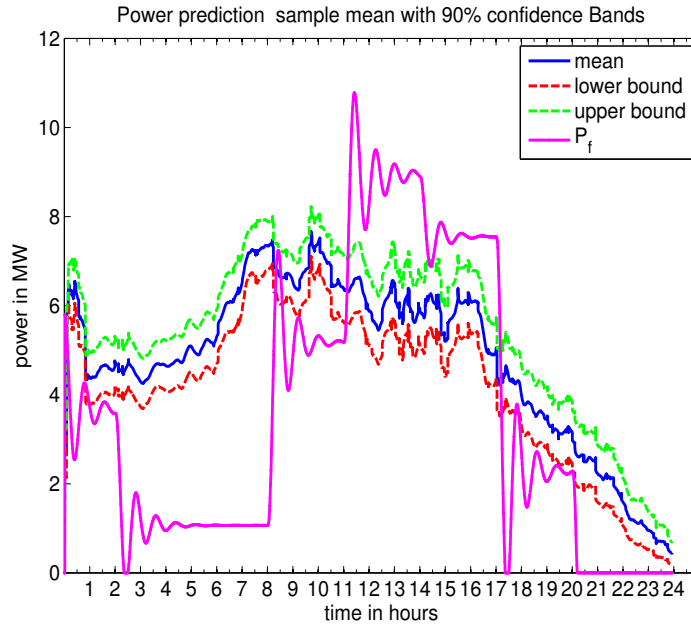


Figure 4.7: Wind power sample mean with 90% confidence bands

From figure 4.7, the \hat{m}_p confidence band lies well above P_f for $02 : 00 \leq t \leq 08 : 00$, so bidding could be aggressive over that interval. Clearly, 75 trials of MCS was sufficient for this assessment.

The above strategies will be more effective if $\hat{\sigma}_p$, the sample standard deviation of P_p , is also taken into account. For example, if \hat{m}_p lies above P_f but $\hat{\sigma}_p$ is large, then it may not be wise to be aggressive in bidding.

To use data $\hat{\sigma}_p$ with assurance we should also check its confidence limits. First we must use equation (4.19) to calculate estimates for the values of kurtosis $\hat{\lambda}$ each one-hourly wind power forecast distribution obtained by performing 75 MCS trials; the results are shown in figure 4.8.

The values of kurtosis were then substituted into equation (4.18) to provide the power prediction confidence intervals with level of confidence 90%, as shown in figure 4.9.

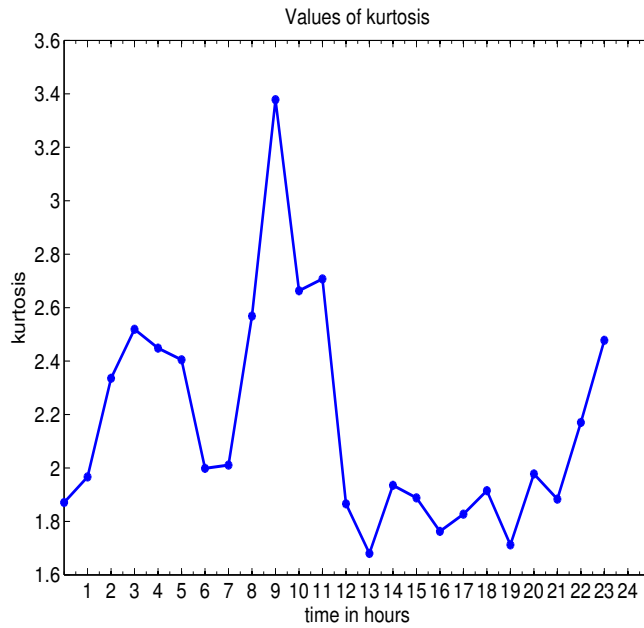


Figure 4.8: Estimated kurtosis

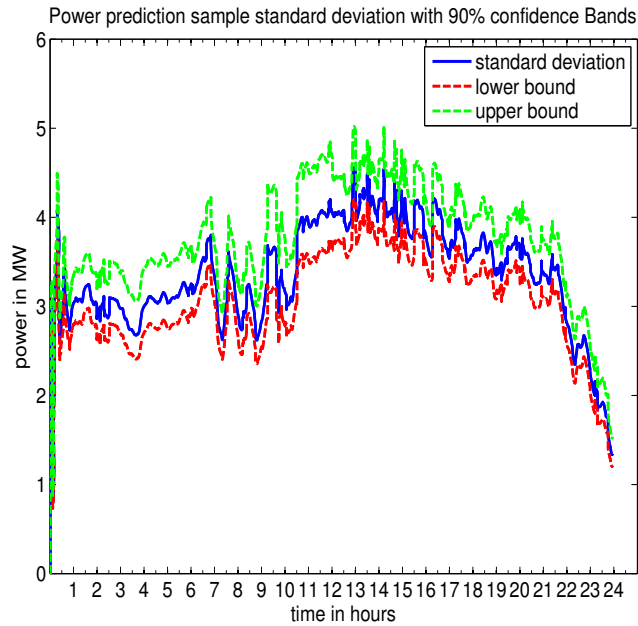


Figure 4.9: Wind power sample standard deviation with 90% confidence bands

From figures 4.7 and 4.9, the WE utility operator might moderate the three strategies (aggressive, careful and neutral) as \hat{m}_p lies above, below and approximately equal to

P_f depending upon the time of the day, noting that the standard deviation $\hat{\sigma}_p$ and its confidence band are quite high (between about 2.4 to 5 MW most of the day) compared to \hat{m}_p ; Therefore an important question then arises, what is the optimal bid? There are penalties for over-production and under-production, so this crucial dilemma is solved in chapter 6.

The statistics of the wind power prediction give an idea of the risk involved in estimating the wind power production. The combination of an uncertain production unit with a certain production unit reduces the overall uncertainty. Therefore, to reduce the variability in wind power production, the prospect of adding a natural gas microturbine was considered since the natural gas microturbines emit very low GHG for electricity generation. However, based on a conservative economic modeling it was shown that the cost of generating electricity from a microturbine is significantly higher than the cost of buying electricity from the grid (discussed in detail in next chapter), thus buying electricity from the grid seems preferable.

Chapter 5

Modeling a gas microturbine

Microturbines are compact, pollution free sources of electricity generation which use natural gas as a primary source of fuel; however they are also able to generate electricity using liquified petroleum gas, biogas or industrial gases (flare gases). The figure 5.1 shows the components of a microturbine system [2].

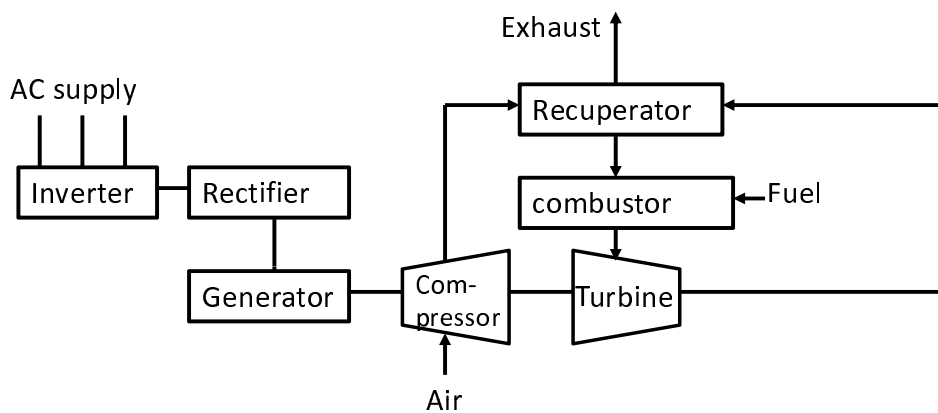


Figure 5.1: Components of a gas microturbine system

The microturbine operates on a thermodynamic cycle known as the Brayton cycle. In the Brayton cycle, the atmospheric air is compressed by the compressor then preheated in a recuperator. The high pressure air passes through the combustion

chamber, where fuel is added and burned at the same pressure as the compressed air. The resulting hot gas increases both in pressure and temperature due to heat energy of burning fuel and is allowed to expand in the turbine section. The gas expansion causes the turbine blades to spin, which then turns the rotor of a high speed permanent magnet generator. The permanent magnet generator converts rotation of a rotor into electric power.

The frequency of the electricity produced by the permanent magnet generator is very high (255 Hz); to make this electric power commercially usable, it is rectified to direct current, and then inverted to 60 Hz alternating current. All the rotating components of the microturbine are mounted on a single shaft supported by air bearings. The exhaust gas exits the turbine to the atmosphere through a recuperator that pre-heats the atmospheric air entering the combustor to improve the efficiency of the system [24].

The efficiency of microturbines depends on the temperature of the pre-heated air entering the combustor; the higher the temperature, the higher the power generation. To sustain a very high temperature, hot sections of the microturbines require special materials; however, to make gas microturbines cost effective, so far alloy steel is used in the microturbines, which can only sustain temperature of well below $700^{\circ}C$ [45].

The microturbines can operate as a power system or as a Combined Heat and Power (CHP) system. In a CHP system, a heat exchanger is placed after the recuperator that recovers energy from the exhaust gas. The heat exchanger has little impact on the power generation of the microturbine. The recovered energy can be used for heating water and/or spaces.

The USA Environmental Protection Agency's Office of Research and Development (EPAORD) operates the Environmental Technology Verification (ETV) program to provide credible performance data for any viable environmental technologies. The ETV is funded by the USA federal government and its purpose is to equip the technology buyers and financiers with credible performance data to make informed

decisions regarding environmental technology purchases and use [2].

The natural gas microturbine used in this thesis is the C60 model of the Capstone Turbine Corporation. The Capstone C60 manufacturer claims to provide up to 60 kW_e of electrical power and 110 kW_{th} of heat for combined heat and power applications [35].

5.1 Performance of a C60 Microturbine

The Capstone Turbine Corporation is the world’s leading producer of low emission microturbines and it has the highest number of microturbines installed all over the world [13]. The manufacturer’s specifications for C60 model is given in the following table at full load [2].

Fuel input	Natural gas 75 – 80 psig, HHV 811,000 Btu/h
Heat rate	12,200 Btu/kWh, LHV
Power	60 kW _e net(+0/ – 2)
Electrical efficiency (LHV)	28% (±2)
NO _x	< 0.00049 lb/kWh
CO ₂	< 2.178 lb/kWh

Table 5.1: Full load specifications

The technical terms used in the above table are explained below.

5.1.1 Fuel Input

Fuel input refers to the amount of natural gas required by the microturbine to generate the rated power. Natural gas quantities are measured in pounds per square inch gauge (psig). The heat content in the natural gas is expressed in British thermal units (Btu). One Btu is the amount of energy needed to heat one pound of water to one degree Fahrenheit . Since Btus are measurements of energy consumption, they can be converted directly to kilowatt-hours (3412.14 Btu = 1 kWh) or joules (1 Btu = 1,055.06 joules) [7].

Natural gas is a fossil fuel composed of a mixture of hydrocarbon gases, primarily

methane (95%), ethane (2.5%), propane (0.2%) and other hydrocarbons (2.3%). The combustion of hydrogen-rich fuels releases water that is subsequently evaporated in the combustion chamber. The water is evaporated by absorbing some heat from the burning of natural gas. That heat is called the latent heat of vaporization. The formation of vapor in the combustion chamber reduces the amount of thermal energy available to move the turbine.

If a process extracts latent heat of vaporization then fuel is said to have High Heating Value (HHV, 1 Btu=1055 joules) and if a process does not extract this heat fuel has Lower Heating value (LHV, 1 Btu=950 joules). In case of a microturbine water vapor passes out of the chamber via the exhaust, thus the fuel has LHV. Commercially, natural gas is sold at its HHV value.

5.1.2 Heat Rate

Heat rate refers to the amount of Btus of heat required to produce a Kilowatt-hour of energy.

5.1.3 Electrical Efficiency

The electrical efficiency is computed by dividing the electrical energy output by the fuel energy input [24]:

$$\eta = \frac{3412.14 \times P_0}{HI} \quad (5.1)$$

where HI =heat input using LHV (Btu/hr) and P_0 = power outputs in kWh.

5.1.4 Heat Recovery

Heat recovery refers to the amount of heat recovered from the exhaust gas leaving the recuperator. The ETV program has tested the performance specifications of a Capstone C60 combine heat and power model and have provided the following results at full load:

The gross power is the actual power developed by the microturbine . The compressor

Fuel input	Natural gas 75 – 80 psig, HHV 795213 Btu/h
Gross power	59.6 kW _e
Net power	54.9 kW _e
Heat rate	13,043 Btu/kWh, LHV
Electrical efficiency (gross)	28.4%
Electrical efficiency (net)	26.2%
Heat recovery	109.32kW _{th}
Thermal efficiency	52.2%
NO _x	0.00015 lb/kWh
CO ₂	1.54 lb/kWh

of the microturbine consumes some of the power, thus net power is the power available to the user. The detailed descriptions of testing and analysis methods are given in the reports [2]. The gas microturbine's NO_x and CO₂ emissions rates at full load are well below the average rate of NO_x (0.0034 lb/kWh) and CO₂(1.76 lb/kWh) for thermal power plants in New Brunswick [46].

5.2 Cost of Power using a C60 Microturbine

Although natural gas microturbines have lower emissions, it is very important to compare the microturbine cost of electricity to the electricity price from the grid; the comparison will determine the competitiveness of natural gas microturbines, as opposed to electricity purchased from the existing electrical grid. The electrical grid cost includes generation, transmission and distribution. To calculate the cost of producing electricity using microturbines following costs must be considered:

5.2.1 Capital Cost Factor

Capital Cost Factor (CCF) refers to the costs of purchasing the generating system itself divided by the life time energy production. The CCF for using a CHP microturbine per kWh at full load is,

$$CCF(\$/kWh)=CC / (L_d \times (kW_e + kW_{th}))$$

where CC is the Capital Cost in \$ and L_d design life or the expected life of microturbine operation in hours. The capital cost of a C60 microturbine provided by manufacturer is \$110,000 without a heat recovery unit, or \$130,000 with a heat recovery unit, and design life is 40,000 hours. It should be noted that the design life is the ideal life one can expect and it varies depending upon the fuel quality, air quality and number of starts and stops.

5.2.2 Fuel Cost

Fuel Cost (FC), is the cost of natural gas consumed for generating electrical and heat energy by the microturbine. The Canadian and U.S. natural gas markets operate as one large integrated market in which gas is traded in US dollars [38]. The natural gas prices are volatile, depending upon the market, but it is likely that as the demand for natural gas increases the cost of natural gas will rise. It is hard to say how fast the price will increase but a study at the Environment and Natural Resources Program, Harvard University believes that gas prices will be lower over the next two decades than during the past two [32], because many new sites have been discovered and as a result production will increase very fast. The work funded by the US Department of Energy predicts that average natural gas price over the next 10 year will be US\$7.24/MMBtu, where 1 MMBtu=1 million Btu [8]. For simplicity, this work will assume that for next few years the average price will be \$7.63/MMBtu (using current conversing rate 1 US\$=1.054 CDN\$). The FC for using microturbine per kWh at full load is,

$$FC(\$/\text{kWh})=(\text{gas cost in } \$/\text{Btu})(\text{gas consumed in Btu/h})/(\text{kW}_e+\text{kW}_{th})$$

5.2.3 Maintenance Cost

Maintenance Cost (MC) refers to the cost of maintenance, such as air filter change, periodical inspections of combustor etc. Most manufacturers offer service contracts for specialized maintenance priced at about \$ 0.01/kWh [32].

5.2.4 Total Cost

Total cost (TC) expressed in \$/kWh is the price of generating one kWh of energy by the microturbine and it is sum of CCF, FC and MC. The TC when microturbine is operating as a power system alone ($kW_{th} = 0$):

CCF(\$/kWh)	FC(\$/kWh)	MC(\$/kWh)	TC(\$/kWh)
0.05	0.11	0.01	0.17

Table 5.2: Cost of energy using microturbine as power system

The total cost when microturbine is operating as combined heat and power system:

CCF(\$/kWh)	FC(\$/kWh)	MC(\$/kWh)	TC(\$/kWh)
0.02	0.035	0.01	0.065

Table 5.3: Cost of energy using microturbine as combined heat and power system

5.3 Comparing a Microturbine vs. Grid-based Power

The cost of buying electricity from the grid in NB is \$.1207/kWh and from the table 5.2 the cost of electricity from a microturbine is \$.170/kWh working as power system alone and from table 5.3 \$.065/kWh as combined heat and power system. Since there is no market developed, where any deviation in electrical energy can be offset by supplying heat energy, it is not economical to dispatch a natural gas microturbine in order to reduce the variability in wind power generation. However, a CHP systems can be very cost effective for any commercial and industrial users who have heat demand as well as electricity demand.

Given the wind production statistics, how much should wind utilities bid into an electricity market to obtain maximum profit in face of regulation prices ? This dilemma is solved in next chapter.

Chapter 6

Bidding under uncertainty

6.1 Overview of an Electricity Market

Electricity markets are virtual markets which facilitate buying and selling of electricity through bidding, under a set of prior known rules and procedures, between market participants. Furthermore, electricity markets must always ensure the stability of the electrical grid by maintaining generation:load balance within $\pm 1.5\%$ limits set by the North American Electric Reliability Council (NAERC) [25]. The participation in the market is completely voluntary, although several necessary agreements have to be signed and fulfilled for participation [36, 27, 42].

Electricity markets operate in a day-ahead framework, i.e., all buying and selling will be done one day before the time of delivery [27, 42]. The day is divided into 24 one hour blocks, and for each block, hourly bids are submitted to the ISO by the participants, from 9.00 am to 11.00 am AST of the previous day [42]. The submitted bids can be made valid up to the next five days. The day-ahead market framework is important because it ensures reliable planning and stable operation of the electric grid [27, 36, 42].

6.1.1 Bids

The bids are the stipulation of both the prices and quantities at which buyers/sellers are willing to buy/sell electricity. The supplier always tries to sell a maximum quantity at the maximum price, while the buyer always tries to buy a maximum quantity at the minimum price. Generally, there are 3 types of bids in an electricity market [36]:

1. **Hourly Bid:** The hourly bid is the most basic and common form of market order. A market order refers to buying or selling electricity at the best available price. The hourly bid consists of price steps and corresponding quantities. There are limits to the price steps; for example, in the New York Electricity Market, the bid may consist of up to 11 price steps not exceeding the ceiling price (maximum price limit). The selection of the price steps and quantities are chosen by the participants individually.
2. **Block Bid:** The block bid consists of an order with a fixed price and quantity for several hours. The initial and the final time can be freely chosen by the participants but it must not be less than three consecutive hours. The block bid gives an opportunity to the participants for executing a ‘nothing or all’ strategy compared to hourly bid.
3. **Flexible Hourly Bid:** The flexible hourly bid is a sales bid for a single hour with a minimum price and a fixed quantity. The hour is not specified; instead, a condition that the bid will only be accepted with the highest price in an hour given that the highest price is more than the bid minimum price.

6.1.2 Accepted Market Price and Quantities

Once the bids are submitted the ISO maximizes the social welfare. In economics, social welfare is the sum of consumer surplus and producer surplus or the area

between the supply curve and demand curve; when this sum or area is maximum, then maximum demand has been fulfilled at minimum cost [55].

6.1.2.1 Consumer Surplus

Consumer surplus is the difference between the price that consumers are willing to pay for a good or service (indicated by the demand curve) and the price that they actually do pay. The shaded region in figure 6.1 shows the consumer surplus.

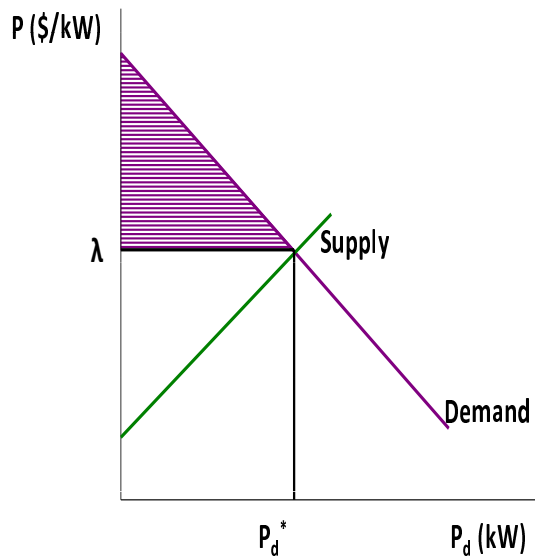


Figure 6.1: Consumer surplus

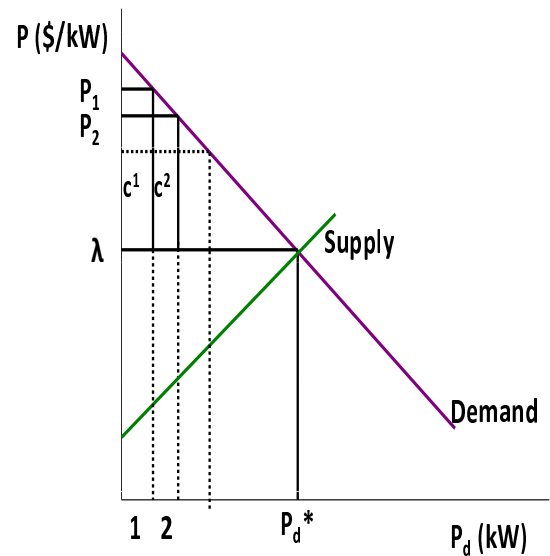


Figure 6.2: Deriving consumer surplus

A graphical representation of consumer surplus can be illustrated by considering the following exercise: suppose there is only 1 kW of power available in the market, figure 6.2, for any hour then it could be sold at price P_1 due to high demand, as shown. This means there is a customer who is willing to pay a very high price P_1 . If the price of electricity decreases than it might induce another customer to purchase power, or, it might induce the first customer to buy two kW. The final price (λ) which prevails in the market is the price where supply equals demand. Now, the consumer surplus for the first person is the difference between the final price (λ) and the price the person was willing to pay P_1 for a kW. The difference between the two prices represents the amount of consumer surplus that accrues to that person. Continuing

this way until the market price λ is reached then the total consumer surplus in the market is given approximately by the sum of the areas of the rectangles in figure 6.2 i.e., c^1 , c^2 and so on. Thus, total consumer surplus can reasonably be measured as the area between the supply curve and the horizontal line drawn at the equilibrium market price [51].

6.1.2.2 Producer Surplus

Producer surplus is the difference between the price producers actually receive for selling a kW of power and the price they would be willing to accept for a kW of power. The shaded region in figure 6.3 shows the producer surplus.

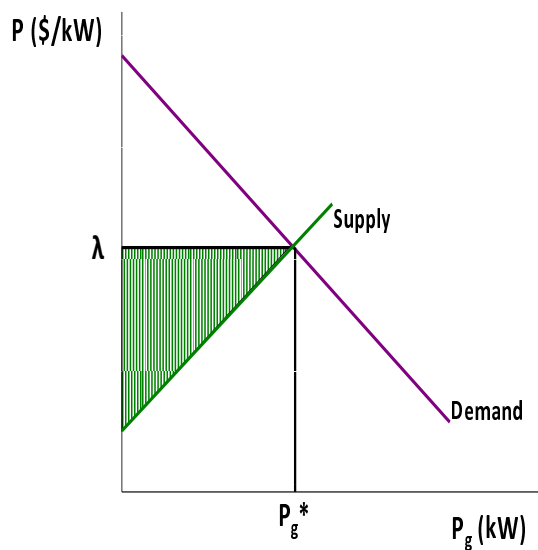


Figure 6.3: Producer surplus

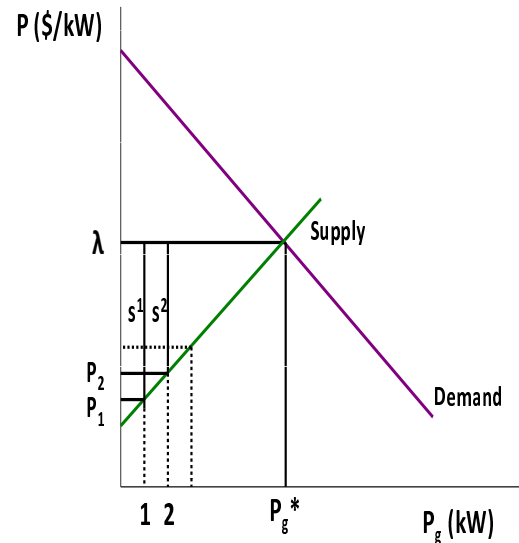


Figure 6.4: Deriving producer surplus

A graphical representation of producer surplus can be illustrated by considering the following exercise: suppose there is only 1 kW of power demand in the market, figure 6.4, for any hour then there would be a supplier willing to accept the price P_1 if only one unit is produced, as shown. If the price of electricity increases than it might induce another supplier to sell power, or it might induce the first supplier to sell two kW. The final price (λ) which prevails in the market is the price where demand equals supply. Now, the producer surplus for the first person is the difference

between the final price (λ) and the price the supplier was willing to accept for a kW, P_1 . The difference between the two prices represents the amount of producer surplus that accrues to that supplier. Continuing this way until the market price λ is reached then the total producer surplus in the market is given by the sum of the areas of the rectangles in figure 6.4, i.e., s^1 , s^2 and so on. Thus, total producer surplus can reasonably be measured as the area between the supply curve and the horizontal line drawn at the equilibrium market price [51], as shown in figure 6.5 .

6.1.2.3 Social Welfare

Social welfare is the sum of consumer surplus and producer surplus, or the area between the demand curve and the supply curve as shown in figure 6.5. From this figure one can see that if this area is maximum then maximum consumer demand has been met at minimum price. The accepted quantities and prices are calculated

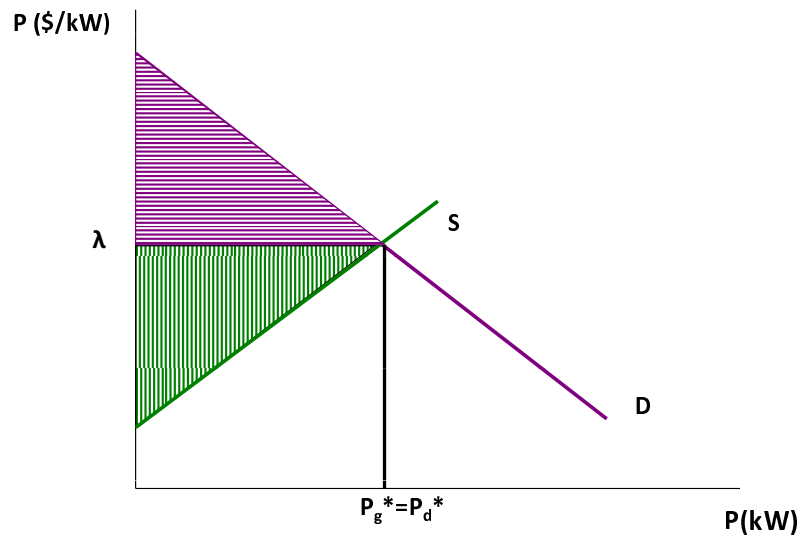


Figure 6.5: Social welfare

by maximizing the social welfare function which can be expressed as a lagrangian

function [55]:

$$L(P_g^*, P_d^*, \lambda) = \max [(area\ under\ demand\ curve) - (area\ under\ supply\ curve)] \quad (6.1)$$

Subject to

$$Power\ balance = 0; \quad (6.2)$$

To elaborate on this, let us assume that there are two suppliers and two buyers who have submitted the following linear bids to the ISO for any hour:

Supplier 1,

$$S_1 = 0.04P_{g1} - 1 \quad (6.3)$$

Supplier 2,

$$S_2 = 0.05P_{g2} - 1 \quad (6.4)$$

Buyer 1,

$$D_1 = -0.04P_{d1} + 5 \quad (6.5)$$

Buyer 2,

$$D_2 = -0.05P_{d2} + 6 \quad (6.6)$$

where, S_1 and S_2 are the offer prices of supplier 1 and supplier 2, in $\$/kW$, for supplying P_{g1} and P_{g2} amounts of electrical power respectively; D_1 and D_2 are the buyers offer prices, in $\$/kW$, for purchasing P_{d1} and P_{d2} amounts of electrical power respectively.

Once the bids are submitted, the ISO then maximizes social welfare, expressed as following lagrangian function (assuming enough transmission capacity to deliver all the demand),

$$L(P_{d1}, P_{d2}, P_{g1}, P_{g2}, \lambda) = \max [(-0.04P_{d1} + 5)P_{d1} + (-0.05P_{d2} + 6)P_{d2}] - \quad (6.7) \\ [(0.04P_{g1} - 1)P_{g1} + (0.05P_{g2} - 1)P_{g2}]$$

$$\begin{aligned}
&\text{subject to } P_{g1} + P_{g2} - P_{d1} - P_{d2} = 0 \\
&P_{d1} \geq 0 \\
&P_{d2} \geq 0 \\
&P_{g1} \geq 0 \\
&P_{g2} \geq 0
\end{aligned} \tag{6.8}$$

For the example above, equation (6.7) can be written as,

$$L(x, \lambda) = \max_x [x^T Hx + f^T x] \tag{6.9}$$

$$\begin{aligned}
&\text{subject to } A_{eq}x = b_{eq} \\
&x \geq lb
\end{aligned} \tag{6.10}$$

where,

$$x = \begin{bmatrix} P_{d1} \\ P_{d2} \\ P_{g1} \\ P_{g2} \end{bmatrix}, H = - \begin{bmatrix} 0.04 & 0 & 0 & 0 \\ 0 & 0.05 & 0 & 0 \\ 0 & 0 & 0.04 & 0 \\ 0 & 0 & 0 & 0.05 \end{bmatrix}, f = [5 \ 6 \ 1 \ 1] \tag{6.11}$$

$$A_{eq} = [-1 \ -1 \ 1 \ 1], b_{eq} = [0], lb = [0 \ 0 \ 0 \ 0]^T \tag{6.12}$$

The above optimization problem was solved using a quadratic programming solver and the optimum quantities ($P_{d1}^*, P_{d2}^*, P_{g1}^*, P_{g2}^*$) and the optimum price (λ), termed as accepted quantities and price, for the submitted linear bids are given in table 6.1.

$P_{d1}^* (kW)$	P_{d2}^*	P_{g1}^*	P_{g2}^*	$\lambda (\frac{\$}{kW})$
69.44	75.55	80.55	64.44	2.22

Table 6.1: Electricity market solution for two participants

6.1.3 Reserve Power

A quite long time period exists between the bidding time and the delivery time. Therefore, there must be reserve at the grid operator's disposal to meet some level of uncertainty. The requirement for reserves in the past has been mainly to offset the variation in the demand, because the buyer's bid is based on the forecast of their consumption 24 hours ahead, and given the complexity of electrical consumption, a perfect forecast is not always expected; many years of experience in forecasting has shown that the electrical demand can be forecasted with a high level of confidence [42].

There are two types of reserve, primary (hour-head market) and secondary (real-time market). The size of the primary reserve is calculated as: the ISO forecasts demand and checks supplies, generally one or two hours before the start of each delivery hour and decides how much additional (or less) supply is required relative to the total accepted supply quantities in the day-ahead market. The ISO then accepts bids, only from the suppliers either as buyer (decrease generation) or supplier (increasing generation).

The ISO promptly optimizes the social welfare (as mentioned above) and provides accepted quantities and prices to the participants. Adding all the accepted quantities will give the size of primary reserve. In case of excess demand, if the size of primary reserve is less than that required to maintain a power balance, then the ISO will make a plan to curtail the excess load until the power balance is satisfied [41].

As the delivery hour starts, the grid operator forecasts demand for each next minute and checks supplies, and any increase in the demand will be meet by the secondary reserves. The ISO again asks for bids and provides accepted quantities to the suppliers. Since the secondary reserves are used for minute to minute balancing, the power generators which can ramp up their production within a fraction of a second are only allowed to participate in the markets, for example NBSO uses gas

turbines and hydropower generators as secondary reserve [25].

After the delivery day, deviations from the accepted quantities are calculated for each market participant and regulation prices (regulation-up or regulation-down) will be charged to any defaulter. The regulation-down price is a salvage price for over-production, i.e., suppose any supplier produces more than its accepted quantity then other suppliers have to regulate-down to maintain power balance, and therefore the excess production will be paid after subtracting the cost of reducing generation.

Regulation-up price is the penalty for under-production, i.e., if power production from any supplier is lower than the bid then other producers will have to regulate-up in order to maintain power balance, and therefore the defaulter has to pay any cost associated with rescheduling of other generators. The regulation-up price is high compared to regulation-down price because the deficit energy is coming from the suppliers whose bids were not accepted in the day ahead market plus a service charge added by the ISO. Thus, it is always in a market participant's interest to fulfill its commitments [26, 54].

6.2 Bidding Quantities Formulation

A WE utility has to sell energy into a day ahead-market. The WE utility receives the market price for every unit of energy delivered. If the actual production is more than the bid quantity then the WE utility will receive the salvage price or regulation-down price for the surplus. If the actual production is below the bid the WE utility will pay the penalty or regulation-up price. Since the ISO accepts bids from 09:00 to 11:00 AST for following day, MCS (chapter 4) performed before 11:00 will give the risk involved in power productions in terms of hourly statistics describing possible power production levels for the delivery day. With this information the WE utility will know how much to bid in order to maximize the expected profit. The bidding

quantities are found by maximizing the expected value of a profit function.

Before formulating an effective bidding strategy, it was important to carefully examine the probability distributions of the MCS power predictions to assess their gaussian-ness. The hourly power prediction data were tested for normality using a statistical Chi-Square (χ^2) test (as mentioned in detail in Chapter 2) and the results are summarized in table 6.2. The table basically tells the probability (in %) that given distribution is normal (the probabilities less than 10^{-4} were rounded off to zero).

0	0	0	0	0	0	0	0	0	0	0	0	0	0	0	0	0	0	0	0	0	0	0	0	1 h block	
																									time in
0	1	2	3	4	5	6	7	8	9	10	11	12	13	14	15	16	17	18	19	20	21	22	23	hours	
All probabilities are in percentage (%)																									

Table 6.2: Summary of chi-square test results

To examine the normality of wind power prediction data further, each 24 hourly distribution were fitted for the normal distribution using MATLAB[®] command ‘normfit’. After that, using the statistics obtained from the ‘normfit’, 1000 power forecasting error samples were generated for each hourly distribution. Then the cumulative distribution was plotted for the synthetically generated sample along with the actual distribution for the same bin width for each hour, as given in Appendix C (using the same approach as discussed in Chapter 2), and from the plot one can see that there is a big difference between the cumulative distribution plots; also the actual distribution does not exhibit a general normal cumulative distribution nature either (as an example, two distribution comparisons plots figure 6.6 and 6.7, one for time 01:00:00 to 1:59:59 and other one for 13:00:00 to 13:59:59 are shown in figure 6.6 and figure 6.7).

Hence it was concluded that wind power prediction is not normally distributed;

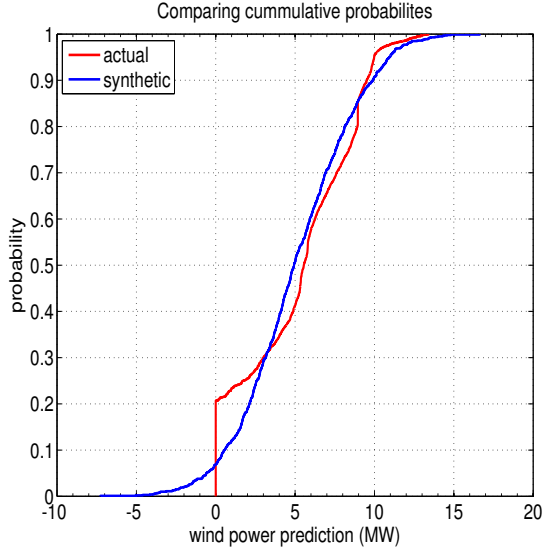


Figure 6.6: Comparing cumulative probabilities for time block 01:00:00 to 1:59:59

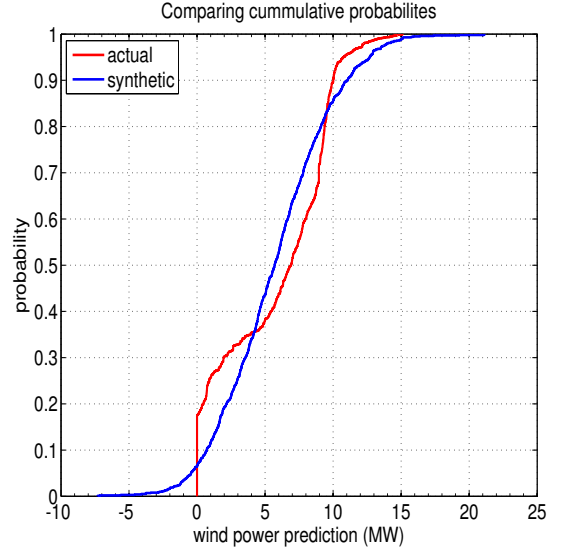


Figure 6.7: Comparing cumulative probabilities for time block 13:00:00 to 13:59:59

rather than looking for a suitable distribution for the wind power prediction, a bidding strategy free of distribution was formulated so that this formulation can be applied to any wind power prediction data.

Let P_g denote the amount of future generation. Also assume that that it belongs to the class F of cumulative distribution functions with mean $\mu = E[P_g]$ and variance $\sigma^2 = var(P_g)$ [21]. Let P_s be the selling price ($P_s > C$, where C is the unit cost of production, \$/kWh). The regulation-up price, R_{up} , is the cost associated with under production, i.e., the penalty minus selling price (P_s). The regulation-down price, R_{dw} , is the cost associated with over-production, i.e., selling price minus cost associated with lowering generation.

If Q is the bid quantity, then $\min(Q, P_g)$ units are sold at the bid price, $(Q - P_g)^+ = \max(Q - P_g, 0)$ units are the deficit and $(P_g - Q)^+ = \max(P_g - Q, 0)$ units are the salvage or over production. The profit function is then given as,

$$\Phi(Q, P_g) = [P_s(\min(Q, P_g)) + R_{dw}(P_g - Q)^+ - R_{up}(Q - P_g)^+ - CP_g] \quad (6.13)$$

The maximum expected profit is:

$$E_{max} [\Phi(Q, P_g)] = \max_Q \{ P_s E[\min(Q, P_g)] + R_{dw} E[P_g - Q]^+ - R_{up} E[Q - P_g]^+ - C\mu_p \} \quad (6.14)$$

where μ_p is the expected WE production, and

C = Cost of generating one unit of energy (\$/kWh)

P_g = Amount of future generation (kW)

Q = Bid quantity (kW)

P_s = Selling price (\$/kWh)

R_{up} = Regulation up-price (\$/kWh) for $P_s > R_{up}$

R_{dw} = Regulation down-price (\$/kWh) for $R_{dw} > R_{up}$

Observing the following two relations,

$$\min(Q, P_g) = Q - (Q - P_g)^+ \quad (6.15)$$

$$(P_g - Q)^+ = P_g - Q + (Q - P_g)^+ \quad (6.16)$$

using the above two equations, equation 6.14 can be rewritten as,

$$E_{max} [\Phi(Q, P_g)] = \max_Q \{ P_s E[Q - (Q - P_g)^+] + R_{dw} E[P_g - Q + (Q - P_g)^+] - R_{up} E[Q - P_g]^+ - C\mu_p \} \quad (6.17)$$

or,

$$E_{max} [\Phi(Q, P_g)] = \max_Q \{ P_s Q - P_s E[(Q - P_g)^+] + R_{dw} \mu_p - R_{dw} Q + R_{dw} E[(Q - P_g)^+] - R_{up} E[(Q - P_g)^+] - C\mu_p \} \quad (6.18)$$

or,

$$E_{max} [\Phi(Q, P_g)] = \max_Q \{ (R_{dw} - C)\mu_p + (P_s - R_{dw})Q - (P_s - R_{dw} + R_{up})E[(Q - P_g)^+] \} \quad (6.19)$$

The $(Q - P_g)^+$ in equation 6.19 can be simplified as,

$$(Q - P_g)^+ = \frac{|Q - P_g| + (Q - P_g)}{2} \quad (6.20)$$

Since the distribution of P_g is unknown, equation 6.19 is maximized against the worst possible distribution F . Using the following Cauchy-Schwarz inequality,

$$E[|Q - P_g|] \leq [E(Q - P_g)^2]^{\frac{1}{2}} = [\sigma^2 + (Q - \mu_p)^2]^{\frac{1}{2}} \quad (6.21)$$

Thus, from equation (6.20) the expectation of $(Q - P_g)^+$ is bounded by,

$$E[(Q - P_g)^+] \leq \frac{(\sigma^2 + (Q - \mu_p)^2)^{\frac{1}{2}} + Q - \mu_p}{2} \quad (6.22)$$

The detailed derivation of equation 6.22 is given in [20, 21]; using the above relation the equation 6.19 can be written as,

$$E_{max} [\Phi(Q, P_g)] = \max_Q \{ (R_{dw} - C)\mu_p + (P_s - R_{dw})Q - (P_s - R_{dw} + R_{up}) \left(\frac{(\sigma^2 + (Q - \mu_p)^2)^{\frac{1}{2}} + Q - \mu_p}{2} \right) \} \quad (6.23)$$

The second derivative of equation 6.23 is,

$$\frac{d^2 E_{max} [\Phi(Q, P_g)]}{dQ^2} = -\frac{(P_s - R_{dw} + R_{up})}{2} \left[\frac{\sigma^2}{(\sigma^2 + (Q - \mu_p)^2)^{\frac{3}{2}}} \right] < 0 \quad (6.24)$$

Therefore, the optimal quantity to be bid Q^* is determined by setting the first-order condition to zero:

$$\begin{aligned} \frac{dE_{max}[\Phi(Q, P_g)]}{dQ} = \frac{d}{dQ} [(R_{dw} - C)\mu_p + (P_s - R_{dw})Q - \\ (P_s - R_{dw} + R_{up}) \left(\frac{(\sigma^2 + (Q - \mu_p)^2)^{\frac{1}{2}} + Q - \mu_p}{2} \right)] = 0 \end{aligned} \quad (6.25)$$

or,

$$(P_s - R_{dw}) - \left(\frac{P_s - R_{dw} + R_{up}}{2} \right) \left[(\sigma^2 + (Q - \mu_p)^2)^{-\frac{1}{2}} (Q - \mu_p) + 1 \right] = 0 \quad (6.26)$$

and the value of Q^* is calculated by solving the above equation, and is given as

$$Q^* = \mu_p + \frac{\sigma}{2} \left[\frac{(P_s - R_{dw} - R_{up})}{(R_{up}P_s - R_{up}R_{dw})^{\frac{1}{2}}} \right] \quad (6.27)$$

6.3 Test Results

The experience of the New Brunswick System Operator (NBSO) with wind integration is developing, and so far there is no market rule as such for the wind power producers. However, all the wind production will be paid at a fixed price 10c/kWh [39]. Let us assume that in the case of under-production the WE utility will buy electricity from the grid at the cost of \$.1207/kWh, which means $R_{dw} = $.0207/kWh$ (cost of buying from grid $- P_s$) and in the case of over-production the salvage price is \$.085c/kWh. i.e,

$$P_s = \$100/\text{MWh},$$

$$R_{up} = \$20.7/\text{MWh},$$

$$R_{dw} = \$85/\text{MWh}$$

Also to elaborate the effects of regulation-down and regulation-up prices on optimal bidding quantities, we considered three cases: we termed the prices mentioned above as case-1 (nominal-case), in case-2 we increased R_{up} to \$30.7/MWh, and in case-3 we

increased R_{dw} to \$95/MWh while keeping the two other prices in both cases the same as the nominal-case. Using the costs for all three cases, the optimal bidding quantities for each case using the statistics of power production obtained by performing 75 MCS (shown in chapter 4) are shown in figure 6.3.

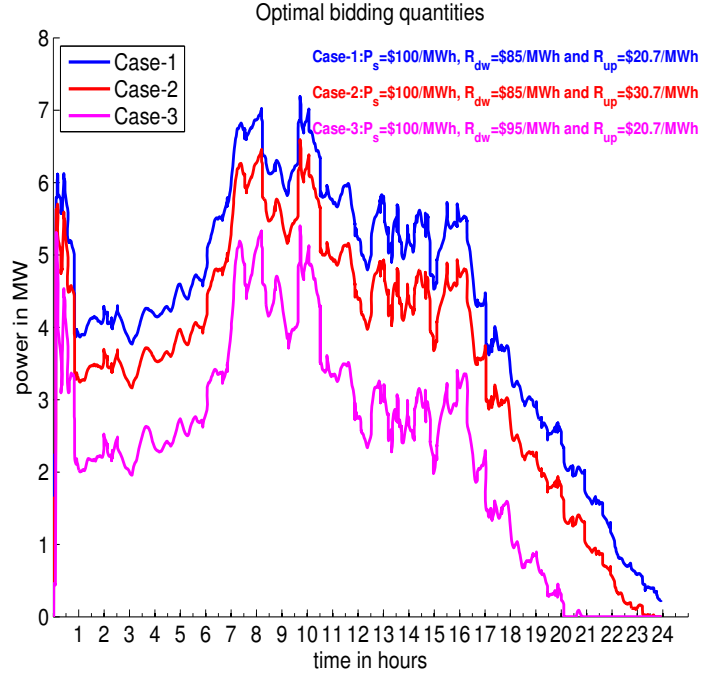


Figure 6.8: Bidding quantities

From figure 6.3, one can notice that the optimal bidding quantities in case-2 are below case-1 because the penalty for under-production increased from \$20.7/MWh to \$30.7/MWh. Also the optimal bidding quantities in case-3 are below case-2 and case-1 because it is in the WE utility's interest to bid low because if it will over-produce then it will get paid very close to the selling price (P_s =\$100/MWh) but if it will under-produce then it will pay \$20/MWh to the ISO which will affect profit significantly.

Chapter 7

Thesis observations

7.1 Summary and Conclusion

The following summary and conclusion can be drawn from the work presented in this thesis:

1. The EC provides wind speed data in GRIB file format. There was no convenient tool available to read GRIB file into MATLAB[®] directly. Therefore, the first task in this thesis was to develop software to read GRIB data directly into MATLAB[®]. With input from Sean Perry, a graduate student of Dr. James H. Taylor, software which reads wind-speed data from any records of actual and forecasted data in GRIB format was developed in MATLAB[®]. Also, the software enables users to calculate wind-speed prediction error, plot and analyze probability distributions for any prediction horizons very easily and effectively.
2. It was shown that the statistics of the wind-speed prediction error do not increase significantly as prediction time increases. This result is very significant because the solution developed in this thesis can be directly incorporated with existing electricity market rules, in contrast to other researchers arguments [26, 31] that for wind utilities the time between bidding and delivery should be

short—the shorter the time gap, the lesser the prediction error.

3. It was shown through statistical analysis that the hourly wind-speed prediction error distributions were quite nearly gaussian in nature. After that, the autocorrelation function of the prediction error distribution was fitted with autocorrelation functions, for first- and second-order markov processes. It was shown that a FOM is a more appropriate fit compared to a SOM. It was shown that solving a FOM using euler's technique for independent initial conditions gave the realizations of the prediction error, and adding those to the forecasted wind speed provided by EC gave the wind speed realizations. The wind speed realizations were then input to an off-the-shelf wind farm model developed in Simulink[®].
4. MATLAB[®] files and Simulink[®] work independently with respect to each other. Therefore, an interface was developed which facilitated the transfer of data from the MATLAB[®] files to the Simulink[®], and *vice versa*.
5. The variability present in the wind speed realizations gets transferred to the wind power realizations by Monte Carlo Simulation. Therefore, it was important to assess the uncertainty in the power production; it was done through MCS.
6. The MCS essentially gave the variability in the wind power production in terms of statistics and histograms. The prospect of adding a natural gas microturbine with a wind farm unit was considered to reduce the overall power production variability, but it was found that economically it is not generally a viable option. A complete economic modeling for a natural gas microturbine was done showing clearly that the cost of electricity from a microturbine is not competitive against the cost of electricity from the grid, unless there is a market for the surplus heat produced.
7. A bidding strategy which facilitates WE producers' participation in an

electricity market to obtain maximum profit was developed based on the statistics obtained by the MCS and electricity market regulations.

8. This research has developed energy and management control software for a wind energy producer which includes: power forecasting, power statistics generation and an optimal bidding strategy.

7.2 Future Work

To continue with the development of this thesis, first and foremost is to test the performance of the energy and management control software developed in this thesis with real electricity market data. We have created the foundation of an effective energy and management control software package which has to be evolved through validation, correction and rigorous testing. Also, as mentioned in section 2.2, it is important to provide a rigorous validation of the gaussian assumption by having more forecast and actual data to process to see if the PDF of the prediction error depends on the forecasted wind speeds.

The limitation on available data (291 days) did not permit a detailed analysis to see if wind-speed forecast error statistics are different for different values of wind-speed prediction (e.g. low, medium and high v_f)—this would make a major difference in generating realizations of wind-speed error compared to generating realizations using hourly wind-speed prediction error statistics.

To perform MCS easily it is recommended that wind turbine generator Simulink[®] model must be replaced with a mathematical model in m-file format, because as the number of trials increases the model stops working due to limit on MATLAB[®]'s memory; also the user does not have any control over these models and therefore does not know precisely what is wrong if any contingencies occur.

Bibliography

- [1] Forecasting intermittent generation in the national electricity market, Tech. report, National Electricity Market Management Company Limited, Australia, February 2004.
- [2] US Environmental Protection Agency, Greenhouse gas technology center verified technologies, <http://www.epa.gov/etv/vt-ggt.html>.
- [3] C. Lindsay Anderson and Judith B. Cardell, Reducing the variability of wind power generation for participation in day ahead electricity markets, HICSS '08: Proceedings of the Proceedings of the 41st Annual Hawaii International Conference on System Sciences (Washington, DC, USA), IEEE Computer Society, 2008, p. 178.
- [4] American Wind Energy Association, The economics of wind energy, Tech. report, February 2005.
- [5] Canadian Wind Energy Association, Wind vision 2025, Tech. report, 2008.
- [6] Candian Wind Energy Association, Backgrounder on wind energy, Tech. report, 2008.
- [7] Bioenergy Feedstock Development Program, Conversion, http://bioenergy.ornl.gov/papers/misc/energy_conv.html.

- [8] Mark Bolinger and Ryan Wiser, 2010 natural gas price forecast to nymex futures prices, Tech. report, Ernest Orlando Lawrence Berkeley National Laboratory, January 2010.
- [9] Brian Blanton, a WMO GRiB file reader for matlab,
<http://www.opnml.unc.edu/OPNML-Matlab/read-grib/read-grib.html>.
- [10] Barbara G. Brown, Richard W. Katz, and Allan H. Murphy, Time series models to simulate and forecast wind speed and wind power, Journal of Climate and Applied Meteorology **23** (1984), no. 8, 1184–1195.
- [11] Erasmo Cadenas and Wilfrido Rivera, Wind speed forecasting in the south coast of Oaxaca, Mexico, Renewable Energy **32** (2007), no. 12, 2116 – 2128.
- [12] Environment Canada, National inventory report: Greenhouse gas sources and sinks in canada, Tech. report, 2008.
- [13] Capstone Turbine Corporation, Press Releases,
<http://www.capstoneturbine.com/news/story.asp?id=561>.
- [14] Matt Coleman and Steve Provol, Wind power economics: Understanding economic risks in wind power projects in the USA, Refocus **6** (2005), no. 4, 22 – 24.
- [15] Global Wind Energy Council, Global wind 2008 report, Tech. report, 2008.
- [16] Toby Couture and Yves Gagnon, An analysis of feed-in tariff remuneration models: Implications for renewable energy investment, Energy Policy **38** (2010), no. 2, 955 – 965.
- [17] Enercon, Canada-wind energy, Tech. report, 2008.
- [18] Environment Canada, Low-resolution CMC GRIB database,
<http://www.weatheroffice.gc.ca/grib/Low-resolution-GRIB-e.html>.

- [19] Luis M. Fernandez, Jose Saenz, and Francisco Jurado, Dynamic models of wind farms with fixed speed wind turbines, *Renewable Energy* **31** (2006), no. 8, 1203 – 1230.
- [20] Guillermo Gallego, A minmax distribution free procedure for the (q, r) inventory model, *Operations Research Letters* **11** (1992), no. 1, 55 – 60.
- [21] Guillermo Gallego and Ilkyeong Moon, The distribution free newsboy problem: Review and extensions, *The Journal of the Operational Research Society* **44** (1993), no. 8, 825–834.
- [22] E. Garcacuteia, The influence of the weibull assumption in monthly wind energy estimation, *Wind Energy* **11** (2008), no. 5, 483–502.
- [23] Gelb, A., Editor, Applied optimal estimation, MIT Press, 1974.
- [24] USA Greenhouse Gas Technology Center, Southern Research Institute, Environmental technology verification report, Tech. report, september 2003.
- [25] Eric Hirst and Jeffrey Hild, The value of wind energy as a function of wind capacity, *The Electricity Journal* **17** (2004), no. 6, 11 – 20.
- [26] H. Holttinen, Optimal electricity market for wind power, *Energy Policy* **33** (2005), no. 16, 2052 – 2063.
- [27] IESO, Independent electricity market operator, <http://www.ieso.ca>.
- [28] M. Jamil, S. Parsa, and M. Majidi, Wind power statistics and an evaluation of wind energy density, *Renewable Energy* **6** (1995), no. 5-6, 623 – 628, *Solar Electricity: Photovoltaics and Wind*.
- [29] National Renewable Energy Laboratory, Estimating the economic value of wind forecasting to utilities, Tech. report, March 1995.

- [30] L. Landberg, Short-term prediction of local wind conditions, Journal of Wind Engineering and Industrial Aerodynamics **89** (2001), no. 3-4, 235 – 245.
- [31] Matthias Lange, On the uncertainty of wind power predictions—analysis of the forecast accuracy and statistical distribution of errors, Journal of Solar Energy Engineering **127** (2005), no. 2, 177–184.
- [32] Henry Lee, Assessing the challenges confronting distributive electricity generation, Tech. report, Belfer Center for Science and International Affairs, Kennedy School of Government, Harvard University, January 2003.
- [33] Sathyajith Mathew, Wind energy: Fundamentals, resource analysis and economics, Springer-Verlag New York, Inc., Secaucus, NJ, USA, 2006.
- [34] Mathworks, Wind turbine, <http://www.mathworks.cn/>.
- [35] Capstone Turbine Corporation, Product data sheet C60, Tech. report, 2004.
- [36] NordPool, Independent Electricity Market Operator, <http://www.nordpool.com/en/>.
- [37] P.E. Morthorst, Detailed investigation of electricity market rules, Tech. report, European Wind Energy Association, April 2007.
- [38] National Energy Board, How Canadian Markets Work, <http://www.neb.gc.ca/clf-nsi/rnrgynfmtn/prcng/ntrlgs/cndnmrk-eng.html>.
- [39] NBSO, Operations, <http://www.nbso.ca/Public/en/op/market/default.aspx>.
- [40] NYISO, Markets & operations, <http://www.nyiso.com/public/index.jsp>.
- [41] Independent System Operator, Nord pool asa’s financial market, Tech. report, March 2010.
- [42] New Brunswick System Operator, New Brunswick electricity market rules, Tech. report, September 2007.

- [43] New York Independent System Operator, Market participants user's guide, Tech. report, November 2008.
- [44] Christos E. Papadopoulos and Hoi Yeung, Uncertainty estimation and monte carlo simulation method, Flow Measurement and Instrumentation **12** (2001), no. 4, 291 – 298.
- [45] John P. Shingledecker Philip J. Maziasz, Bruce A. Pint, Austenitic stainless steels and alloys with improved high-temperature performance for advanced microturbine recuperators, Tech. report, Oak Ridge National Laboratory Metals and Ceramics Division, 2004.
- [46] NB Power, Environmental performance report 2007, Tech. report, 2007.
- [47] Sancho Salcedo-Sanz, Angel M. Perez-Bellido, Emilio G. Ortiz-Garcia, Antonio Portilla-Figueras, Luis Prieto, and Daniel Paredes, Hybridizing the fifth generation mesoscale model with artificial neural networks for short-term wind speed prediction, Renewable Energy **34** (2009), no. 6, 1451 – 1457.
- [48] Surya Santoso and Ha Thu Le, Fundamental time-domain wind turbine models for wind power studies, Renewable Energy **32** (2007), no. 14, 2436 – 2452.
- [49] A. Shamshad, M.A. Bawadi, W.M.A. Wan Hussin, T.A. Majid, and S.A.M. Sanusi, First and second order markov chain models for synthetic generation of wind speed time series, Energy **30** (2005), no. 5, 693 – 708.
- [50] S.N. Singh and I. Erlich, Strategies for wind power trading in competitive electricity markets, IEEE Transactions on Energy Conversion **23** (2008), no. 1, 249–256.
- [51] Steve Suranovic, Producer surplus, <http://internationalecon.com/Trade/T90-6A.php>.

- [52] J. H. Taylor, Statistical performance analysis of nonlinear stochastic systems by the Monte Carlo Method, *Trans. on Mathematics and Computers in Simulation* **23** (1981).
- [53] J.L. Torres, A. Garca, M. De Blas, and A. De Francisco, Forecast of hourly average wind speed with ARMA models in Navarre (Spain), *Solar Energy* **79** (2005), no. 1, 65 – 77.
- [54] J. Usaola and J. Angarita, Bidding wind energy under uncertainty, *International Conference on Clean Electrical Power*, 2007. ICCEP '07 (2007), 754–759.
- [55] James D. Weber and Thomas J. Overbye, An individual welfare maximization algorithm for electricity markets, *IEEE Trans. Power Syst* **17** (2002), 590–596.
- [56] D. Weisser, A wind energy analysis of Grenada: an estimation using the weibull density function, *Renewable Energy* **28** (2003), no. 11, 1803 – 1812.
- [57] Jinn-Chang Wu, Novel circuit configuration for compensating for the reactive power of induction generator, *IEEE Transactions on Energy Conversion* **23** (2008), no. 1, 156 – 162.

Appendix A

χ^2 test results

The following terminology has been used for χ^2 test results,

$H_0 = 1$, Hypothesis has been rejected

$H_0 = 0$, Hypothesis has been accepted

P_a = The probability of observing the given result, given $H_0 = 0$

w = Prediction time block

A.1 24 hour Prediction block test result

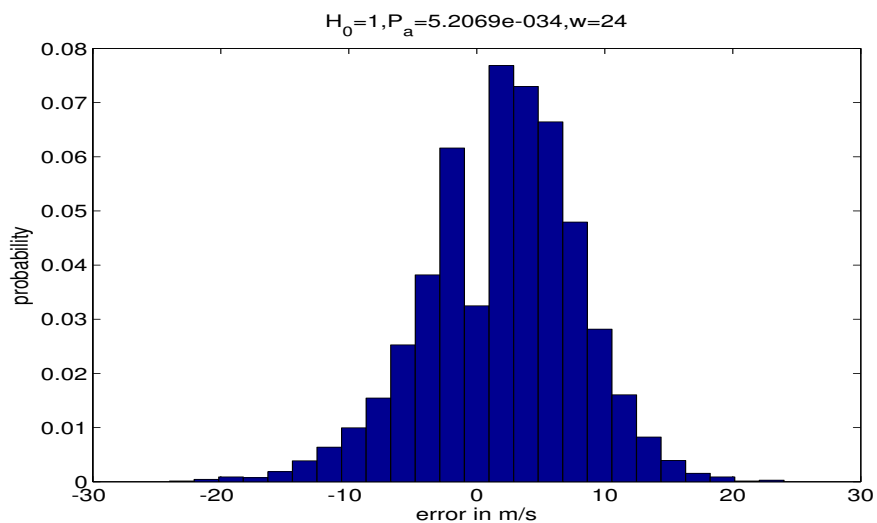


Figure A.1: Prediction block 00:00 to 23:59:5

A.2 12 hour Prediction block test results

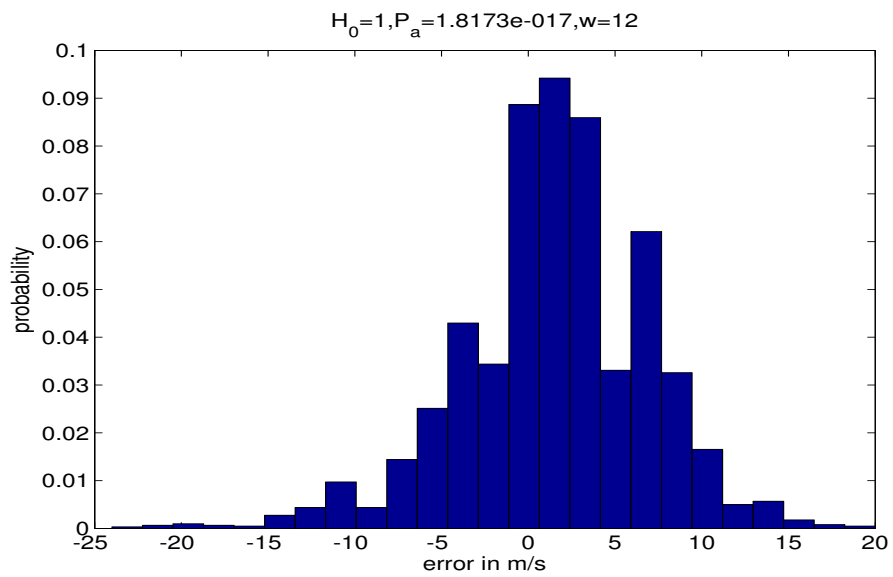


Figure A.2: Prediction block 00:00 to 11:59:59

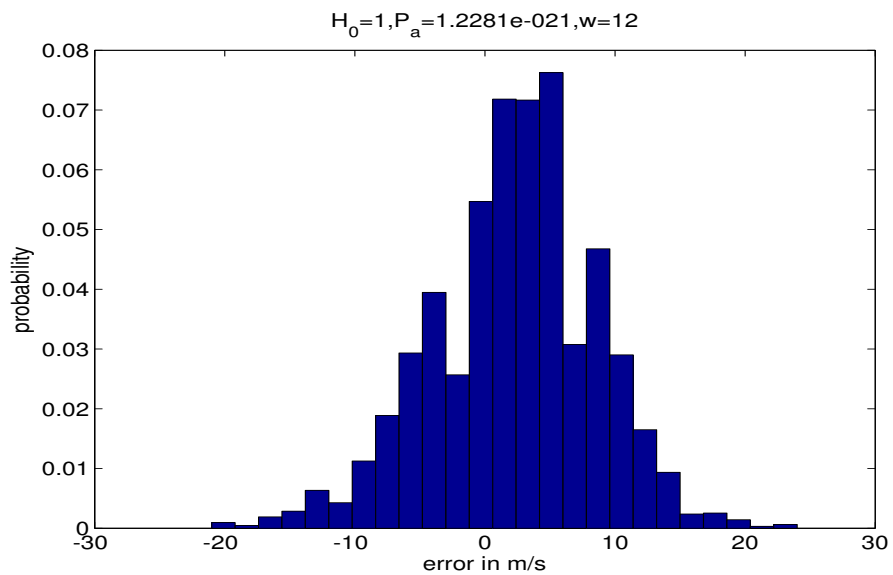


Figure A.3: Prediction block 12:00 to 23:59:59

A.3 6 hour Prediction block test results

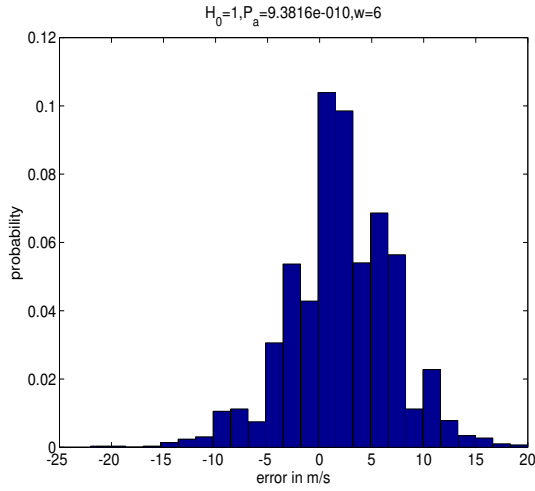


Figure A.4: Prediction block 00:00 to 05:59:59

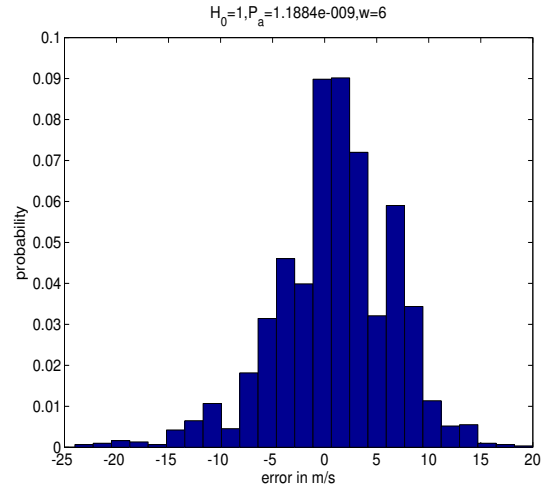


Figure A.5: Prediction block 6:00 to 11:59:59

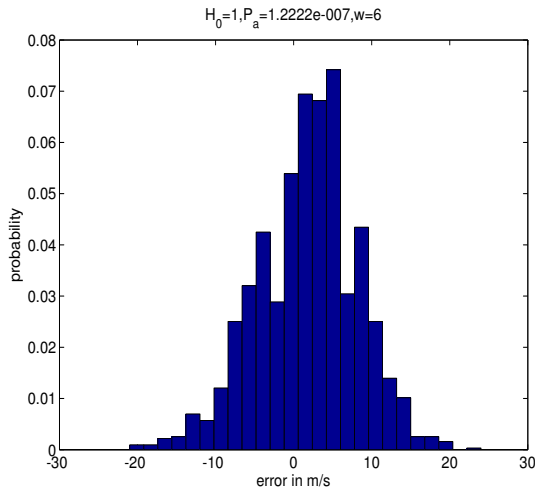


Figure A.6: Prediction block 12:00 to 17:59:59

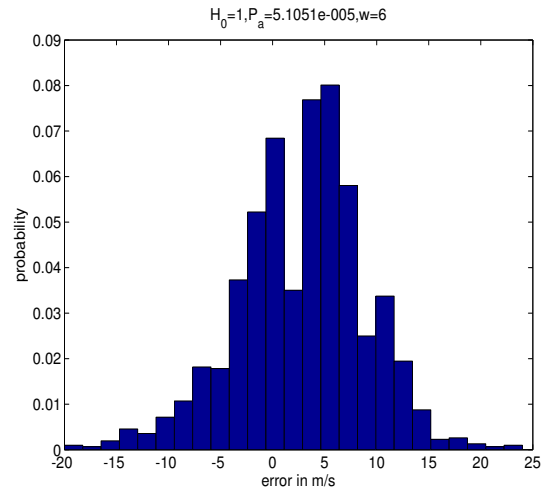


Figure A.7: Prediction block 18:00 to 23:59:59

A.4 3 hour Prediction block test results

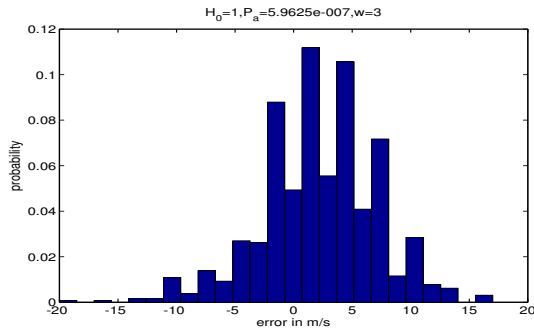


Figure A.8: Prediction block 00:00 to 2:59:59

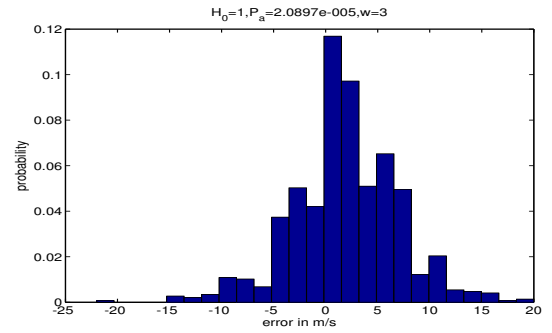


Figure A.9: Prediction block 3:00 to 5:59:59

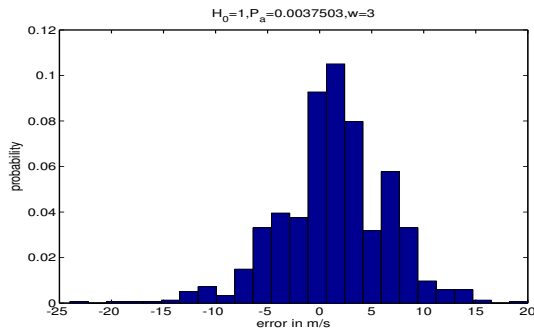


Figure A.10: Prediction block 06:00 to 8:59:59

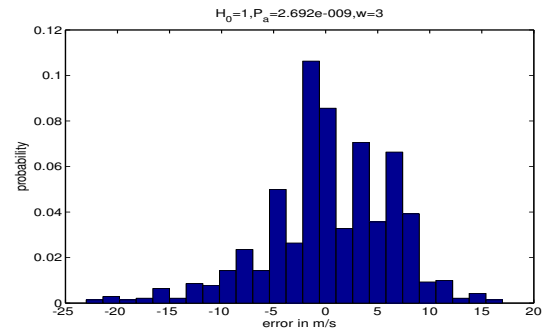


Figure A.11: Prediction block 9:00 to 11:59:59

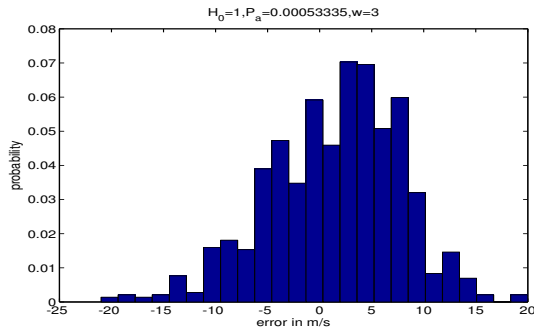


Figure A.12: Prediction block 12:00 to 14:59:59

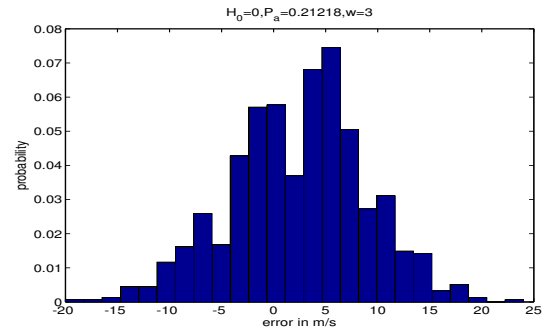


Figure A.13: Prediction block 15:00 to 17:59:59

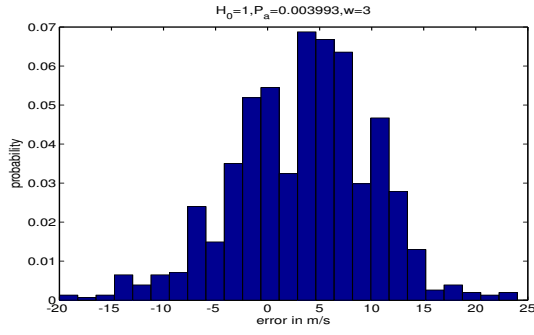


Figure A.14: Prediction block 18:00 to 20:59:59

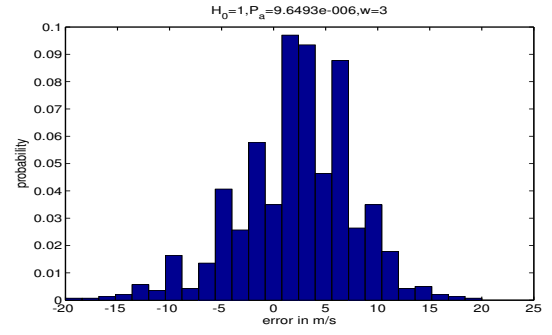


Figure A.15: Prediction block 21:00 to 23:59:59

A.5 1 hour Prediction block test results

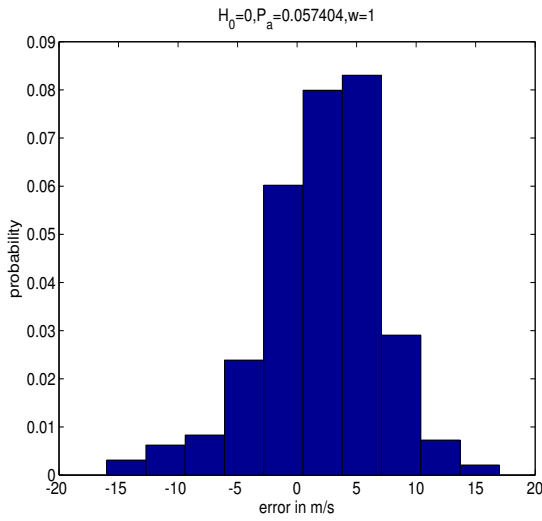


Figure A.16: Prediction block 00:00 to 0:59:59

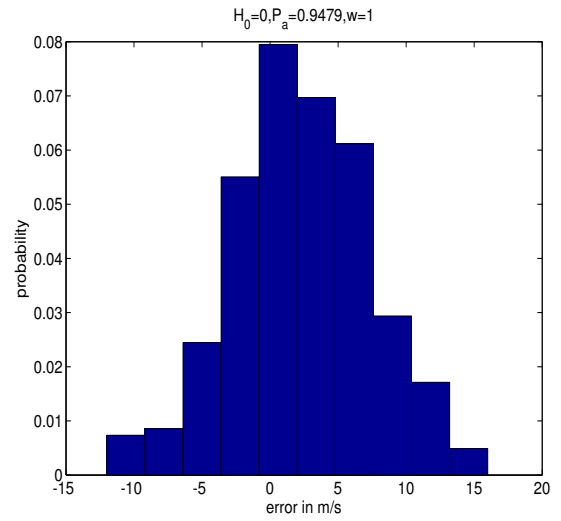


Figure A.17: Prediction block 1:00 to 1:59:59

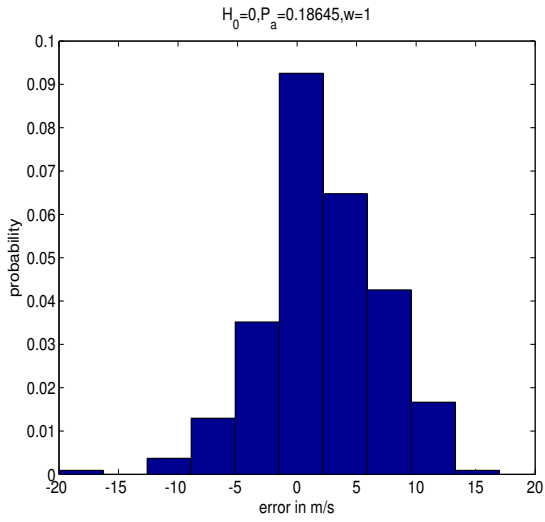


Figure A.18: Prediction block 2:00 to 2:59:59

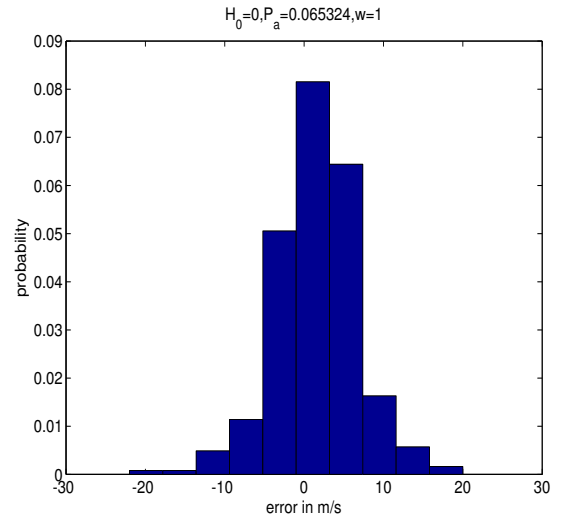


Figure A.19: Prediction block 3:00 to 3:59:59

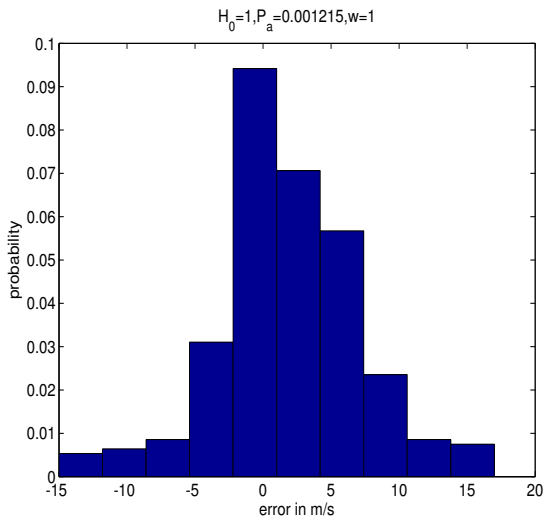


Figure A.20: Prediction block 04:00 to 4:59:59

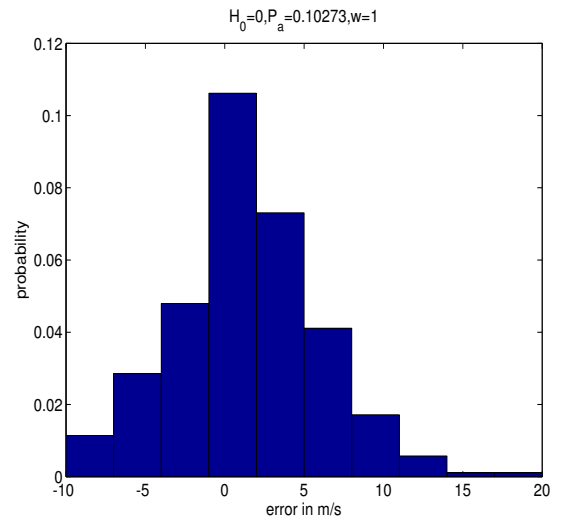


Figure A.21: Prediction block 5:00 to 5:59:59

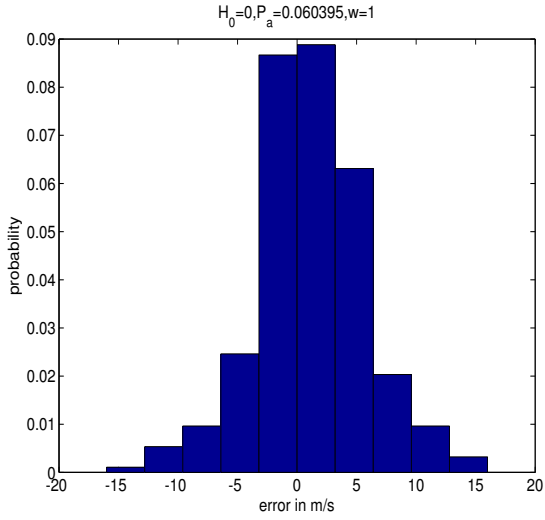


Figure A.22: Prediction block 6:00 to 6:59:59

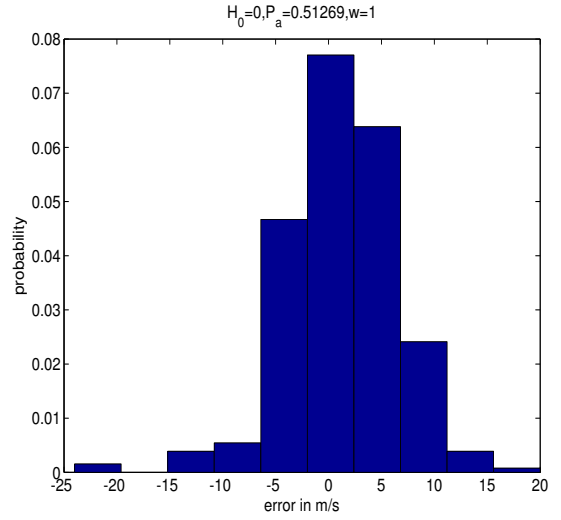


Figure A.23: Prediction block 7:00 to 7:59:59

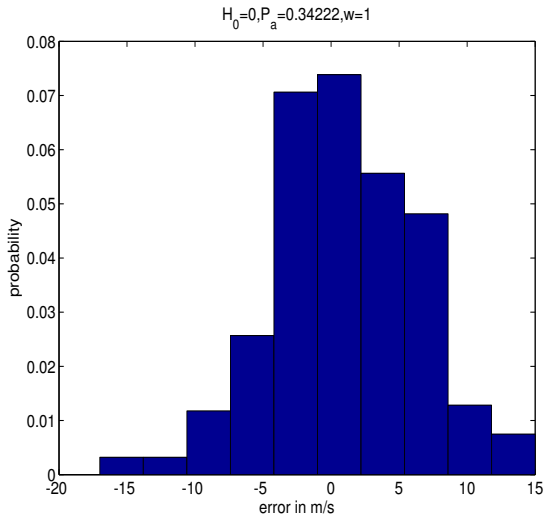


Figure A.24: Prediction block 8:00 to 8:59:59

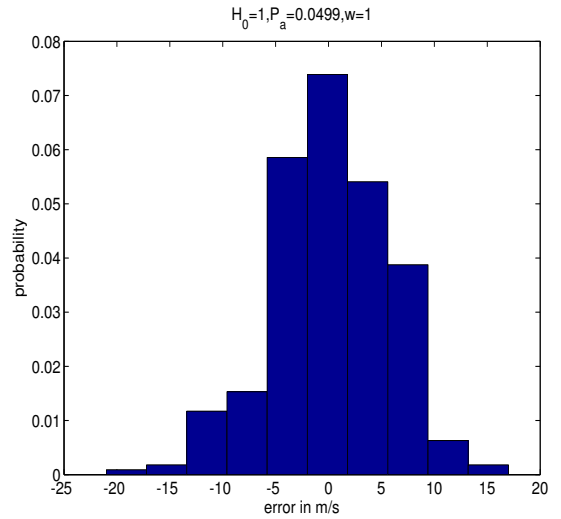


Figure A.25: Prediction block 9:00 to 9:59:59

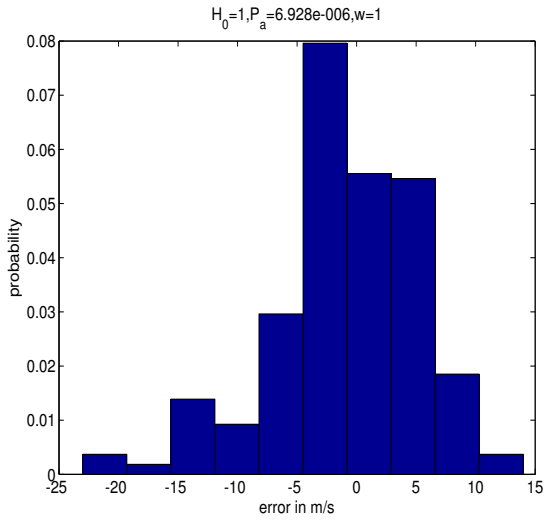


Figure A.26: Prediction block 10:00 to 10:59:59

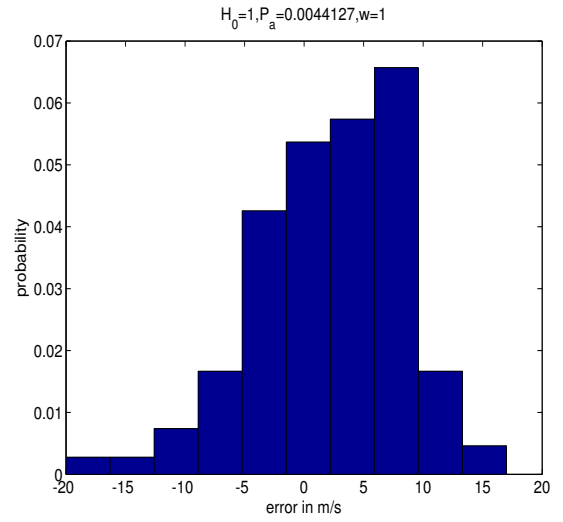


Figure A.27: Prediction block 11:00 to 11:59:59

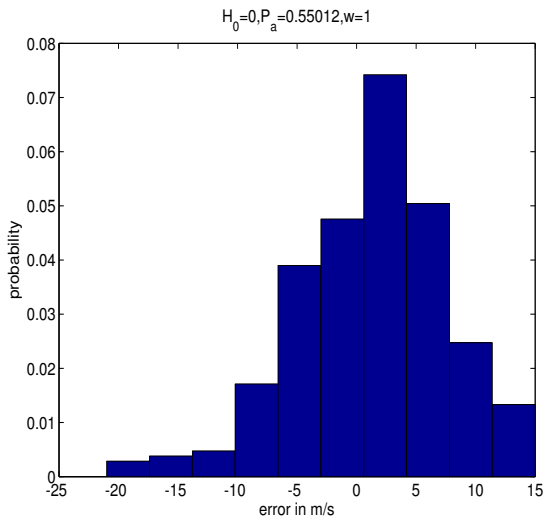


Figure A.28: Prediction block 12:00 to 12:59:59

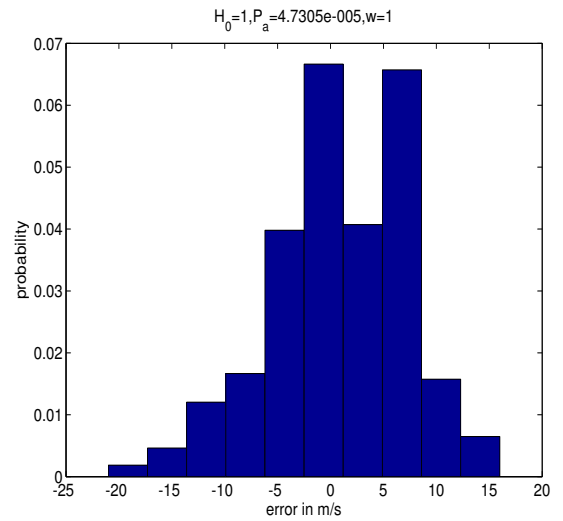


Figure A.29: Prediction block 13:00 to 13:59:59

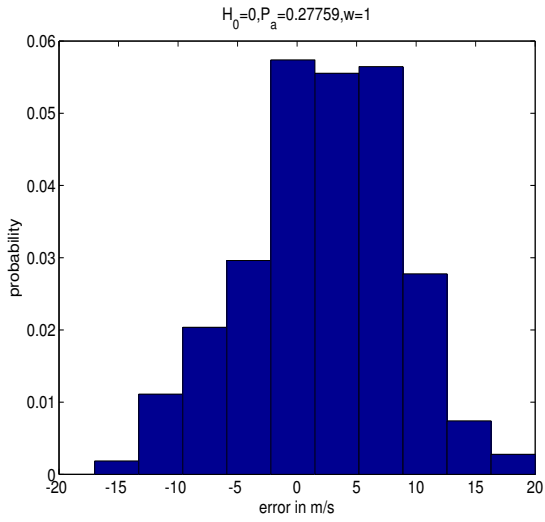


Figure A.30: Prediction block 14:00 to 14:59:59

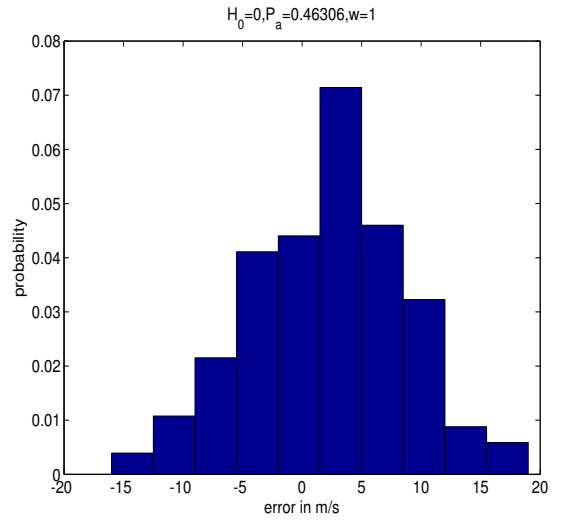


Figure A.31: Prediction block 15:00 to 15:59:59

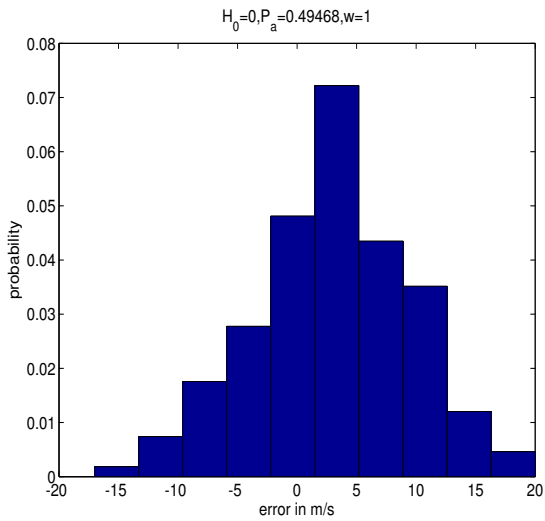


Figure A.32: Prediction block 16:00 to 16:59:59

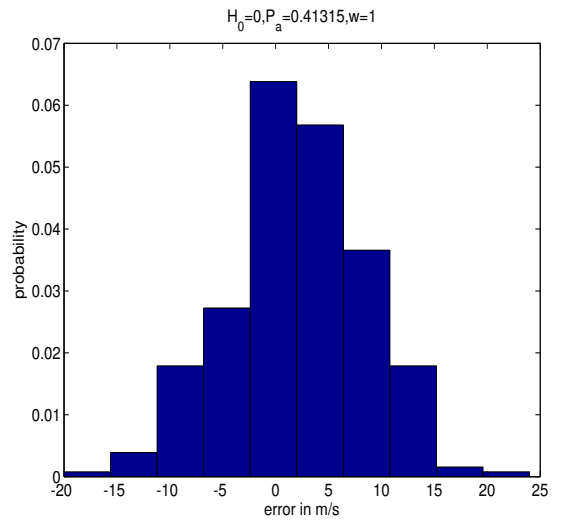


Figure A.33: Prediction block 17:00 to 17:59:59

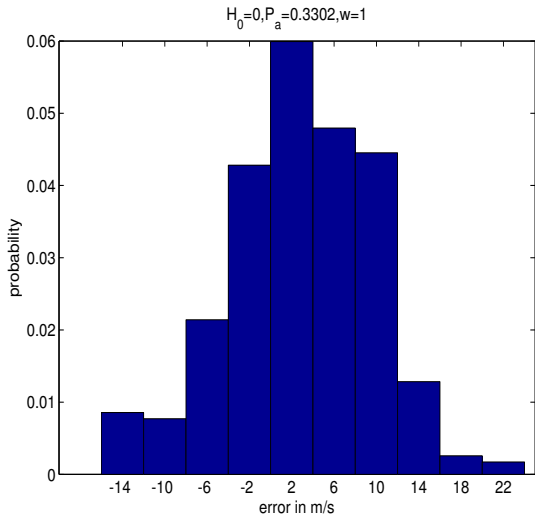


Figure A.34: Prediction block 18:00 to 18:59:59

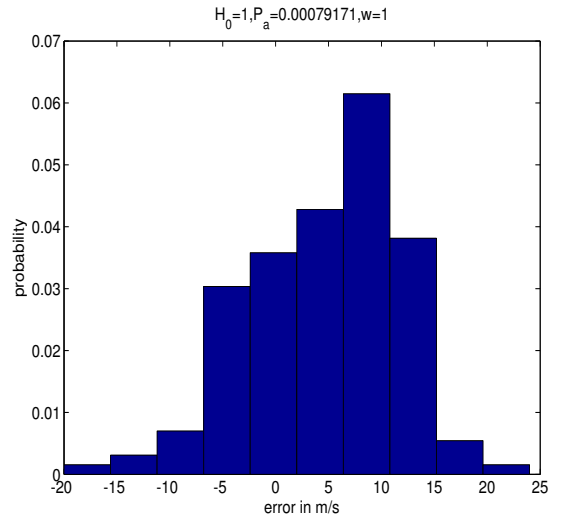


Figure A.35: Prediction block 19:00 to 19:59:59

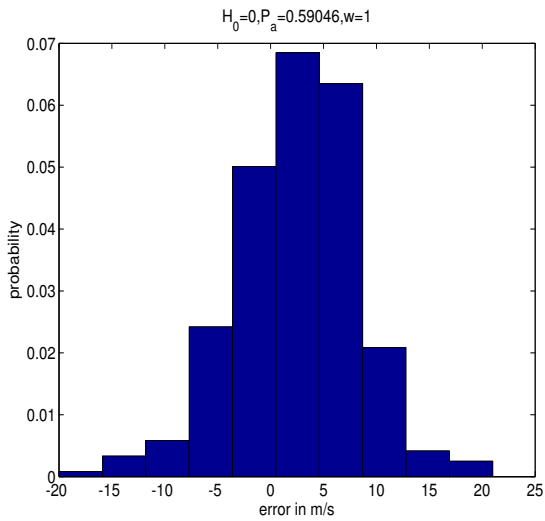


Figure A.36: Prediction block 20:00 to 20:59:59

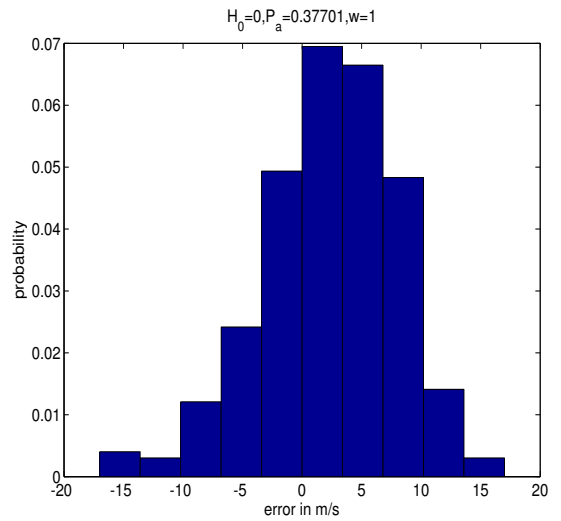


Figure A.37: Prediction block 21:00 to 21:59:59

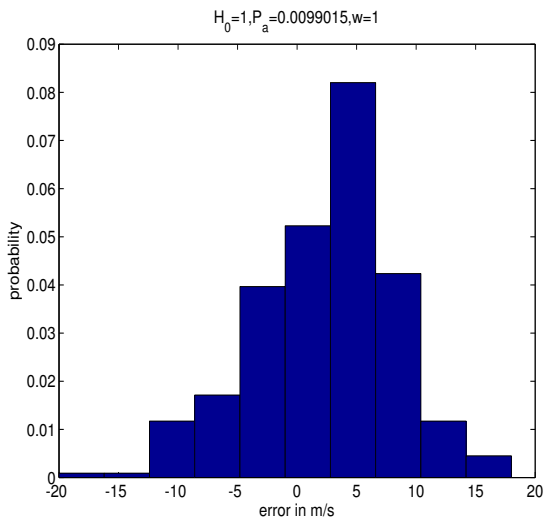


Figure A.38: Prediction block 22:00 to 22:59:59

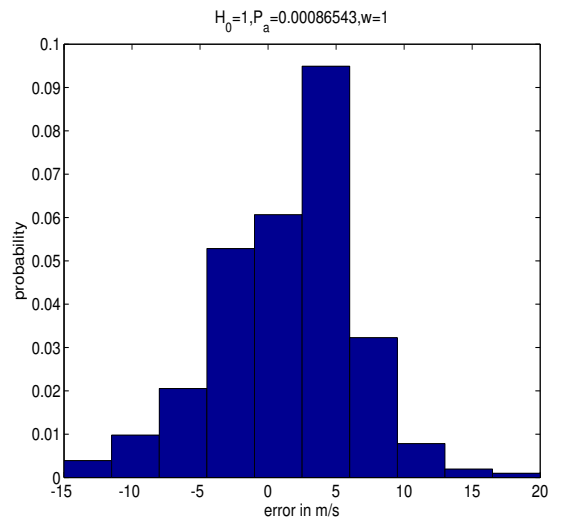


Figure A.39: Prediction block 23:00 to 23:59:59

Appendix B

Comparing cumulative probabilities (wind-speed forecast error)

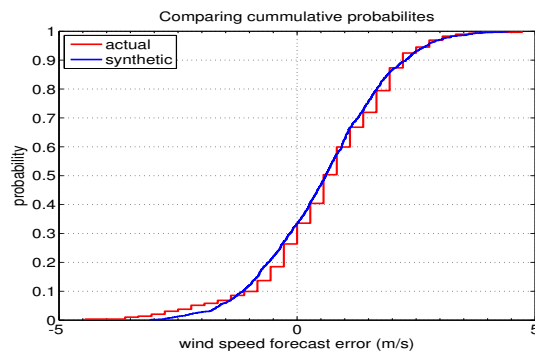


Figure B.1: Prediction block 00:00 to 0:59:59

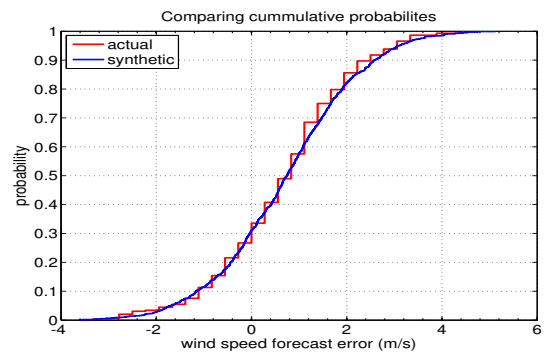


Figure B.2: Prediction block 1:00 to 1:59:59

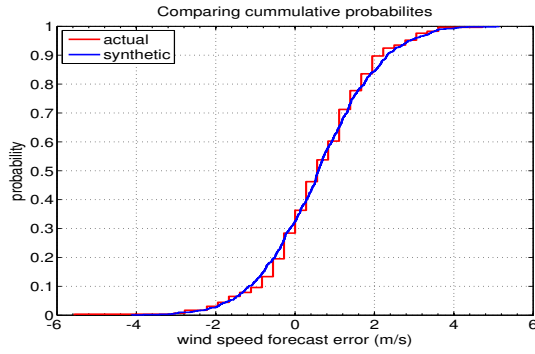


Figure B.3: Prediction block 2:00 to 2:59:59

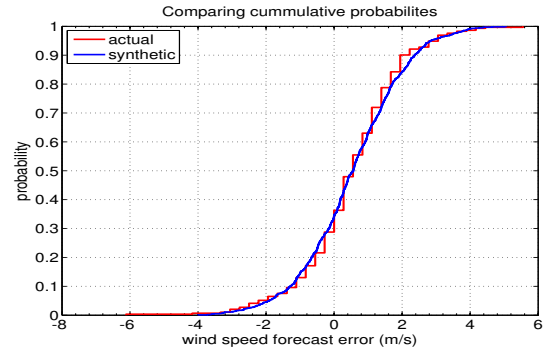


Figure B.4: Prediction block 3:00 to 3:59:59

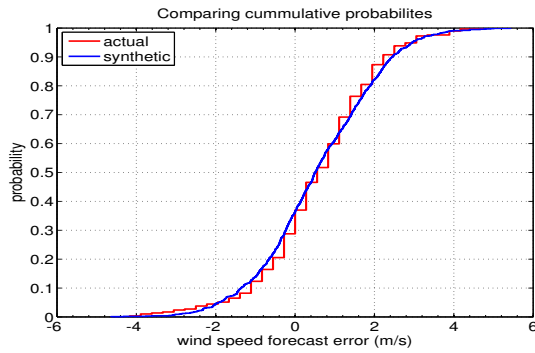


Figure B.5: Prediction block 04:00 to 4:59:59

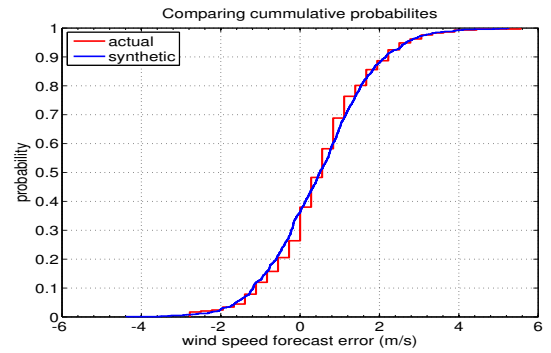


Figure B.6: Prediction block 5:00 to 5:59:59

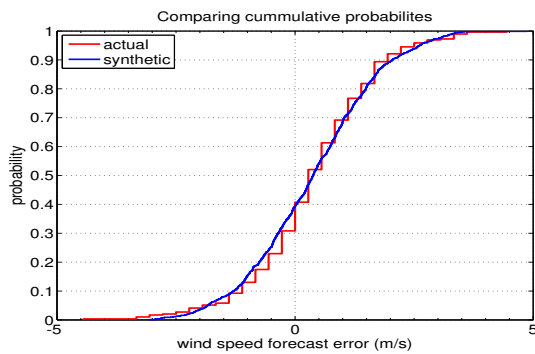


Figure B.7: Prediction block 6:00 to 6:59:59

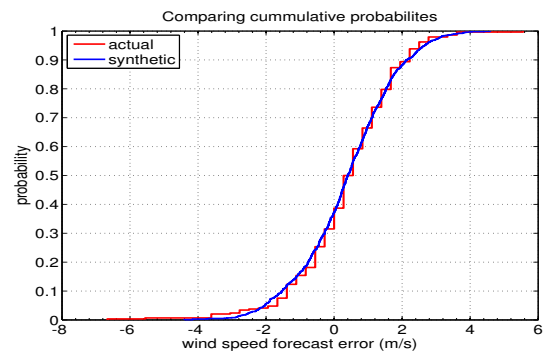


Figure B.8: Prediction block 7:00 to 7:59:59

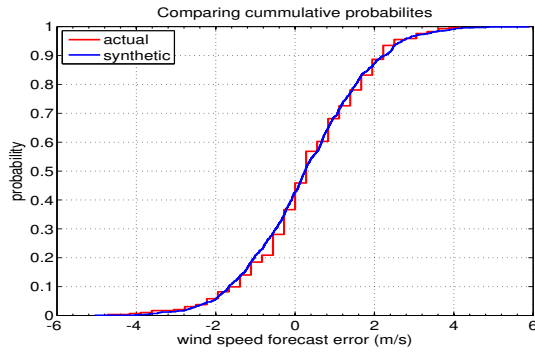


Figure B.9: Prediction block 08:00 to 8:59:59

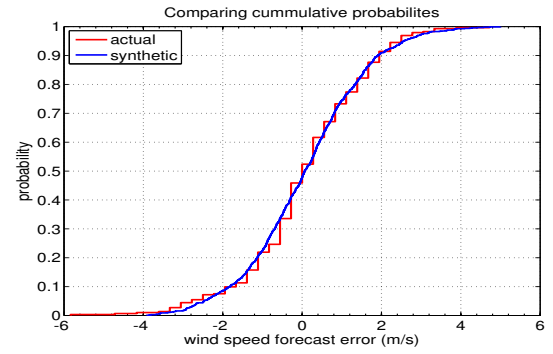


Figure B.10: Prediction block 9:00 to 9:59:59

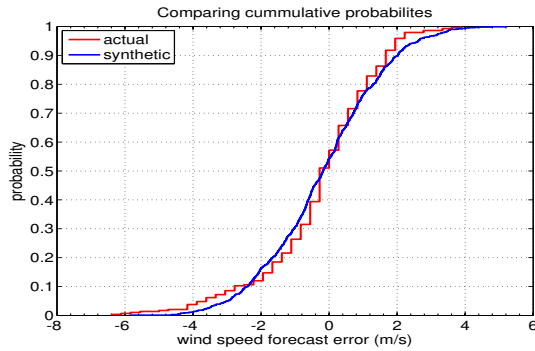


Figure B.11: Prediction block 10:00 to 10:59:59

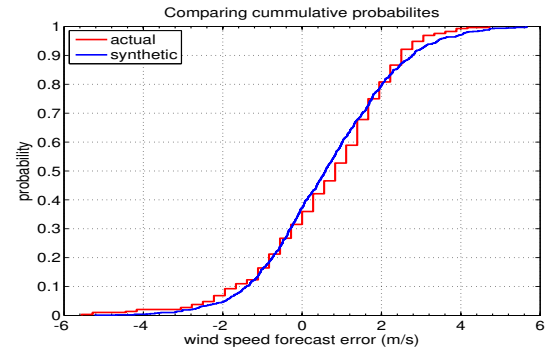


Figure B.12: Prediction block 11:00 to 11:59:59

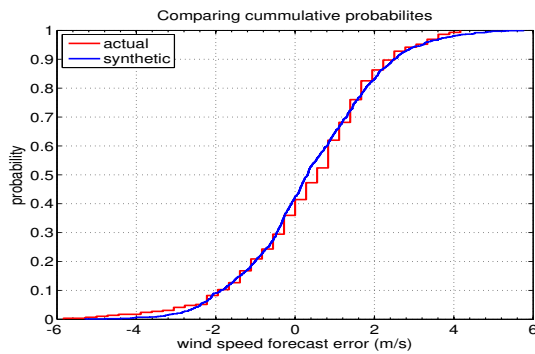


Figure B.13: Prediction block 12:00 to 12:59:59

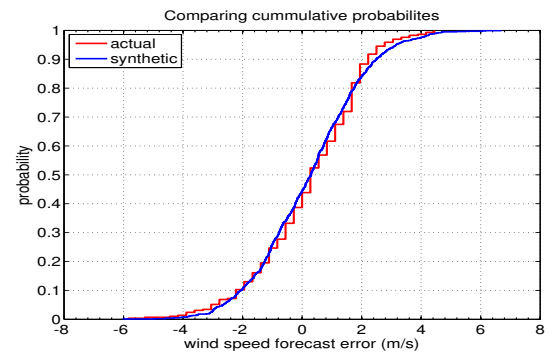


Figure B.14: Prediction block 13:00 to 13:59:59

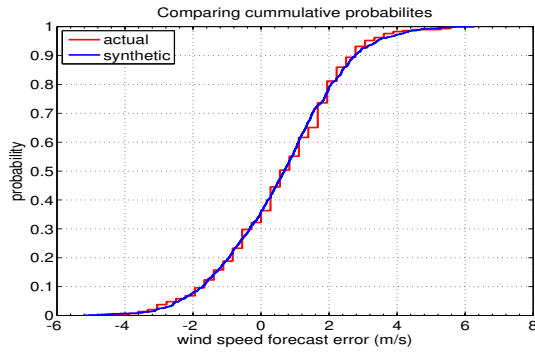


Figure B.15: Prediction block 14:00 to 14:59:59

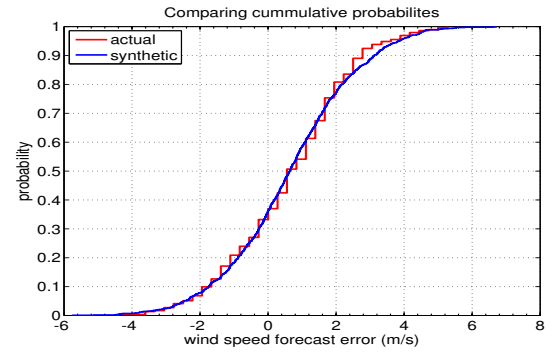


Figure B.16: Prediction block 15:00 to 15:59:59

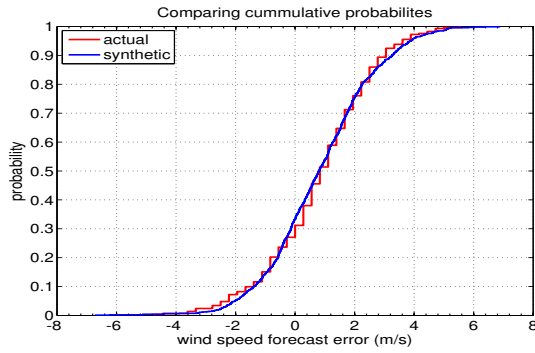


Figure B.17: Prediction block 16:00 to 16:59:59

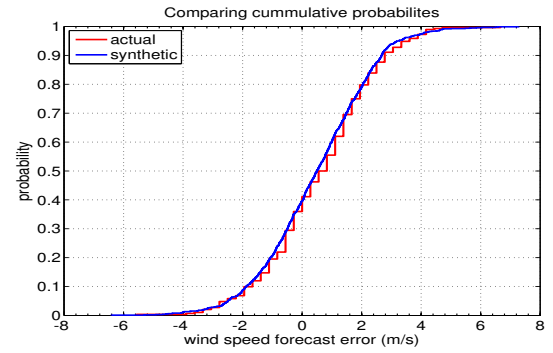


Figure B.18: Prediction block 17:00 to 17:59:59

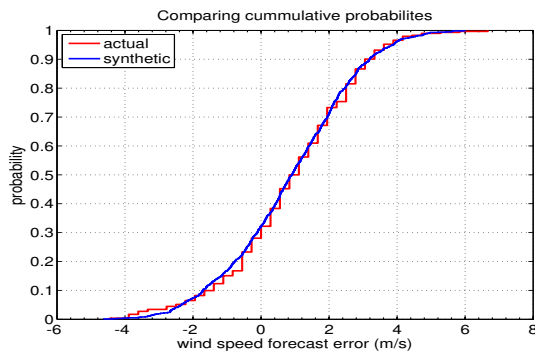


Figure B.19: Prediction block 18:00 to 18:59:59

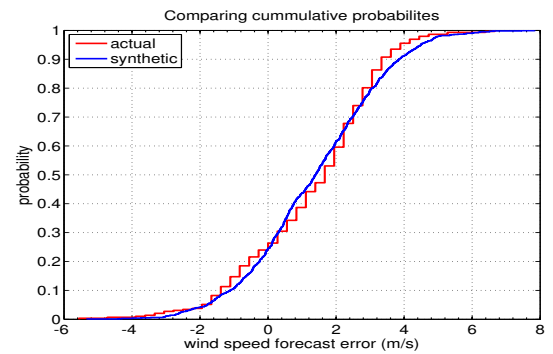


Figure B.20: Prediction block 19:00 to 19:59:59

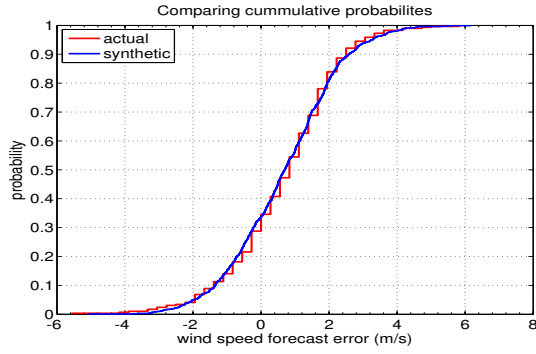


Figure B.21: Prediction block 20:00 to 20:59:59

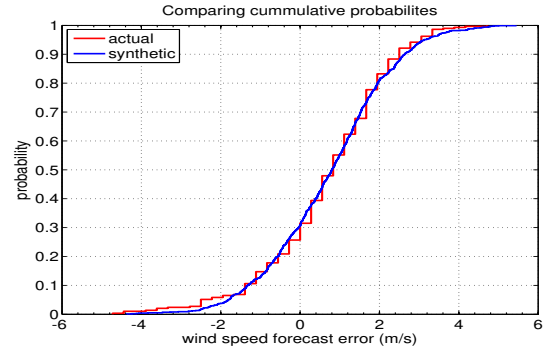


Figure B.22: Prediction block 21:00 to 21:59:59

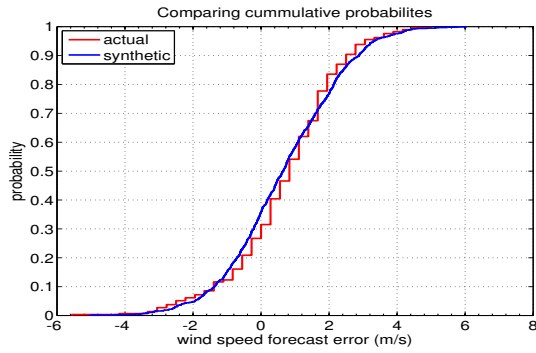


Figure B.23: Prediction block 22:00 to 22:59:59

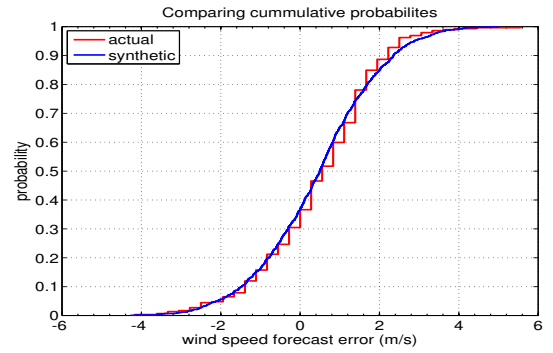


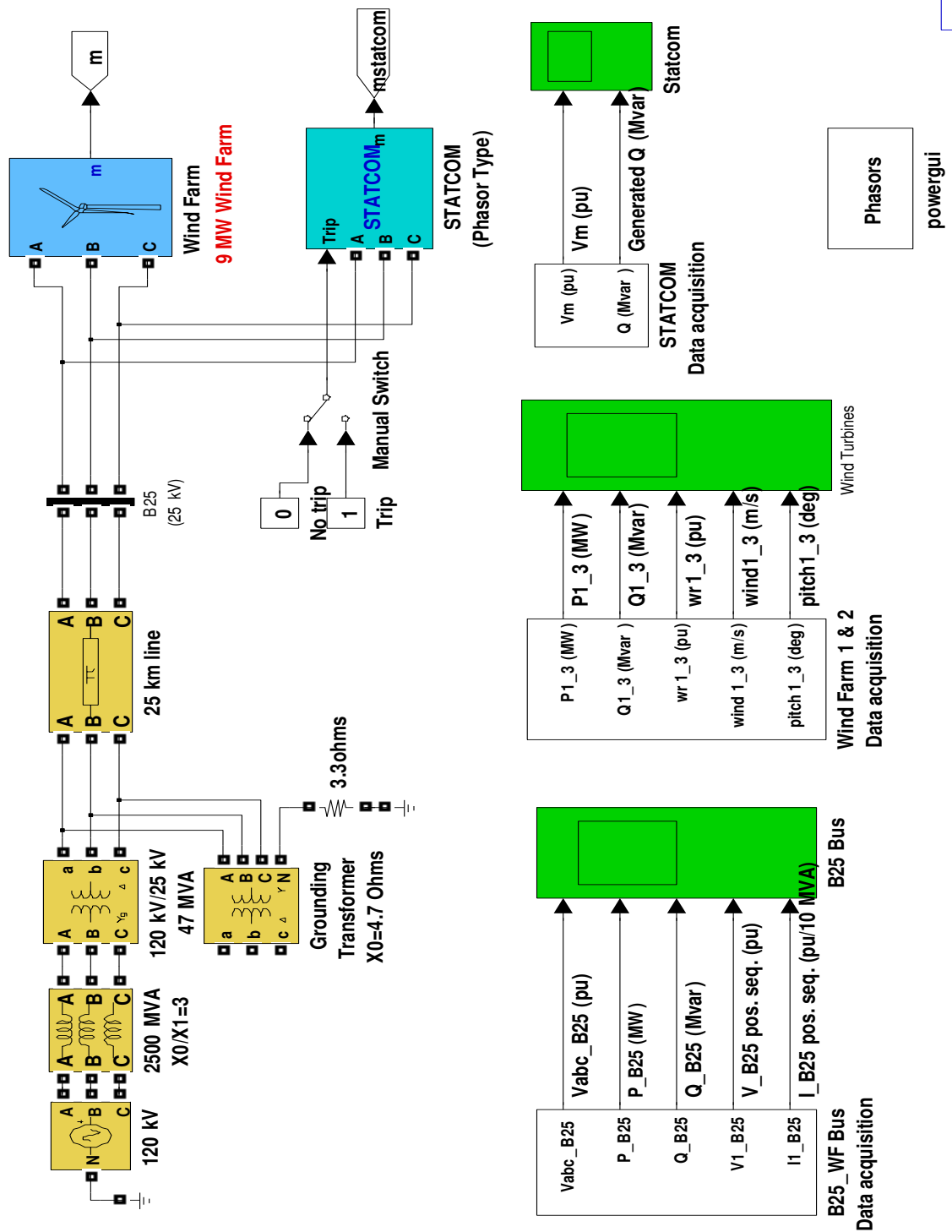
Figure B.24: Prediction block 23:00 to 23:59:59

Appendix C

Grid-connected wind power generator

Figure C.1 shows a 9 MW fixed-speed, grid connected wind power generator used in this thesis. The 'Wind Farm' model is explored further as shown in the figure C.2. m connected to the 'Wind Farm' model is called as sink node and from this node the following performance values of the 'Wind Farm' model can be obtained:

1. Active Power
2. Reactive Power
3. Pitch Angle
4. Angular speed of turbine rotor



Wind Farm (IG)

Figure C.1: Grid-connected wind power generator model [34]

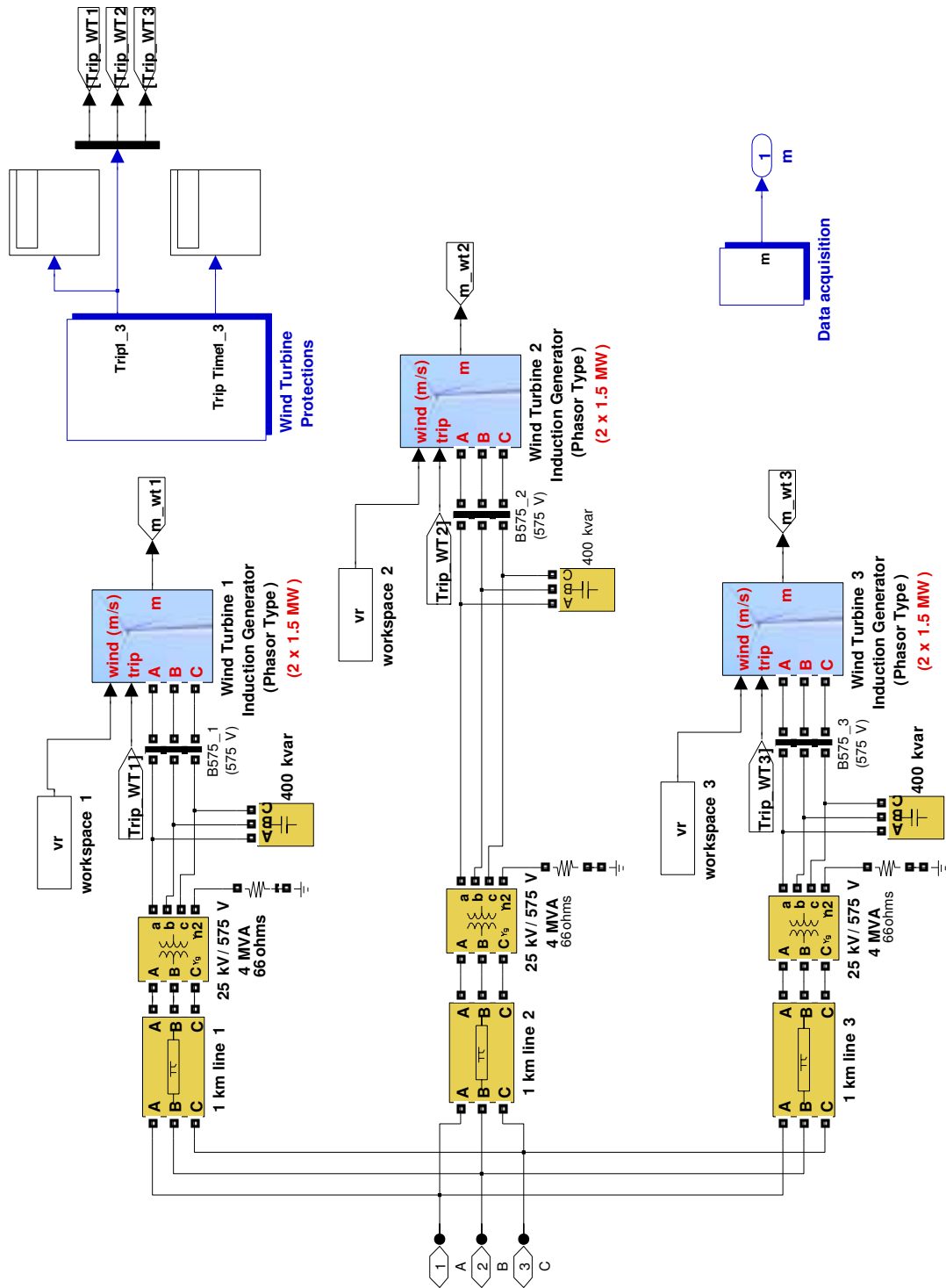


Figure C.2: Nine MW wind farm model [34]

Appendix D

Comparing cumulative probabilities (wind power prediction)

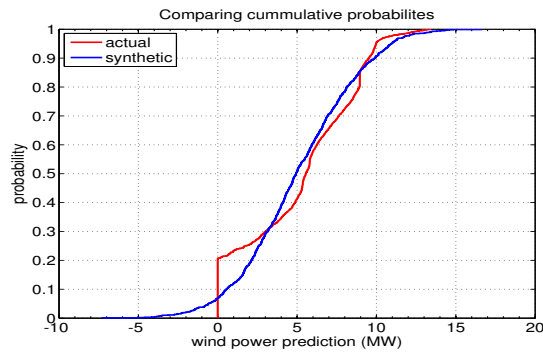


Figure D.1: Prediction block 00:00 to 0:59:59

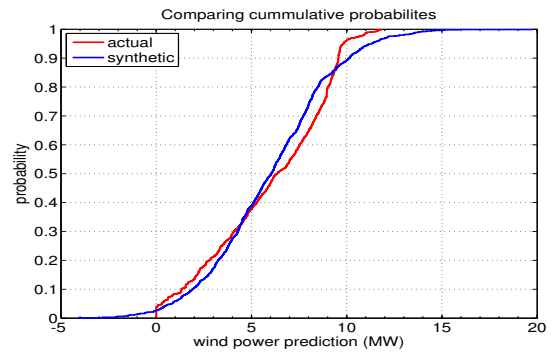


Figure D.2: Prediction block 1:00 to 1:59:59

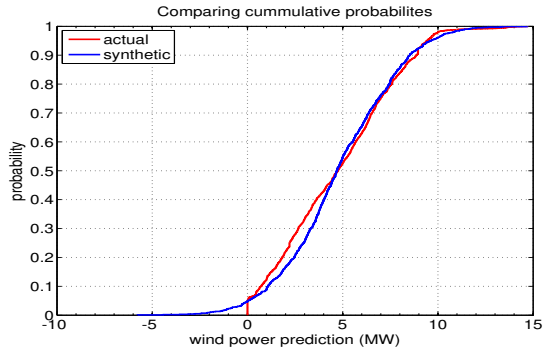


Figure D.3: Prediction block 2:00 to 2:59:59

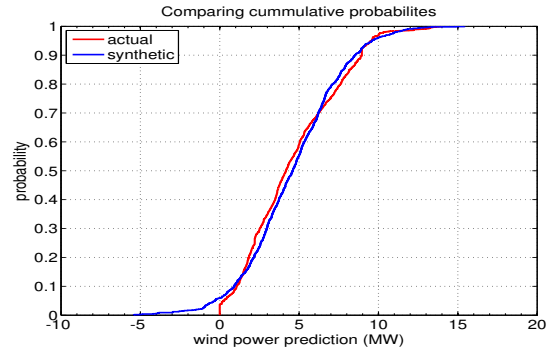


Figure D.4: Prediction block 3:00 to 3:59:59

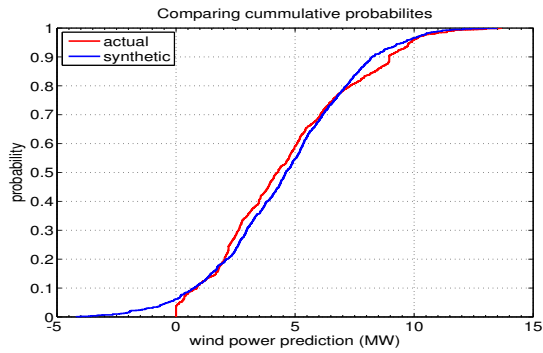


Figure D.5: Prediction block 04:00 to 4:59:59

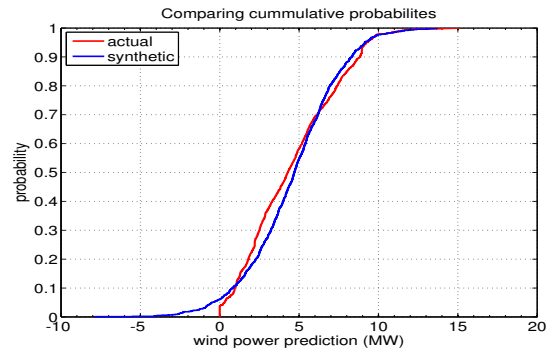


Figure D.6: Prediction block 5:00 to 5:59:59

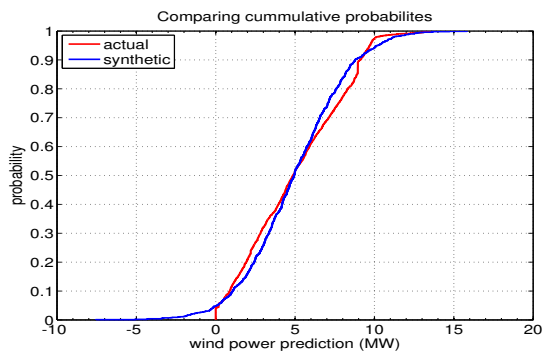


Figure D.7: Prediction block 6:00 to 6:59:59

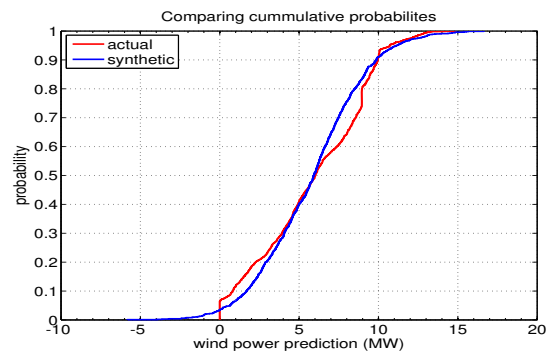


Figure D.8: Prediction block 7:00 to 7:59:59

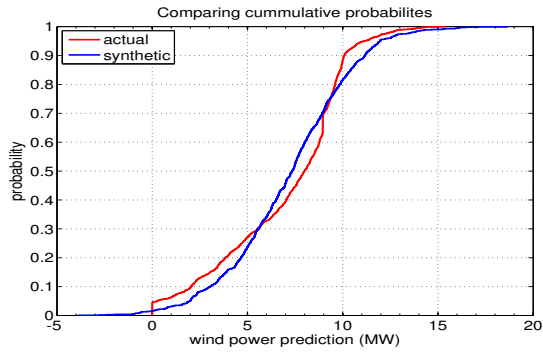


Figure D.9: Prediction block 08:00 to 8:59:59

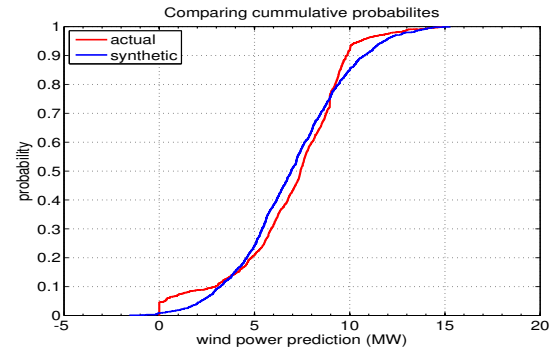


Figure D.10: Prediction block 9:00 to 9:59:59

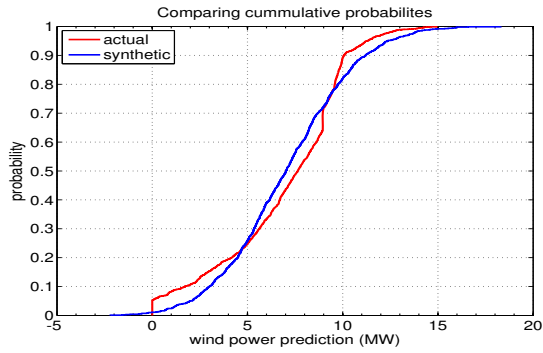


Figure D.11: Prediction block 10:00 to 10:59:59

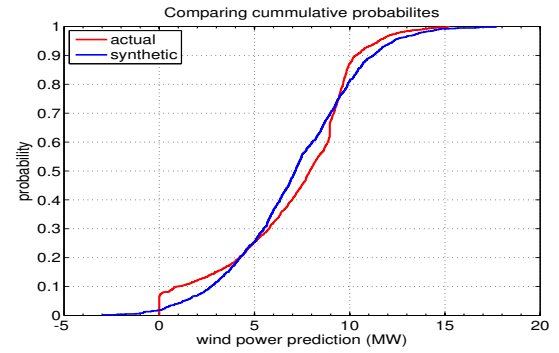


Figure D.12: Prediction block 11:00 to 11:59:59

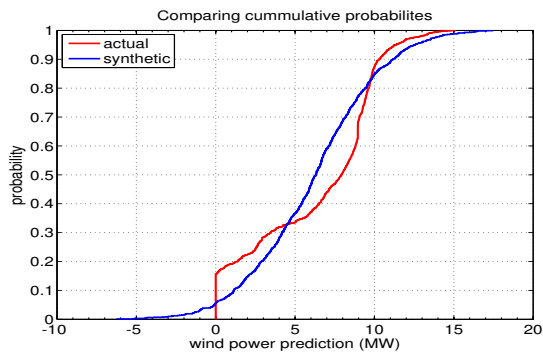


Figure D.13: Prediction block 12:00 to 12:59:59

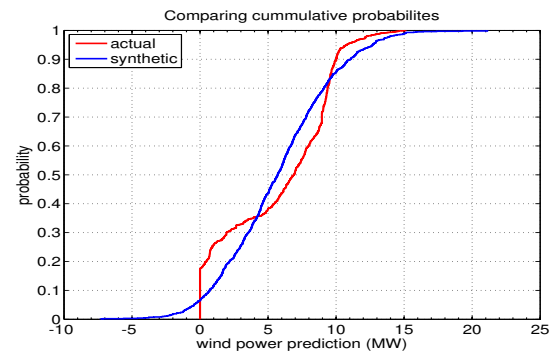


Figure D.14: Prediction block 13:00 to 13:59:59

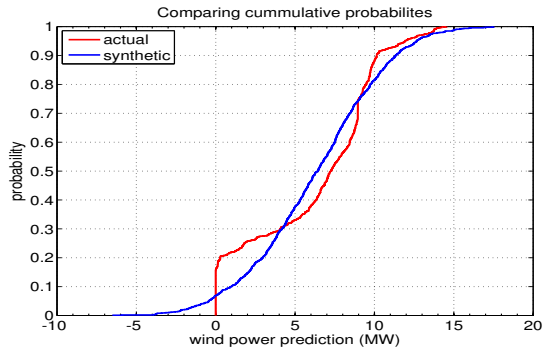


Figure D.15: Prediction block 14:00 to 14:59:59

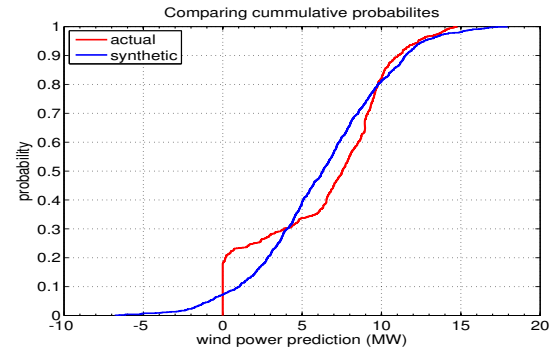


Figure D.16: Prediction block 15:00 to 15:59:59

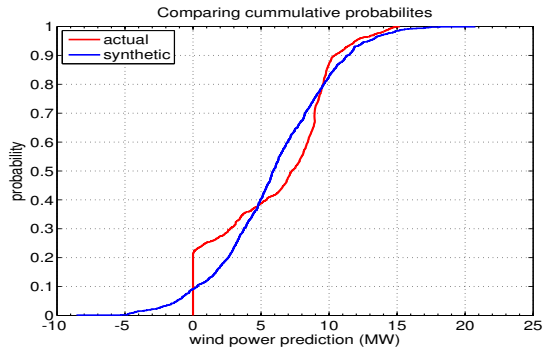


Figure D.17: Prediction block 16:00 to 16:59:59

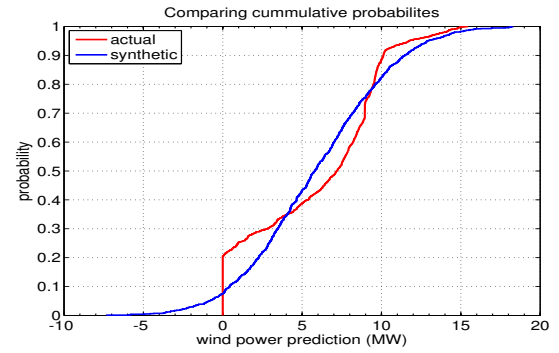


Figure D.18: Prediction block 17:00 to 17:59:59

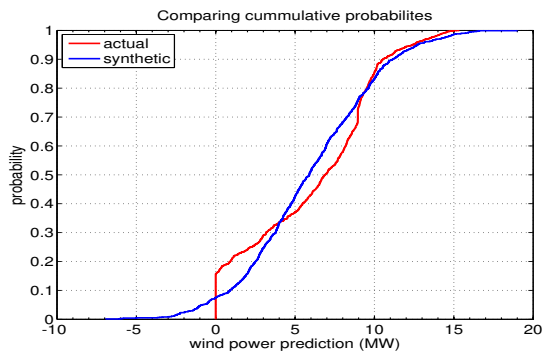


Figure D.19: Prediction block 18:00 to 18:59:59

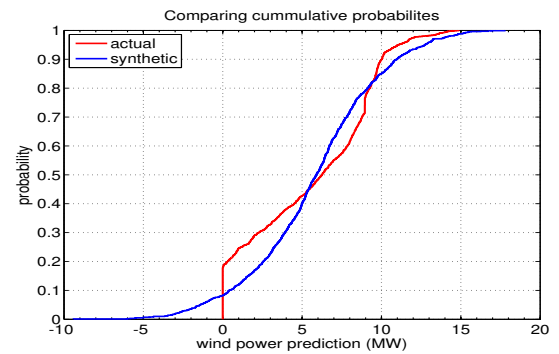


Figure D.20: Prediction block 19:00 to 19:59:59

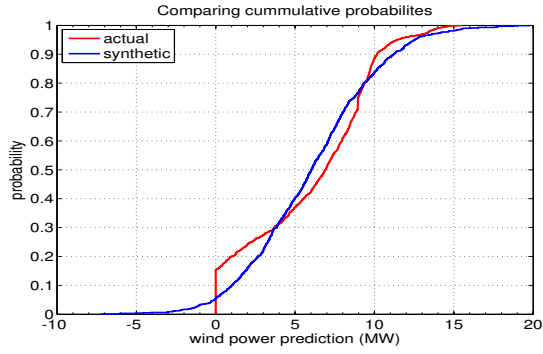


Figure D.21: Prediction block 20:00 to 20:59:59

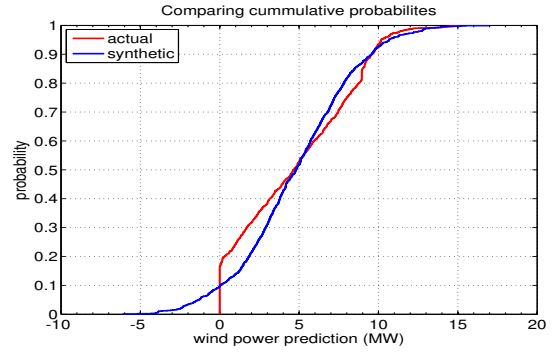


Figure D.22: Prediction block 21:00 to 21:59:59

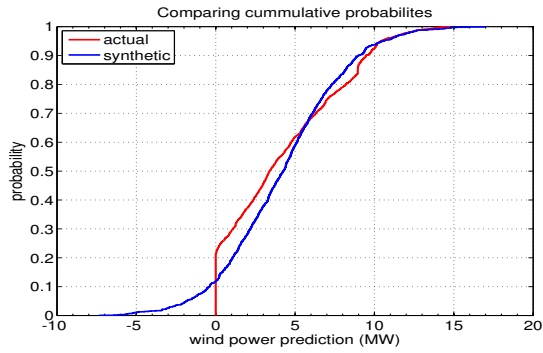


Figure D.23: Prediction block 22:00 to 22:59:59

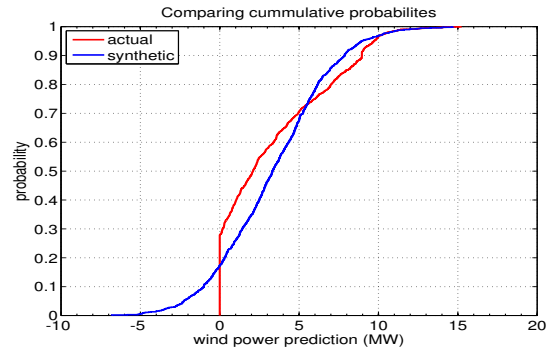


Figure D.24: Prediction block 23:00 to 23:59:59